
GEOMETRICAL ERROR ANALYSIS AND CORRECTION IN ROBOTIC GRINDING

A thesis submitted in partial fulfilment of the requirements of Liverpool John
Moore's University for the degree of Doctor of Philosophy

Mohammed Towfick Sufian

May 2020

PGR Declaration Form

COMPLETED BY THE PGR

Declaration:

I declare that while registered as a candidate for the University's research Degree

I have not been a registered candidate or enrolled student for another award of LJMU, or other university or institute of learning

I was, with the University's specific permission, a registered candidate/enrolled student for the following award.

Award	PhD
-------	-----

Materials:

I declare that no portion of the work referred to in this thesis has been submitted in support of an application for another degree or qualification of this or any other university or institute of learning.

Where work referred to in the thesis has been submitted in support of an application for another degree or qualification of this any other university or institute of learning, please provide details including reference to joint authorship of published materials which might have been included in a thesis submitted by another student of this university or any other institution of learning.

Click or tap here to enter text.

Thesis:

From January, we are moving to electronic submission of the thesis for examination. You can submit an electronic copy of your thesis to this email address (PGRExaminations@ljmu.ac.uk). The examiners can request a paper copy by exception. If they do then we can advise at that point about how to do this.

Signature:

Applicant Signature:	
Print Name:	Mohammed Towfick Sufian
Date:	27/11/2019

Abstract

The use of robots in industrial applications has been widespread in the manufacturing tasks such as welding, finishing, polishing and grinding. Most robotic grinding focus on the surface finish rather than accuracy and precision. Therefore, it is important to advance the technology of robotic machining so that more practical and competitive systems can be developed for components that have accuracy and precision requirement.

This thesis focuses on improving the level of accuracy in robotic grinding which is a significant challenge in robotic applications because of the kinematic accuracy of the robot movement which is much more complex than normal CNC machine tools. Therefore, aiming to improve the robot accuracy, this work provides a novel method to define the geometrical error by using the cutting tool as a probe whilst using Acoustic Emission monitoring to modify robot commands and to detect surfaces of the workpiece. The work also includes an applicable mathematical model for compensating machining errors in relation to its geometrical position as well as applying an optimum grinding method to motivate the need of eliminating the residual error when performing abrasive grinding using the robot.

The work has demonstrated an improved machining precision level from **50 μ m** to **30 μ m** which is controlled by considering the process influential variables, such as depth of cut, wheel speed, feed speed, dressing condition and system time constant. The recorded data and associated error reduction provide a significant evidence to support the viability of implementing a robotic system for various grinding applications, combining more quality and critical surface finishing practices, and an increased focus on the size and form of generated components. This method could provide more flexibility to help designers and manufacturers to control the final accuracy for machining a product using a robot system.

Acknowledgement

Taking first steps towards presenting a new understanding of knowledge in the manufacturing field is a worthy experience. Therefore, the time and experience during the production of this work cannot be seen without the help and support of some valuable people to me.

I am grateful and would like to express my sincere gratitude to my supervisor Prof. Xun Chen for his incredible ideas, continuous encouragement and constant support in making this work possible. He has always impressed me with his professional conduct and his strong conviction for science. I appreciate his consistent support from the first day and it has been a pleasure to work under his supervision. I would also like to thank with much appreciation the role of staff in the mechanical laboratory Thomas Byrne and Anthony Dunmore for their continuous assistance and help using the robot facility.

I must also give special thanks to my family for their love, dream and constant encouragement during this journey. I would like to thank them for their suggestions and comments which was part of the successful completion of this PhD Project.

Nomenclature

Upper Case

<u>Symbol</u>	<u>Description</u>	<u>S.I Unit</u>
A	Matrix of values solved simultaneously, from regression of point detection experiment.	N/A
A_0	Matrix of origin point values.	N/A
\hat{A}	Rotary Axis of an Industrial Robot.	(Degree)
\hat{B}	Rotary Axis of an Industrial Robot.	(Degree)
\hat{C}	Rotary Axis of an Industrial Robot.	(Degree)
D_x	Deviation in the X plane.	mm
D_y	Deviation in the Y plane.	mm
D_z	Deviation in the Z plane.	mm
E	Matrix of error values in each plane.	N/A
N	Unit of Force.	Newton
\vec{P}_z	Plane vector attributed to the Z axis.	N/A
R	Repeatability of a single process cycle.	N/A
\bar{R}	Average Repeatability over a given number of cycles.	N/A
X	Linear Axis of an Industrial Robot.	mm
$X_{\text{Experimental}}$	Actual point in the X plane, determined by practical experimentation.	mm
$X_{\text{Theoretical}}$	Theoretical value of X from regression experiment.	mm

$X_{\Delta d}$	Average Depth of Cut in the X plane.	μm
X_0	Real datum point of X found mathematically.	mm
Y	Linear Axis of an Industrial Robot.	mm
$Y_{\text{Experimental}}$	Actual point in the Y plane, determined by practical experimentation.	mm
$Y_{\text{Theoretical}}$	Theoretical value of Y from regression experiment.	mm
\vec{Y}_w	Y workpiece vector.	N/A
$Y_{\Delta d}$	Average Depth of Cut in the Y plane.	μm
Y_0	Real datum point of Y found mathematically.	mm
Z	Linear Axis of an Industrial Robot.	mm
$Z_{\text{Experimental}}$	Actual point in the Z plane, determined by practical experimentation.	mm
$Z_{\text{Theoretical}}$	Theoretical value of Z from regression experiment.	mm
F_n	Normal Force	N
$Z_{\Delta d}$	Average Depth of Cut in the Z plane.	μm
Z_0	Real datum point of Z found mathematically.	mm

Lower Case

<u>Symbol</u>	<u>Description</u>	<u>S.I Unit</u>
a	Constant that defines the position of the X plane.	N/A
\vec{a}	Vector that corresponds to the X plane.	N/A
\dot{a}	Coefficient of component vector in \vec{a} .	N/A
a_0	Origin point of X as a matrix constituent.	mm
b	Constant that defines the position of the Y plane.	N/A
\vec{b}	Vector that corresponds to the Y plane.	N/A
\dot{b}	Coefficient of component vector in \vec{b} .	N/A
b_0	Origin point of Y as a matrix constituent	mm
c	Constant that defines the position of the Z plane.	N/A
\vec{c}	Vector that corresponds to the Z plane.	N/A
\dot{c}	Coefficient of component vector in \vec{c} .	N/A
c_0	Origin point of Z as a matrix constituent.	mm
d	Constant that defines the regression function of a given plane.	N/A
i (subscript)	Minimum trials of a process or initial point or component value of a vector.	Various
j	Component of a vector in the Y direction.	N/A
k	Component of a vector in the Z direction.	N/A

kg	Base unit of mass, used interchangeably with weight for simplification in this report.	Kg
kHz	Unit of frequency defined as one cycle per second.	KHz
m	Base unit of length, distance, or span from which the majority of measurement units in this report are derived.	m
mm	Reflective of one millionth of the base unit 'Metre'. Used in the context of this report to describe axial positions in each plane.	mm
n (subscript)	Maximum trials of a process or final point of value.	Various
s	Base unit of time.	Second
w (subscript)	Denotes workpiece vector in corrective mathematical modelling.	N/A

Greek

<u>Symbol</u>	<u>Description</u>	<u>S.I Unit</u>
ε	Deformation	μm
Y	Matrix form given by the coordinate points found.	mm
Δ_d	Depth of cut in robotic grinding exercises.	μm
Δ_{plane}	Error in any given plane.	μm
Δ_R	Repeatability error.	μm
ε	Measurement Error	Mm
ε_X	Error in the X plane as a matrix constituent.	mm
ε_Y	Error in the Y plane as a matrix constituent.	mm
ε_Z	Error in the Z plane as a matrix constituent.	mm
α	Matrix form of Standard Deviation of Repeatability values.	N/A
α_X	Standard Deviation of Repeatability values in the X plane.	μm
α_Y	Standard Deviation of Repeatability values in the Y plane.	μm
α_Z	Standard Deviation of Repeatability values in the Z plane.	μm
δ	Real Depth of Cut	Mm
δ'	Nominal Depth of Cut	Mm
α	coefficient of deformation	N/A

List of Figures

Figure 2 - 1: Six-axis robot coordinate system. Hurco (2017).....	5
Figure 2 - 2: Belt grinding process Zhang et.al (2005).....	8
Figure 2 - 3: a) Manual grinding operation large-scale components b) human assisted grinding operation	9
Figure 2 - 4: Robotic welding application	10
Figure 2 - 5: Accuracy and Repeatability formation (Shiakolas, et al., 2002).....	15
Figure 2 - 6: Probing Examples Nageswara (2006)	16
Figure 2 - 7: Reverse Engineering Process Bagci (2009).....	22
Figure 2 - 8: Surface reconstruction and NC measurement of the core die Zhang (2003)	24
Figure 3-1: Methodology Flow Chart.....	28
Figure 3-2: a) KR 16 view of Robot b) Robot kinematic joint axis	29
Figure 3-3: Robot Control Panel Kuka (2010).....	30
Figure 3-4: Types of coordinate systems (Gadit & Damle, 2015)	31
Figure 3-5: Tool calibration layout Kuka (2010)	32
Figure 3-6: Base Calibration Kuka (2010).....	33
Figure 3-7: Electric circuit Connection	34
Figure 3-8: Electric Circuit Diagram.....	35
Figure 3-9: SBC Balance System Model SB-5500	36
Figure 3-10: Workpiece, Clamps and AE sensor	37
Figure 3-11: Single Point Diamond Dresser	37
Figure 3-12: Grinding Wheel.....	38
Figure 3-13: i-Series Talysurf Surface Machine	39
Figure 3-14: Bruker Machine.....	39
Figure 3-15: Romer 3D scanner	40
Figure 5-1: (a) Schematic Diagram for Experimental Setup, (b) Grinding Locations and Sensor illustration.....	86
Figure 5-2: Schematic of tool path generation.....	88
Figure 5-3: Fine Dressing Results	90
Figure 5-4: Coarse Dressing Results	90
Figure 5-5: Decay Chart for all Selected Speeds	95
Figure 5-6: Time constant representation graph.....	97
Figure 5-7: Grinding wheel interaction with work piece.....	98
Figure 5-8: Infeed process	100
Figure 5-9: Spark-out process	102

Figure 6-1: Grinding Strategy Flow Chart.....	105
Figure 6-2: (a) Weld view of the block, (b) weld size measurement.....	106
Figure 6-3: Mesh Converge Graph.....	107
Figure 6-4: Stepper schematic	109
Figure 6-5: Schematic view of weld and block surface.....	111
Figure 6-6 – Theoretical schematic view of material removal depth of cut	112
Figure 6-7: Roughing Stage Theoretical Cuts	113
Figure 6-8: Finishing Stage Theoretical Cuts	114
Figure 6-9: Experimental schematic view of material removal depth of cut	116
Figure 6-10: Roughing Stage Comparison	117
Figure 6-11: Finishing Stage Comparison	118
Figure 6-12: Final achieved positions	118
Figure 6-13 – physical profile measurement view	120
Figure 6-14: Surface profile of grinding area	121
Figure 6-15: Surface profile of grinding area	121
Figure 6-16: Detection of total measurement area	122

List of Tables

Table 1: Comparison of CNC machine and industrial robots for machining (Klimchik, et al., 2017)..	6
Table 2: Benefits and Drawbacks.....	22
Table 3: Robot Control Variables	30
Table 4: Electrical Repeatability Results.....	46
Table 5: AE Repeatability Results uner 0.01m/s	51
Table 6: AE Repeatability Results uner 0.005m/s	52
Table 7: Repeatability Comparison Results	57
Table 8: Measurment Results of XY Plane.....	68
Table 9: Measurment Results of YZ Plane	68
Table 10: Measurment Results of XZ Plane	69
Table 11: Error Correlation of palne ZX	70
Table 12: Standard devation of calculated error	70
Table 13: Error Correlation of palne YZ	71
Table 14: Standard devation of calculated error	71
Table 15: Error Correlation of palne XZ	72
Table 16: Standard devation of calculated error	72
Table 17: Regressed Values calculated from software.....	73
Table 18: Datum Error for each set of sqaure.	76
Table 19: Overall outcome results of two different speeds.....	81
Table 20: Experimental parameters of grinding.....	87
Table 21: Fine Dressing Results.....	89
Table 22: Corase Dressing Reuslts.....	89
Table 23: Experimental grinding results.....	92
Table 24: Grinding Stratagy Experimental Parameters	105
Table 25: Mesh convergence reuslts	107
Table 26: Tool path setup parameters.....	108
Table 27: Experimental Roughing Results	115
Table 28: Experimental results comparisions	117

Table of Contents

Abstract	III
Acknowledgement.....	IV
Nomenclature.....	V
List of Figures.....	X
List of Tables	XII
Table of Contents.....	XIII
Chapter One. Introduction.....	1
1.1 Aims & Objectives	2
1.2 Novelty & Academic Contribution	2
1.3 Thesis Layout.....	3
Chapter Two. Literature Review	4
2.1. Research Motivation.....	4
2.2. Robotic Grinding Overview, Applications and Challenges	4
2.2.1 Robots and CNC Machines	6
2.2.2 Robot Grinding Applications.....	8
2.2.3 Robot Grinding Challenges	10
2.3. Robot Grinding Strategies & Alternative Solutions.....	13
2.3.1 Precision measurement.....	13
2.3.2 Tool path planning	18
2.3.3 Process Parameter Optimisation	19
2.3.4 Machine Error Compensation.....	20
2.4. Digitizing and Repair Engineering.....	20
2.4.1 Digitizing devices and methods.....	21
2.4.2 Repair Engineering.....	22
2.5. Summary, Gaps and Challenges	24
Chapter Three. Methodology & Experiment Instrumentation	26
3.1. Methodology.....	26
3.2. Experimental Instruments.....	29

3.2.1 Robot control panel.....	30
3.2.2 Robot Coordinate system.....	31
3.2.3 Electric Circuit.....	33
3.2.4 Data accusation log.....	36
3.2.5 Workpiece.....	36
3.2.6 Single Point Diamond Dresser.....	37
3.2.7 Grinding Tool.....	38
3.2.8 Surface Measurement Machine.....	38
3.2.9 Bruker machine (Microscope).....	39
3.2.10 3D Scanner.....	40
Chapter Four. Geometrical Error Analysis.....	41
4.1. Repeatability Tests.....	41
4.1.2 Mechanical Method.....	43
4.1.2 Electrical Method.....	46
4.1.3 Acoustic Emission Probing Method.....	48
4.1.4 Accuracy Error Comparison.....	57
4.2. Mathematical Model for Error analysis.....	58
4.2.1 Position Modelling.....	58
4.2.2 Model Establishment Implementation.....	66
4.2.3 Error Comparison.....	81
4.3. Summary.....	82
Chapter Five. System Compliance Model.....	83
5.1. Influential Factors for Robotic Grinding.....	84
5.1.1 Dressing.....	84
5.1.2 Grinding.....	85
5.1.3 Tool Path Generation.....	88
5.2. Results & Discussions.....	88
5.3. Mathematical Model.....	97
5.4. Summary.....	103

Chapter Six. Grinding Strategy for Repair	104
6.1. Component Repair Strategy Development and Validation.....	104
6.1.1 Robot setup and grinding parameters	105
6.1.3 Toolpath setup.....	108
6.1.4 Contact Registration and Model Alignment using Acoustic Emission	110
6.1.5 Theoretical Grinding Analyses	110
6.1.6 Experimental Results & Validations	115
6.2. Summary.....	123
Chapter Seven. Conclusion.....	124
Chapter Eight. Recommendations & Future Work	126
References.....	127
Appendices.....	136
Appendix 1.....	136
Appendix 2.....	142
Appendix 3.....	147
Appendix 4.....	149
Appendix 5.....	151

Chapter One. Introduction

Robotic manufacturing is becoming an alternative approach in efficient machining due its flexibility, cost efficiency and intelligence particularly in comparison with the current manufacturing modes. Many industrial robots are currently used for grinding operation and they operate in a constrained way were grinding tool is mounted on the robot arm in a conventional way. Applications such as aerospace, automotive, defence and medical industries have been implementing repair technologies to reduce the cost, time of the manufacturing process and increase service life of the component. The manufacture of these complex shapes is extremely expensive and time consuming. Therefore, the use of robots has been very efficient recently in terms of proving manufacturing purposes, they have the ability to create an enormous amount of cutting cycles in X, Y and Z directions and A, B rotary orientations which makes it flexible to machine or repair complex parts and grind surfaces. This rotary axis can tilt the position of the tool or the workpiece in many different ways, which adds flexibility and uncertainty in machining parts Tao et.al (2019). Due to the limited robot rigidity and payload, the applicable depth of cut and feed rate must be kept small which limits the material removal rate and the machining efficiency. Therefore, most robotic grinding focuses on the surface finish improvement, but not on the accuracy of component size and form in the process.

The proposed new development of robotic grinding technology will consider all quality measures in grinding as well as the accuracy of size and form. Such development will open up huge flexible application potentials in precision component manufacturing. It also presents a significant challenge in robot application, because the kinematic accuracy of robot movement is much more complex than a normal CNC machine. This causes inaccuracies and error which occurs from several sources such as set-up error, machine error and tool path that affect the datum and target features of the workpiece which leads to errors in position and orientation of machined features on the workpiece which strongly affects the product quality. Therefore, a fixture must be accurately located in a position and orientation with respect to the cutting tool Neto & Moreira (2013).

This thesis focuses on improving the level of accuracy in robotic grinding precision, which is a significant challenge in robot applications. The work includes steps involved in defining the datum on a closed workspace to support the process monitoring and control strategy to

provide an accurate movement to the robot and to ensure smooth grinding and surface finishing. The proposed project will consider typical quality measures in robotic grinding including the accuracy of size and form.

1.1 Aims & Objectives

The aim of this thesis will focus on improving the level of accuracy in robotic grinding precision by eliminating the influence of errors on the geometrical accuracy, which is the key for controlling the robot to conduct grinding process. By establishing the geometrical relationship between reference datum and probe point of measurement, the error level could be assessed based on the repeatability and defined measuring points on the surface of the workpiece. The goal is to present a practical method to improve the machining accuracy by compensating the geometrical error and to motivate the need to eliminate the residual error when performing abrasive grinding using the robot. The project will consist of the following objectives:

- Understanding the knowledge of available repair processes which includes critical analyses on machining strategy through literature review.
- Establish suitable sensing and metrological monitoring method to improve error compensation in robotic abrasive processing.
- Establishing a model to provide a fundamental material removal mechanism under conditions and guidelines for robotic grinding and its optimization.
- Developing a machining strategy for the repair of components.

1.2 Novelty & Academic Contribution

This research provides a suitable solution for precision measurement to repair components in manufacturing and maintenance operation using a robot in many industrial sectors. The main novel contributions are as follows:

- A novel method to define the error accuracy by using the cutting tool as a probe in the robot system using acoustic emission monitoring technology that modifies robot commands accordingly for detecting surfaces.
- A novel mathematical model for compensating machining errors in relation to its geometrical position by utilising system relaxing technique.
- Novel improvement of repair accuracy by taking advantages of abrasive machining that has minimum depth of cut.

- Novel grinding method to motivate the need to eliminate the residual error when performing abrasive grinding using the robot.

It has been identified that the development of next generation robotic abrasive machining technology is a research forefront to provide suitable solutions for precision component manufacturing and maintenance operation in broad industrial sectors Bagci (2009). The developed repair method consists of establishing a new technique for robotic abrasive machining which will provide a high inspection quality, best fit reconstruction and effective machining strategy to restore geometric and dimensional attributes. Therefore, this work provides a fundamental step using robots for grinding purposes in manufacturing.

1.3 Thesis Layout

The layout of this thesis is as follows:

- Chapter Two includes a review of literature which aims to present a relevant research in the field of robotic grinding till this date, it presents a critical review of aspects robotic grinding, focusing on problems and challenges arising and their impact on the machined workpiece geometry.
- Chapter Three presents a methodology to give a detailed description of the thesis work including its instruments.
- Chapter Four presents the proposed geometrical error analysis and implements a mathematical model for analysing and compensating errors aiming to improve machining accuracy.
- Chapter Five presents an empirical model to obtain a clear and appropriate method to perform grinding using the robot. The goal is to have the maximum workpiece quality, minimum machining time and economic efficiency by making a selective adaptation strategy and chosen parameter selection.
- Chapter Six implements the developed grinding method to improve the machining accuracy by compensating errors to improve surface finish.
- Chapter Seven and Eight concludes the work of thesis and presents the main outcomes with future recommendations that may help to improve the work further.

Chapter Two. Literature Review

2.1. Research Motivation

Robotic grinding is considered as an alternative machining towards an efficient and intelligent machining of components due to its flexibility, intelligence and cost efficiency, particularly in comparison with the current mainstream manufacturing modes such as CNC machines. Components such as turbine blades, wind blades and high speed rail body are widely used in aerospace, energy, rail and automotive industries and their manufacturing level presents a core competitive to the manufacturing industry. Researchers have attempted to observe key technologies to develop the relevant machining system. The advances in robotic grinding during the past years aims to solve problems of precision machining in small scale complex surfaces and other emphasizes on the efficient machining of large scale complex surfaces. Therefore, achieving efficient and intelligent grinding of such components that are highly complex poses a serious challenge in the manufacturing industry.

This review of literature aims to present a relevant research in the field of robotic grinding till this date, it presents various applications of successful robotic grinding systems used industries along with a critical and comprehensive review of aspects robotic grinding, focusing on the problems and challenges arising and their impact on the machined workpiece geometry. Strategies and alternative solutions to overcome challenges is also discussed. Finally, repair engineering literature is also discussed presenting methods and previous strategies to observe current key technologies to be able to develop a relevant machining strategy.

2.2. Robotic Grinding Overview, Applications and Challenges

Grinding process is applied to various products that are utilised in both quality and safety-critical environments (Caggiano & Teti, 2013). It is essential for the manufacturing organisation to be able to finish products with the utmost precision. In order to achieve the accuracy required from abrasive processing activities, Computer Numerical Control (CNC) machinery is the traditional manufacturing method used in the current industry. In this technique, a programme is developed to generate a tool path that specifies the trajectory of the cutting tool. These tool paths follow the Cartesian coordinate system and work from parametric data commands allowing the machining procedure (Chiles, et al., 2002) & (Overby, 2010). Geometrical surfaces are widely used in the design of complex geometry products, these

surfaces are normally produced by three or five axis CNC machines using appropriate cutters. Methods of generating tool paths, selection of cutting tools and the determination of parameters such as, scallop height, machining tolerance, tool path interval and interference check are all effective elements for a successful machining process. A multi axis CNC grinding machines have become the mainstream approach for manufacturing such parts. It is a complicated application and has a high cost machining tools, fixed manufacturing modes and complex configuration without integrated machining to measurement function (Chen, 2014).

An alternative to CNC is the use of robots which offers an a large extendable workspace and competitive price that makes them a cost effective solution for machining such components particularly equipped with powerful sensing functions, optimising parameters in real time and multi-sensor feedback information promising cost saving and flexible alternatives for many machining applications. According to the robotic industries association, robotic production constitutes more than 5% robotic sales and was seen a as growth over the next 10 years, Robotic Industries Association (2012). Applications using robots involve pre-machining or welding, finishing, de-burring, polishing and grinding. Robots have the ability of performing machining cycles across three directional planes in linear three dimensional space: X, Y, & Z, in addition to two or three rotational axes as \hat{A} , \hat{B} , and \hat{C} shown in figure 2-1 (Niku, 2001). This rotary axis can tilt the position of the tool in many different ways, which adds flexibility to the robot when dealing with complex geometries. This breaks through the limitations of traditional manufacturing equipment which mainly focuses on movement axis and speed control leading to active control of the equipment on the process. Robot exercises are primarily concerned with the overall surface finish, rather than with the precision that can be achieved by the grinding exercise (Sufian, et al., 2017).

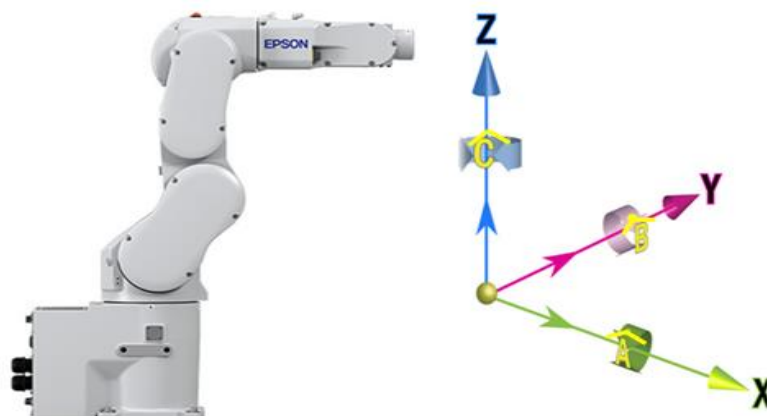


Figure 2 - 1: Six-axis robot coordinate system. Hurco (2017).

2.2.1 Robots and CNC Machines

A significant challenge to the use of an industrial robot for grinding exercises is the accuracy limitations associated with the flexibility of the robot arm, with the potential for further discrepancies incurred by the stiffness and rigidity at each joint (Zhifeng, et al., 2018). As a consequence to the limitations of the robot, the kinematic trajectory of the robot arm is significantly more complex than that of the conventional CNC machinery cutting tool, and for that reason the optimised accuracy and repeatability of the CNC machinery is considered the superior medium to perform the grinding operation on industrial products (Nof, 1999). The table below shows a detailed comparison of CNC machine and industrial robots for machining (Klimchik, et al., 2017).

Table 1: Comparison of CNC machine and industrial robots for machining (Klimchik, et al., 2017)

Indicator	CNC Machine	Industrial Robot
Accuracy	-0.005mm	-0.1-1.0mm
Repeatability	-0.002mm	-0.03-0.3mm
Workspace	Limited	Large
Workspace Extending	Impossible	Possible by adding extra axis
Kinematic architecture	Cartesian	Serial
Number of axis	3 or 5	6+
Kinematics redundancy	None	Yes, 1 DOF at least
Complexity of trajectory	Suitable for 3/5 axis	Any complex geometry
Relation between actuated and operational space	Linear	Non-linear
Mechanical compliance	Relatively High	Relatively Low

Dynamic properties	Moderate, homogenous within workspace	High, homogenous within workspace
Control algorithm	Continues path control	Point-to-Point, Linear and Circular
Programming language	Standard G-code	Manufacturing Specified languages
Manufacturing flexibility	Single or several similar operations	Any type of operation
Price	Competitive for 3 to 5 axes	Competitive for 6 axis

Regardless to such issues and limitations, a large number of effective solutions have been proposed to reduce the stiffness as well as improving accuracy and positional errors in the machining fields. In particular for grinding operations the robots are gradually replacing the multi-axis CNC machines tools and become an alternative. During the past decade, research on robotic grinding have gradually increased and published literatures mainly focus on the feasibility study of the robotic machining (Ren, et al., 2006), As well as modelling machining dynamics (Nahavandi, 2007), position/posture optimization (Gao, et al., 2011), calibration and measurement (Li, 2008), tool path generation (Huang, et al., 2002) , material removal control (Song, et al., 2011) , force control (Mohammed, et al., 2018) and many more. In the past year, researchers have recently published papers that are directly related in robotic machining. For example, Verl et.al (2019) focused on the machining of robots and identified the theoretical foundations related to the static and dynamic stiffness of robot joints and links in milling, forming and polishing machining types. Ji and Wang (2019). focuses on machining of high and low level material removal rate according to their machining properties by introducing the configuration, machining quality and monitoring and compensation Tao et.al (2019). focuses on large complex components with mobile robots, they introduced structure optimization, dynamic modelling and control of mobile robots. Finally, Yuan et.al (2018). reviewed chatter in robotic machining process regarding both regenerative and mode coupling mechanism in the roughing/finishing process.

2.2.2 Robot Grinding Applications

Applications using robots involve pre-machining or welding, finishing, de-burring, polishing and grinding. Most robotic grinding focuses on the surface finish improvement. It was argued that in robot grinding the surface finish is normally better than the three axis CNC machine due to the fact that it can produce better surface roughness because of the robot ability to easily change the tool orientation which makes it more flexible to produce grinding. Applications such as manual robotic belt grinding and disc grinding currently exists for its having high efficiency and good level accuracy control Xiang et.al (2005) . The grinding belt is the cutting tool and consists of coated abrasives attached around a rotating wheels were the workpiece is pushed onto to the contact wheel as shown in figure 2-2 below.

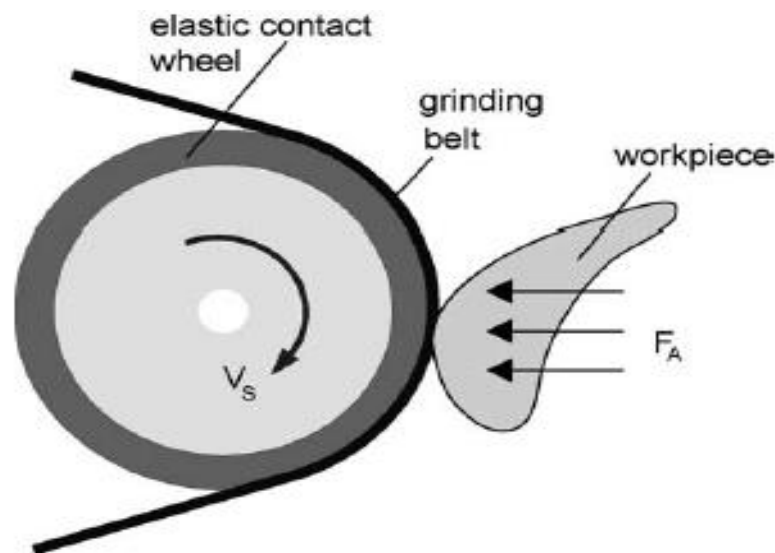


Figure 2 - 2: Belt grinding process Zhang et.al (2005)

For example, turbine blades are mainly finished by manual grinding and multi axis belt grinding, both the curvature and machining path change accordingly and this poses challenge to the precision blades being grinded (Xiao & Huang, 2015). The large randomness of positioning and the uncontrollable contact force between the tool and the workpiece interfere during the manual machining operation creating poor accuracy control. Theoretically, belt grinding can be applied to manufacture geometries like the turbine blade but programming is still a difficult issue particularly for complex geometries.

In another hand, large scale structures such as high speed rail body, energy vehicles, wind turbine blade and core components of power aerospace industry involves multiple grinding

operations, and the quality directly affects the coating performance in later stage and product production cycle (Tao, et al., 2019). Figure 2-3 illustrates the manual grinding operation in large-scale disc grinding with human assisted operation.

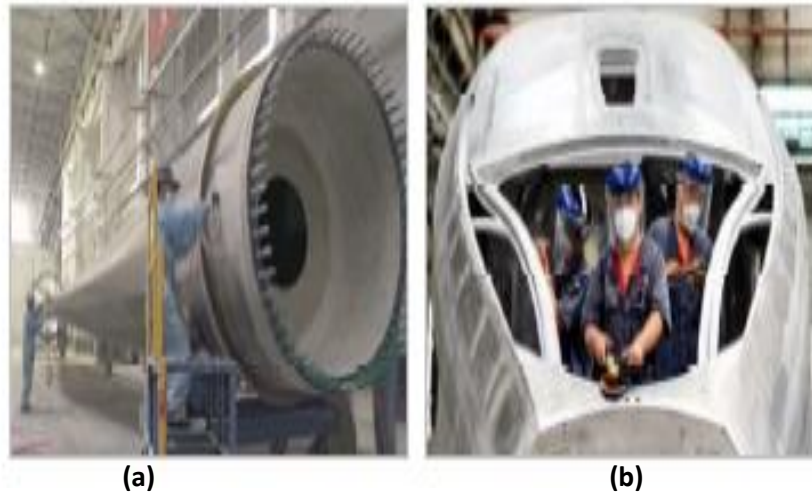


Figure 2 - 3: a) Manual grinding operation large-scale components b) human assisted grinding operation

Robotic grinding system for large-scale components mainly includes robots, guide rails, grinding tools, measurement and total control system. A local measurement and matching analysis of the workpiece is firstly constructed, mapping between the workpiece and the design model is then established and the robot path is than planned. The programming software is used to generate the robot control program for the adaptive machining and process optimization. The total system integrates software and hardware efficiently for central dispatching which greatly reduces the human intervention, and finally can ensure the realization of intelligent grinding of large and complex components.

Finally, Robotic welding is one of the most common applications of industrial robot manipulators. In fact, a huge number of products require robotic welding operations when reaching their assembly process. The welding process is complex and difficult to parameterize in order to monitor and control the robot effectively. Welding in most cases has extremely high temperature concentrated in all zones around the product, these benefit from robot manipulators which is cheaper and has more advantage in terms of cost and quality.



Figure 2 - 4: Robotic welding application

The robot stores the position data and then makes adjustments automatically to the entire weld path before the arc start (Damle & Gadit, 2015) . The time required for welding is very less if we use robot for welding purpose as compared to manual welding of work piece which leads to a cheaper productivity and quality to be increased. Several researches have been undertaken to investigate robotic welding. One of which is Damle & Gadit (2015) were they used a touch sensing technique for robot welding. It works by using the welding electrode, wire, or other sensing pointer to make electrical contact with the part. Latifinaid and Konukseven (2017) also used robot for abrasive grinding. They have developed a force model to predict the normal and tangential forces based on a chip formation energy. The proposed model has been validated by comparing the model outputs with experimentally obtained data which resulted in predicting the surface grinding forces. Huang and Lin (2013) investigated the efficiency of robot machining on a dual machine robot system. In their system, the stock is installed and fixed at the working able and robots were used to machine a 3D part. Similar to Owen et.al (2006) used two robotic arms one as a stock fixture and the other as a machining were it allowed the robot to have more degree of freedom to grinding complex parts.

2.2.3 Robot Grinding Challenges

Robotic grinding produces a significant challenge due to its flexibility and accuracy particularly in comparison with the current mainstream manufacturing methods. The main issue that causes restriction for the practical implementation of robotic grinding is discussed as follows:

Accuracy Control

The Precision concerns in the robotic grinding systems in the manufacturing industry are considered a huge challenge. This is related to measuring the area associated of the workpiece then matches its theory to accurately locate the measured position. The relationship between the measured points and the designed model is crucial to analyse the geometric error of the surface of the component.

The challenge in measuring the accuracy control is that it is difficult to accurately measure the actual position of the robot when scanning the workpiece (Tao, et al., 2019). Also, the significant elements for affecting the favourable rigid transformation may include the local data missing as well as the uneven point compactness. It tends to provide the failure to the traditional algorithm for matching purposes (Xie, et al., 2019). This provides incorrect values and may include the profile errors as well as the allowance distribution problems.

It can be said the designed models as well as the measured points needs to have a direct relationship to achieve the required accuracy & the precision. This is considered to be the key parameter for making the robotic grinding systems perform accurately in the workspace environment. In general, the geometrical accuracy of the machined product mainly depends on the kinematics of the machine, location of workpiece and tool location (Quin, et al., 2006). The geometric errors influence the location and orientation of the location of the workpiece and lead to mis- alignments of the workpiece. Researchers have proposed different methods based on error models, these models focus on the position and posture in relation to the joints of the robot. For example, Xiong et.al (2002) discussed the inner force distribution and load capacity of fixtures as well as the contact forces. Marin and Ferreria (2003) discussed the impact of error on the location of geometry and tolerance of the workpiece.

Compliance Control

Compliance control is the contact state between the workpiece and the tool or in another word the force control of machining. Components such as turbine blades require a high level of geometrical accuracy control. Such research has published work on the control strategies applied in robotic belt grinding and not mobile robots. For example, Chen et.al (2019) and Zhu et.al (2018) proposed a force control algorithm that was implemented in the end effector of the robot to control the contact force which have particularly improved the surface roughness. But In general, the force control is still less in engineering applications compering to CNC

machines, this is mainly due to the difficulties in accurate modelling of robotic dynamics which is linked to the position and orientation of the robot joints. Meanwhile, the existing force and position control in robotic grinding aims to reduce the surface roughness of parts and pays less attention to the accuracy of form and position.

Sensing/Positional Control

When machining such components, it is difficult to obtain information of the without building a relationship between the workpiece and the robot. This machining mode involve multi sensor data combination to allow the robot motion to provide the necessary outputs to avoid any system of error development which is caused due to improper sensor resolution and installation (Kubla & Singule, 2015). Therefore, is necessary to put forward robot motion control strategies which are suitable for collaborative machining and develop collaborative control software to realize the task allocation and interference avoidance.

Vibration & Chatter Control

One of the issues preventing the adaptation of robots for machining process is chatter. Chatter is the vibration of the tool or workpiece due to the revolutions being affected by the cutting force. The effect of stiffness causes vibration in different directions of the robot arm which affects the cutting accuracy. Therefore, relationship between vibration and chatter is related to machining parameters which must be taken into consideration to improve robot accuracy.

Given the fact that the stiffness of a robot arm may cause machining errors, several researchers have developed different methods to compensate it. For example, Zhang and Pan (2006) investigated the effect of chatter in robotic machining by highlighting a control method based on compensations of deflections and adaptive material removal rate. The deflection was based on a matrix theoretical model and the material removal rate was adaptive to the cutting forces. It was reported that the machining accuracy in belt grinding could be improved from 0.9 to 0.3mm. Bisu et.al (2011) used a frequency based method to measure the dynamic response of the robot when cutting at designated points, his method was not directly involved to machining path. Dumas et.al evaluated joint stiffness based on consideration of translational and rotational displacement of the robot end effector at a given force and torque, They concluded that joint stiffness values can be used for motion planning to optimize robot

machining process but results were not validated making it un-reliable to use (Dumas, et al., 2011).

2.3. Robot Grinding Strategies & Alternative Solutions

Challenges obviously produce significant issues to the robotic grinding. To overcome challenges, based on detailed research has been constructed on strategies and alternative solutions that can be conducted to such to solves challenges such as construct measurement, manipulation and machining function for robotic grinding system.

2.3.1 Precision measurement

Repeatability

Repeatability is the ability of a robot to return to the same spot with minor slightest variation whereas accuracy is a measure of the distance error associated with the desired and achieved point. These two factors are interrelated and most commonly used amongst all performance characteristics. Environmental conditions, calibration issues and machine wear may influence the accuracy and repeatability, which may be improved by applying suitable compensation algorithms. Therefore, it is important to determine the repeatability of a robot when considering them for specific applications such as grinding of components.

By conducting academic research into the use of robots for grinding purposes, it can be determined that there is an industry preference for the application of robots in belt grinding exercises, as recorded by Yun and Wang (2011), and corroborated in the works of both Qi et.al (2017) and Wu et.al (2013). For example, in their publication: Accurate robotic belt grinding of workpieces with complex geometries (turbine blades) using relative calibration techniques such as mathematical modelling or CAD systems.

Sun et.al (2009) attempt to develop a methodology to improve the accuracy and of the grinding robot by calibration and force control techniques. in order to reduce the error observed when grinding turbine blades. Through a relative calibration process and force adaptation to maintain homogenous force distribution over the workpiece, the study demonstrates a viable technique of error compensation in reducing the position error from 100 μm to 50 μm .

Brethe et.al (2005) investigated the repeatability of a KUKA industrial robot and the distributions of the angular positions of the joints to show that these distributions can be considered as Gaussian. They computed a repeatability test at different locations within the

workspace of the robot using the experimental angular covariance matrix and the stochastic ellipsoid modelling. A high variability was observed in the measured data and a method of drawing the distribution of the 30sample repeatability index is used to compare the computed and measured repeatability. Riemer and Edan (2000) evaluated the impact of target location on robot repeatability, his experimental results showed a significant statistical difference between repeatability at different work-volume locations. Especially the height of the target point was found to be a major factor determining the repeatability of a point within the workspace.

However, the most common used method of performing repeatability on industrial robots is based on the requirement of ISO 9283:2003 standard which is used to manipulate the performance and related test methods for repeatability. This standard has the scope of conductance of specified tests to develop and verify individual robot specifications, prototype or acceptance testing. The method is used to determine the error in repeatability of robot positioning in order to conduct a series of measurements in the workspace. It is used by robot manufactures and yet it is not highly practical for users' due to the limited information obtained in this manner (Brink, et al., 2004).

The current experiment is designed to evaluate the repeatability of an articulated industrial KUKA robot based in the university laboratory of Liverpool John Moores University (LJMU). The fundamental objective of repeatability test is to observe how well the robot will return to its programmed location at selected positions. Absolute accuracy and repeatability describe the ability of a robot to move to a desired location without any deviation. Therefore, the dynamic ability of the robot is set to follow a dynamic trajectory with little variance. In repeatability, the ability of the robot to move back to the same position and orientation over and over again gives a good accuracy to the robot to precisely move into the desired position on the work place, this concept is shown in figure 2-5 below taking from (Shiakolas, et al., 2002).

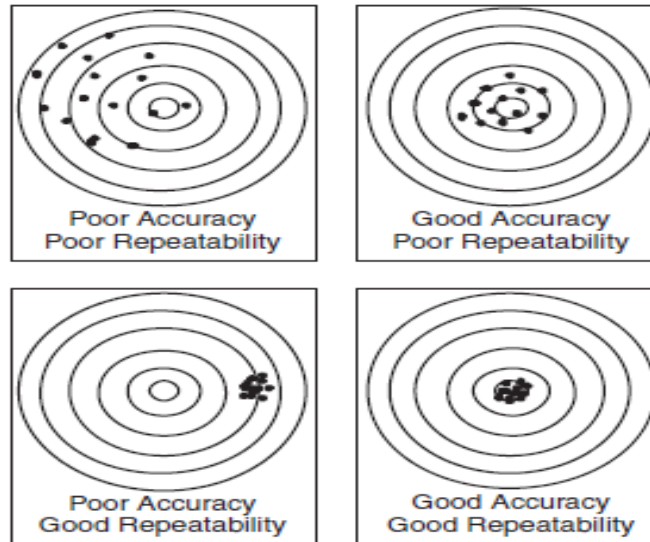


Figure 2 - 5: Accuracy and Repeatability formation (Shiakolas, et al., 2002).

If the primary aim of improving the precision of robotic grinding in this project can be successfully achieved, the recorded data and associated error reduction would provide significant evidence to support the viability of implementing a robotic system for various grinding applications, combining more quality-critical surface finishing practices, and an increased focus on the size and form of generated components. However, statistical evaluation of the literature available indicates that the geometrical error recorded through robotic grinding practices show $50\mu\text{m}$ error level (Cui & and Zhu, 2006). When considering how this influences the methodology in this project, the results determined by experimentation will be evaluated by benchmarking them against the standards found.

Datum Reference

Datum-ing is a procedure used to position and tolerate an object in the robot work envelop to create a reference system for measurement. One of the challenges in robot manufacturing machines tools is the determination of the datum to find a reference point to perform the grinding procedure. Therefore, the traditional method used in many robotic applications to determine the workpiece datum is mainly using CMM (Coordinate measuring machine) touch probe to establish the reference point. Before measuring the surface, it is important to find a reference point to define the location of the workpiece corresponding to the tool as this is crucial in order for the robot program to be activated to perform the grinding procedure. However, probing can be carried out to check that the generated features to be machined are accurate to avoid damaging the component. Two examples of inspection using a probe are

shown in Figure 2-6. The inspection procedure can be in many different ways by in-cycle process or post-cycle process. All techniques may or may not be used depending on the dimension to be measured. However, the types of tools to be used for probing may also be different from one to another too. For example, sensors or dial gauge method can be used to detect the surface of the workpiece to obtain the tool offset.

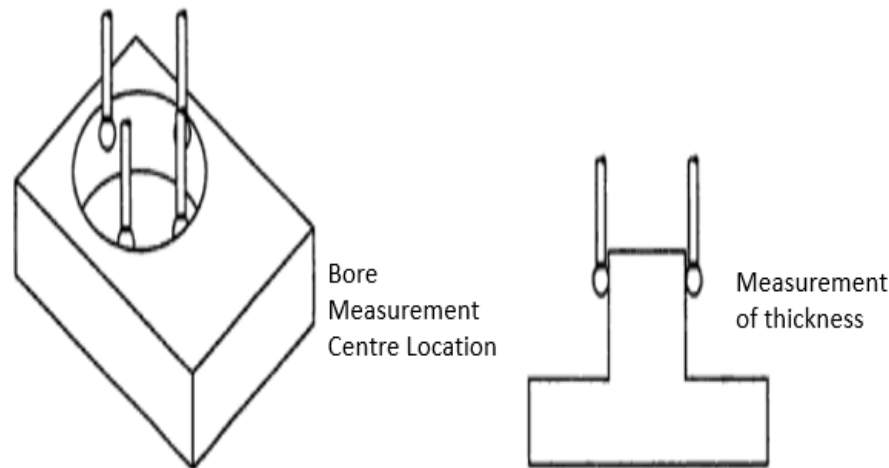


Figure 2 - 6: Probing Examples Nageswara (2006)

Several researchers have approached different methodologies to define a datum location. For example, Batako & Goh (2014) explored a potential use of acoustic emission (AE) to detect workpiece lobes by analysing the acoustic emission signals in the frequency domain whereas Lizarralde et.al (2005). presented a simulation software tool to facilitate centreless grinding machine to achieve stable conditions.

Inaccuracies in the workpiece location lead to errors in the position and orientation of the workpiece and can strongly affect quality of the product. Therefore, the workpiece must be accurately located in a position with respect to the cutting or the measuring device to avoid anomalies affecting the grinding procedure. Researchers have investigated the effect of machining error with the aim of proposing more precise methods for eliminating error effects, which is a key for controlling the robot to perform machining. In early research stages, Choudhuri and DeMeter (1999) presented a model that illustrates the datum error to the geometry locator. The proposed model is limited to dimensional profile tolerances in the machined workpiece surface. As development occurred in the 2000s, Qin et.al (2006) presented a method that enables to characterise the effect of locating the error based on orientation and

position of the workpiece. Jin & Jiyong (2007) developed a measurement algorithm using three different coordinate systems to find the closest point to the workpiece. The method uses datum point data in different coordinates to calculate the rotation and translation matrix and transform measurement data to coordinate system that's applied in the robot being used. Chaiprapat and Rujikietgumjorn (2008) developed a math model to predict the geometrical variation of the workpiece surface and datum features are given workpiece.

Use of Acoustic Emission Sensing

Acoustic emission is a phenomenon defined as the energy of stress waves by materials that occur in internal structures in grinding. It is an intelligent manufacturing method used to maintain machining accuracy and monitoring the cutting state of the machined product. In grinding operation, Acoustic Emission signals are released due to applied stress and strain. These signals can be crucial in understanding and monitoring the grinding operation (Kim, et al., 2001). Therefore, when using the cutting tool as a probe acoustic emission can be used to give feedback to the system to monitor and control the detection points. These acoustic emission rays are much sensitive and have far better responsive rate to the control measure applied due to its high frequency range (Ha, et al., 2004).

Materials normally possess elasticity and become strained under external forces causing the creation of forces under elastic deformation. If the material exceeded fracture it may cause the material to break under certain deformation. This will emit acoustic emission signals were the waves will propagate through the material releasing elastic energy by the AE sensor. Moon et.al (2006) has looked at the effect of cutting force by different feed and depth of cut to look at how the waveform behave under AE signals. He mentioned forces are affected by the material removal which is a result of the depth of cut, feed rate and the cutting speed in grinding. The interaction between the grinding tool and the workpiece can easily define the result of the grinding process. Many researchers have investigated on different parameters of grinding based on acoustic emission and how they relate with the grinding results.

Tool structure and chatter characteristics have been found to have significant effect over the particular grinding process. These two characteristics with the help of acoustic emission can help to optimize the grinding cycle (Maksoud & Atia, 2007). The associated vibrations with the tool and workpiece increase gradually with later resulting in instability. Researchers have suggested seven traditional steps to follow in order to avoid instability of vibration. These

includes dressing the wheel, decreasing feed rate, replacing grinding wheel with larger one, improving the stiffness of wheel, reducing depth of cut, using grinding fluid and reducing the process speed. These steps can help to recover from wheel regenerative chatter. In work regenerative chatter the waves generated through the grinding process will make the grinding surface unstable. These vibrations increase based on continuous wave generation will result in non-acceptable grinding results. Acoustic emission is the most suitable technique to identify roundness error and chatter characteristics (Quintana & Ciuranab, 2011).

However, no research is currently available for using the cutter probe along whiles using the AE sensor for monitoring the operation to define the datum. Therefore, in this thesis work this initiative method is considered as one way to assist to define the datum reference of the workpiece.

2.3.2 Tool path planning

The trajectory tool path planning for robotic machining is based on the relationship of tool location and workpiece interface. Modelling of the tool path data exists in CAD/CAM software packages which lacks the consideration of robotic machining causing low machining accuracy. Compared with CNC machining, very little literature is published on robot path planning can be found. It is true that there is some similarity between CNC path planning and robot machining path, but the difference is substantial. For example, the impact of stiffness on robot machining path planning is significant and has much smaller impact on CNC path planning (Chen & Dong, 2013).

Past research on robotic machining has mainly focused on the influence of the dynamics on the machining accuracy and efficiency. Dumas et.al (2011) valuated joint stiffness values that can be used for motion planning and optimise machining. Liu et.al (2013) proposed a time optimal planning method for robot manipulators and obtained smooth tracking performance. Wang et.al (2018) looked at the adjusting the machining parameters and changing the robot posture. Xiao et.al (2011) proposed a robot trajectory method based on cutter location data generated by CAD/CAM software when doing inverse kinematics to avoid singular configurations and joint limits.

However, for robotic path planning most of the existing literature are based on offline programming of CAD model or analysis of dynamics in machining, while less consideration is given to the situation of high complexity and randomness of robot tool path planning. The

planning of robotic grinding path starts from the initial point to the target point should be complex free and therefore the tool path planning method needs to adapt to the shape and size uncertainty of the workpiece.

2.3.3 Process Parameter Optimisation

One way to improve the surface integrity using the robot to machine a workpiece is by implementing process parameter optimization. Robot arms are normally flexible with good accessibility when used for machining. Accuracy of part making is actually not the main concern, in fact it is the stiffness of the robot that presents the bigger problem because varies significantly in different directions. For example, the static stiffness of robot machining system has reported to be $83.65\mu\text{m/N}$ in X-direction, $20.35\mu\text{m/N}$ and $68.76\mu\text{m/N}$ in the Z-direction (Chen & Fenghua, 2013).

Despite differences of stiffness in different directions, machine process optimization have been proposed by researchers to improve the machining accuracy. For example, El.Mansori et.al (2007). analysed the effects of cycle time and frequency oscillation in belt grinding to improve the surface finish on a hardened steel. Zaghbani et.al (2011) have collected the cutting forces signals and vibrations in order to find a reliable dynamic stability machining with respect to spindle speed. Rech et.al (2008) used finite element method to investigate the residual stresses generated by belt finishing grinding, results have demonstrated that the surface integrity had significantly improved by the induction of strong compressive residual stresses on the surface of the hardened steel. Zhao et.al (2014) investigated the effects of grain sizes, contact force, linear velocity and feed rate on the surface roughness in abrasive belt grinding of aviation blades by analysing the response of surface.

However, material removal rate is one key indicator for measuring the profile accuracy in robotic grinding. Like any grinding operations, the material removal rate is influenced by the process parameters, geometric information and material properties. Researchers have investigated the effect of material removals as force distributions in the contact zone of the workpiece. For example, Huang et.al (2002) investigated the effects of contact force between the tool and workpiece during robotic belt grinding of a turbine vane, they have found that the material removal has been increased with the increase of the contact load and belt speed with less feed rate applied. Xia et.al (2019) regarded the material removals as the force distribution in contact in the contact area and developed an algorithm to define the real material removal rate. Due to the complicated material removal operation involving ploughing, cutting,

modelling the material removal depth of workpiece surface could be an alternative to calculate the material removal rate. An articulated robot has a diverse stiffness within its working envelope, therefore it will be best for a robot to perform machining within its possible range of best stiffness. By selecting the most suitable pose of the robot with respect to the workpiece, the best process parameter can be selected and a better surface finish can be reached.

2.3.4 Machine Error Compensation

System stiffness including tool, workpiece and robot is considered to be the cause of deviation of machining accuracy during robotic grinding. The machine error should be controlled in order to extend robot machining to more applications. However, due to the limited robot stiffness machining feed rate, depth of cut, and cutter diameter must be kept at small values because it limits the material removal rate or machining efficiency. Therefore, some machining strategies have been developed focusing on different aspects to improve the machining error in grinding. For example, Latifinavid & Konukseven (2017) derived a grinding force model and real-time tool deflection algorithm to predict the grinding forces. The effect of elastic deformation between the tool and workpiece have been investigated by establishing the average contact force to evaluate the coefficient of friction and abrasive wear. In order to control the error created by the abrasive wear, a feasible way is to reduce the volume of abrasive wear choosing the correct tool size.

More research focuses on the characterization of the grinding tools to fully understand the grinding process and to increase the machining accuracy. Tahvilian et.al (2015) measured different wheel grain protrusion under different robotic grinding conditions. The wheel is measured using a laser microscope and his results indicated that sharper edges exist on the wheel surfaces with a higher depth of cut. Finally, it is important to consider process variables when machining to decrease machining error and to ensure the robot exhibits a continuous process with minimum error deviation according to the published paper of International Organization for Standardisation in (1998).

2.4. Digitizing and Repair Engineering

Digitizing is a process of converting information into a digital format. When measuring and inspecting mechanical components that require re-manufacturing a skilled technical person uses mechanical gauges and template to take dimensions of worn parts and inspect its physique. This process has become not efficient and accurate anymore because of the implementation of

the new modern digitizing devices such as CMM and laser/optical scanning measurement systems. The new measurement methods smoothen the measurement and inspection of parts in order to achieve the best outcome as possible.

However, there are two types of measurement data techniques a contact measurement and a non-contact measurement. A contact measurement is type were single points is take from the surface of the geometry using tactile sensors such as gauges and probes. According to the Exact Metrology website published in (2012) a non-contact measurement use 3D dimensional sensing devices to capture the geometry such as laser and optical scanner & X-rays. The touch probe is a common device used in a contact measurement and can be manually operated by an operator or it may be controlled by a computer. Measurements are defined by a probe that contacts points on workpiece, depending on the geometry features the points can be measured with a range of accessories in terms of probe types and shapes. Laser and optical scanner provides accurate scans with detailed resolution of the object. When a laser line project onto the surface of the object, the distorted laser image is acquired through a device which captures the object full surface geometry and creating a polygon mesh were a large quantity of point data is collected from the surface of the geometry.

2.4.1 Digitizing devices and methods

According to many industrial applications, it is obvious that the CMM machine with the touch probe is the most accurate device to measure objects with widely varying size and geometric configuration. It is ideal to measure features such as diameter of a hole, radius of an arc and distances between edges. Laser optical scanner is considered to be flexible and portable to measure complex geometries with free form surfaces were it digitally converts the images as two-dimensional digital files and send them to the computer. With optical scanners, the geometry can be editable into a design format allowing you to get full details and giving you freedom to examine the shape before remanufacturing. If CMM is to be used for reverse engineering and inspection purposes for parts that are damaged of worn it will take extremely a long time to digitize the surface than a laser of optical scanner. Therefore, Benefits and drawbacks of both techniques are as follows:

Table 2: Benefits and Drawbacks

Touch Probe		Optical Sensor	
Benefits	Drawbacks	Benefits	Drawbacks
High Precision	The touch probes are less portable	Provides good accuracy of geometry	Cannot be used to scan shiny surfaces
High Accuracy	Measuring machines are very costly	Cheap in cost	Very sensitive
Robustness against external force and error accumulation.	If the operating software fails, it is difficult to restart the entire system	Provides excellent depth resolution to measure detailed features such as curves and cracks.	Slow when measuring objects with many complex details

2.4.2 Repair Engineering

Repair or reverse engineering is very important in the design and manufacturing application area and it is generally applied in many fields such as manufacturing engineering, software engineering, chemical engineering and many more. Repair Engineering is a process in which a model is constructed using a digitized data to study the physical dimensions of geometry. This technology defines a tool path where input parameters are entered into the software interactively for simplicity. In applications such as aerospace, automotive, marine and medicine it is difficult to construct a CAD model from an existing product that has a free form surface. The process of reverse engineering is usually subdivided into five stages. 1) Digitizing of the part, 2) Data capturing, 3) Processing data measurement & Surface approximation using CAD modelling and 4) NC programming for part manufacturing which can be shown in figure 2-7 below.

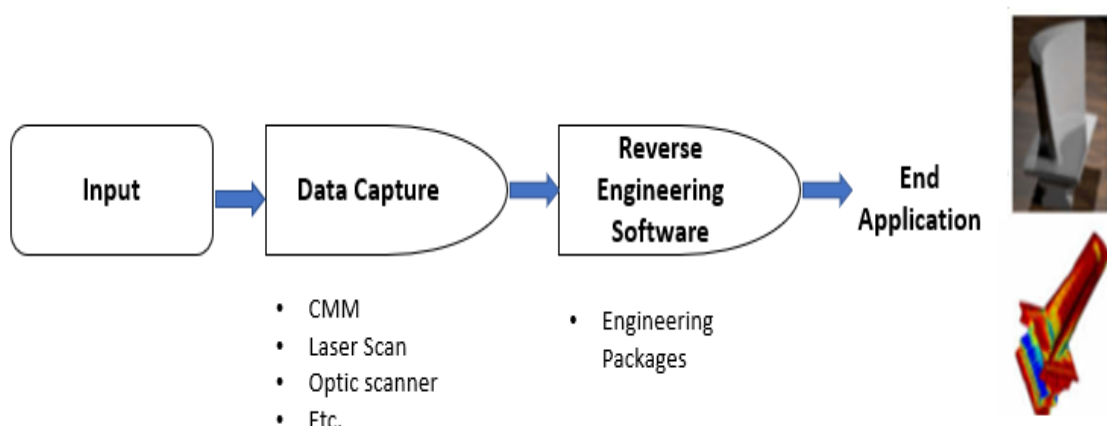


Figure 2 - 7: Reverse Engineering Process Bagci (2009)

Reverse engineering significantly reduces the product development cycle, inspection and deviation analysis of a digitized model. An example of implementing reverse engineering on complex geometries is presented by Dix (2004), where he developed an adaptive machining solution for repairing blades in order to achieve accuracy and repeatability. He used a digitizing measurement technique to collect 3D points from the surface of the blade, these points are collected using a touch probe attached to a CNC machine and then processed to create the blade curves for tool path generation in order to remove excessive weld from the surface of the blade.

As with Huffman (2013), he developed a laser powder welding machine which integrates with a 2D vision system for blade repair. The vision system locates the part and adjusts it so that it generates a CNC program through the software attached to carry out the welding process. Once the image is captured by the vision system, the software can rapidly provide a profile for the geometry in the x and y coordinates as well as tool paths and welding parameters for welding process. Due to the limitation of vision system it is difficult for the machine to be used for complex geometry components. Bagci (2009) established the possibilities of using reverse engineering methodologies in three different samples a cam, turbine blade and a bust. The method includes digitizing the surfaces using CMM touch probes, processing the measurement data to create a 3D model of the part and tool path generation based on the continuity analysis Zhang (2003). selected a core die of the inlet of a diesel engine as an example of reverse engineering from digitization, CAD model reconstruction to NC machining. In his work the measurement data is obtained by scanning the physical part using a three-dimensional 5mm diameter CMM probe to collect data point from the surface of the shape, the number of measurement points is automatically determined and automatically according to the curvature change on the surface of the object. After that, the output results of the CMM measurement points are transformed into an x-y-z format were it is used directly for the creation of a CAD model. The CAD model is then created directly from the measurement data of the CMM machine using a free form feature modelling. In this way, the construction curves are generated from the measurement data and then the surface can be created through mesh generated. The surface generated through shading is to check the shape continuity and smoothness of the surface to ensure a minimum error. Finally, after the CAD model is generated the NC machining process can be planned and tool path can be generated by machining codes to start the manufacturing process. Figure 2-8 below shows the results obtained by Zhang (2003) of NC measurement and surface reconstruction of the core die of the inlet of the diesel engine.

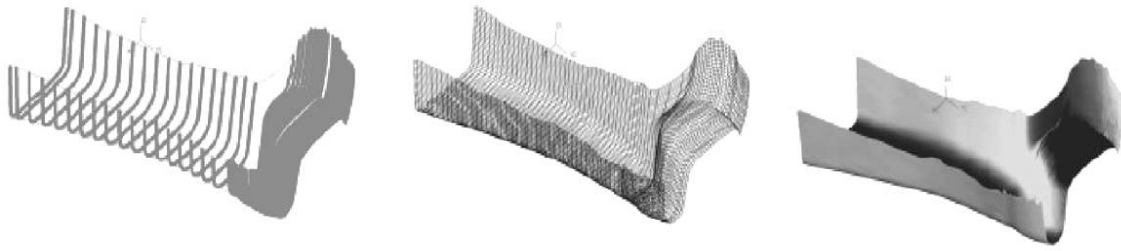


Figure 2 - 8: Surface reconstruction and NC measurement of the core die Zhang (2003)

Repair engineering is an efficient approach to significantly reduce the product cycle and ensure product quality in the design and manufacture of surfaces. However, the aerospace and automotive industry is a highly competitive and is difficult engineering area. Each component needs more attention during its production process. Shape, geometry, material, manufacturing method, working conditions of each part are all factors for performance. Design changes on the parts to improve functionality and efficiency as well as manufacturing difficulties and repairing requirements of these components might be a great reason for choosing reverse engineering. Wu et.al (2013) reviewed several algorithms based on geometric reconstruction for gas turbine blades. The paper includes different types of algorithms for repairing solutions of damaged blades. The process of repair included a five stage process: pre repair inspection, identification, surface reconstruction of defected surface, welding, milling and grinding. They concluded that the available reconstructing approaches are not efficient, so future work is required in this field. Finally, depending on the used digitizing method and measurement process researchers have aimed to improve existing repair techniques by applying it to different products and engineering areas.

2.5. Summary, Gaps and Challenges

Based on the research framework and outcomes of the initial literature key gaps have been identified as follows;

- 1) Due to time consuming and cost of manufacturing there is a substantial demand to repair shapes using robots
- 2) There is no dedicated strategy developed to make robot more accurate and robust to perform the grinding.
- 3) Aiming to improve accuracy of robot, there is no a model developed for analysing and compensating machining errors in relation to geometrical shape.

- 4) Currently there is no dedicated method to use the probe as the cutting tool so that positional error between the tool and sensor can be eliminated. Therefore, a practical method will be developed to improve the machining accuracy by compensating the geometrical error to achieve smooth surface by tolerating the depth of cut.

Chapter Three. Methodology & Experiment

Instrumentation

3.1. Methodology

This chapter describes the methodology and the experimental set up of this thesis. It gives a detailed description of the steps and tools used in the experimental environment. The work will comprise developing a methodology for component repair and error compensation in robotic grinding by preceding the following steps:

1. Geometric Error Analyses

This method aims to improve the accuracy of the robot. For that to be done, a repeatability test is firstly constructed to evaluate the uncertainty of the data collected throughout three different stages 1) Mechanical, this includes using a dial gauge method 2) Electrical, this includes using an electric circuit that is built to communicate with the robot controller 3) Acoustic emission is used to monitor the movement of the robot and modifies the trajectories accordingly. Each stage will define the level of error relative to its response. After that, a mathematical model based on the best repeatability is constructed to define a general relationship between the workpiece and the cutting tool for error compensation and to predict the datum reference point. The datum is then modified accordingly to the robot position in order to provide a reliable and accurate grinding movement.

2. System Compliance Model

This method is designed to obtain a clear a characteristics of grinding system to achieve a best workpiece quality, minimum machining time and economic efficiency by making a selective adaptation strategy and parameter selection. In this part, the proposed work will give a clear insight to build up a reliable model to eliminate the residual error when performing abrasive grinding using the robot.

3. Grinding Strategy Repair

This method demonstrates the developed grinding strategy to improve the machining accuracy by compensating all sorts of error to achieve smooth surface finish when performing

robotic grinding in order to further improve the grinding performance capability, this part provides a strategy repair that can improve the surface quality of the component. However, despite to the obvious advantages that the robot has such as production flexibility, dexterity and functional integration, there are still improvement margin in machining accuracy and surface quality by robotic grinding compared to the CNC machine tools.

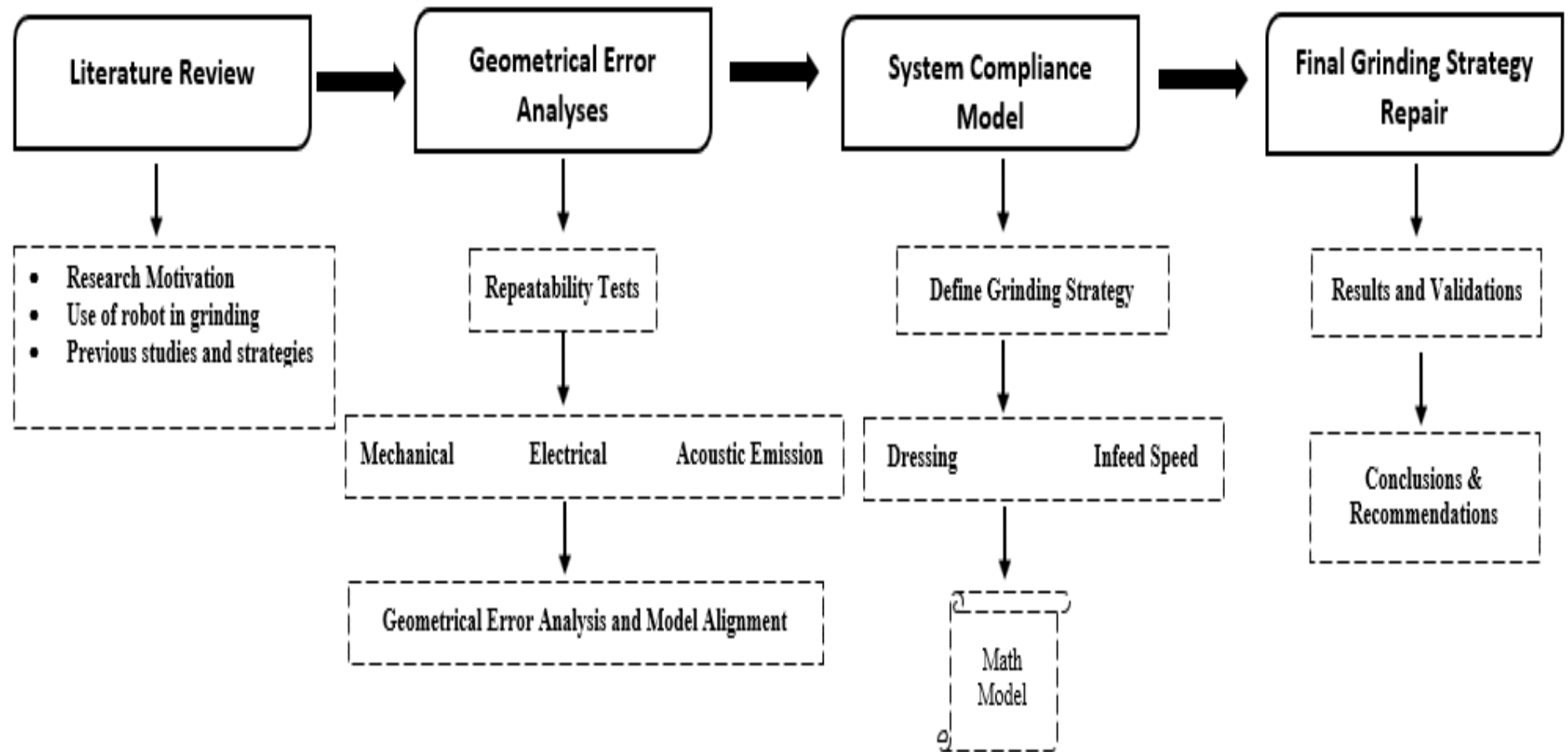
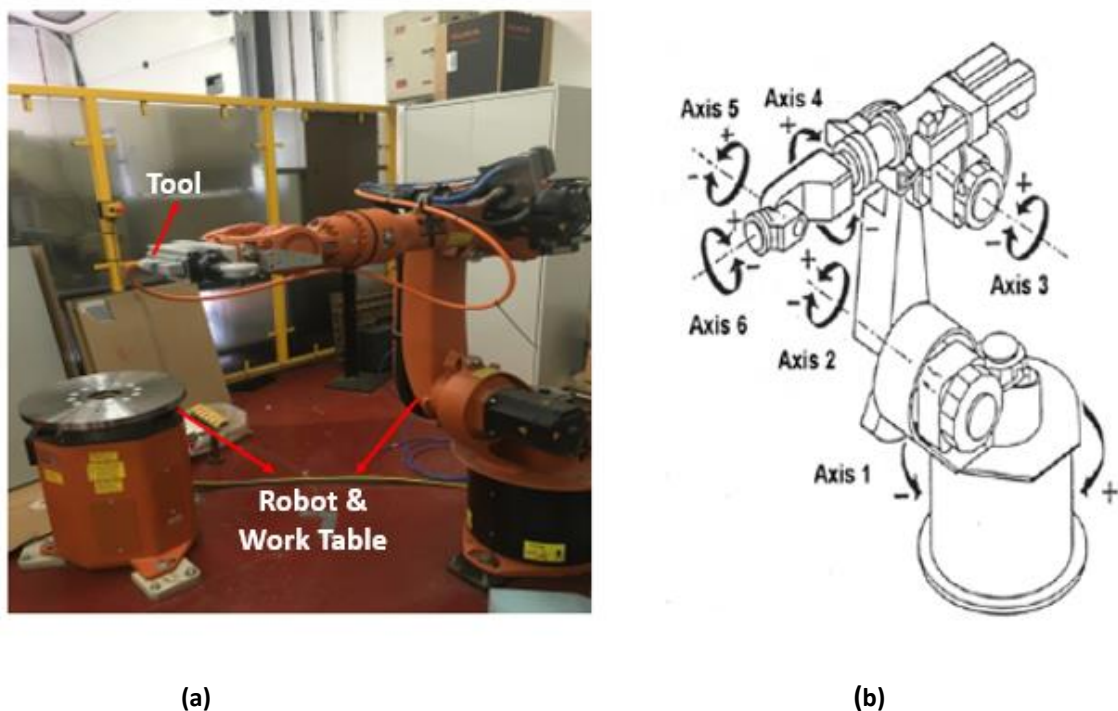


Figure 3-1: Methodology Flow Chart

3.2. Experimental Instruments

A KUKA (KR-16) robot with a six degree of freedom located in the department of engineering workshop have been used in this project. The KR-16 has the following specifications reported by the KUKA website: a payload capacity of 16kg, a weight of 235kg, and maximum reach of 1610mm. The robot is mounted in upright position with a large work space and load capacity which allows KR-16 to be utilized for a wide variety of applications including material handling, assembly, and material removal. The Robot used in this study is shown in figure 3-2 below.



(a) (b)
Figure 3-2: a) KR 16 view of Robot b) Robot kinematic joint axis

Throughout the planning phase of the experiment some control variables were determined to analyse the repeatability of the robot. These variables were chosen based on the working knowledge of the robots by the faculty. The control variables varied in the experiment are presented in the table below which lists related information considered for each factor. Robot speed, payload, work envelope location, motion type and the presence of points to create the desired path are all shown in Table 3 below.

Table 3: Robot Control Variables

Control Variable	Normal Range	Measurement Accuracy	Setting
Speed	0 – 2 m/s	N/A	1 m/s
Payload	0 – 16 kg	Kg	None
Workspace location	0 – 1610mm	variable	4 points within workspace
Motion type	Discrete	Variable	Point to point, Linear
Intermediate points	More than one point to create the desired path	Store random points than span the entire workspace	Store couple of points to target location

3.2.1 Robot control panel

To be able to make the robot move and create paths, a control panel is used. The control panel is the heart of the system which is designed to function the robot to transfer information and communicate with external systems or advanced tasks.

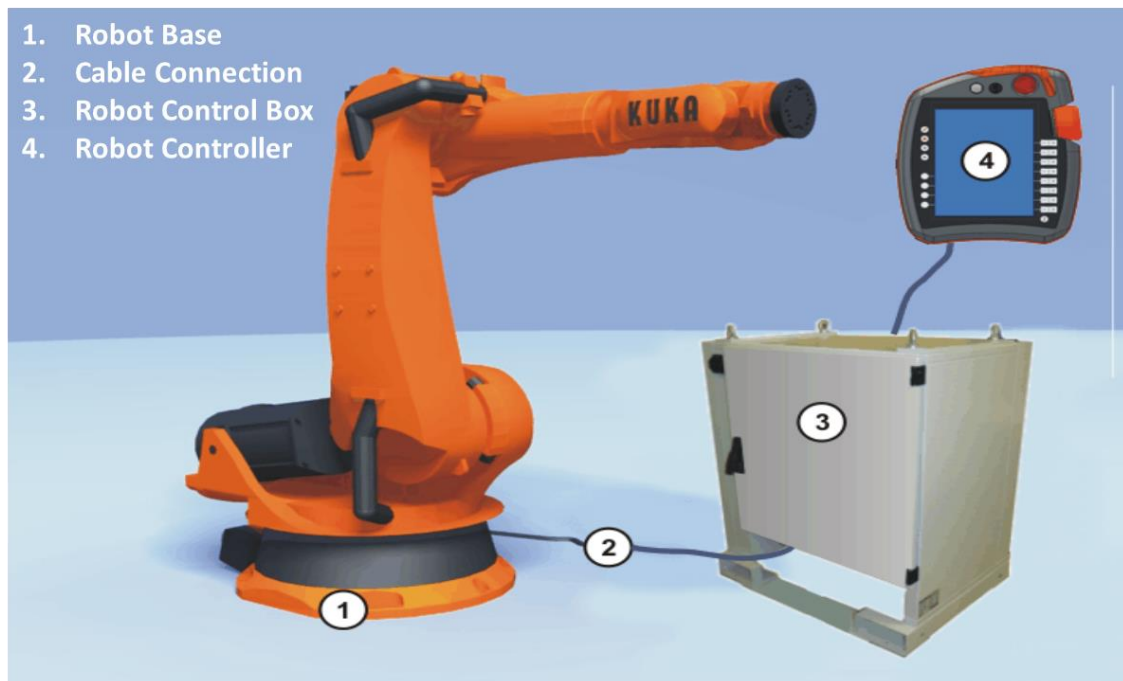


Figure 3-3: Robot Control Panel Kuka (2010)

3.2.2 Robot Coordinate system

The definition of coordinate system is based on where reference point is to be considered for measurement in programming. For example, The Base coordinate system has its reference point on the workpiece whereas tool coordinate system has a reference point at the tool centre point (TCP). Figure 3-4 below shows the type of existing coordinate systems

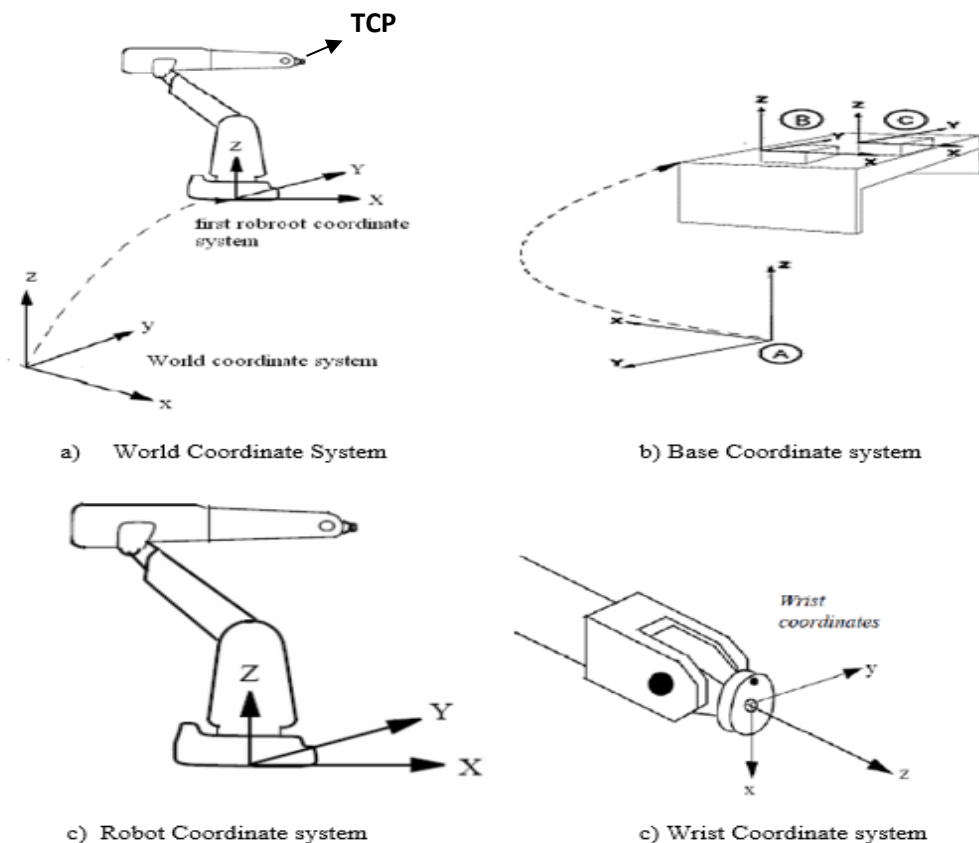


Figure 3-4: Types of coordinate systems (Gadit & Damle, 2015)

Motion specification

There are three types of motion that can be used for programming trajectory of path for grinding. These are point-to-point motion (PTP), linear motion (LIN) and Circular motion (CIRC). The LIN and CIRC motion are termed as continuous path motions. In PTP motion, the robot guides the TCP along the fastest path to the end point. As the motions of the robot axes are rotational, curved paths can be executed faster than straight paths. The exact path of the motion cannot be predicted. Therefore, the LIN motion is best used because the robot guides the TCP at a defined velocity along a straight path to the end point.

Tool calibration

The tool calibration is the determination of the centre point of the tool with reference to flange position that is termed as TCP. In tool calibration, the user assign Cartesian coordinate system to the tool mounted on the flange. The data saved are Origin of the tool (X, Y, Z) and orientation of the tool (A, B, C) with reference to the workpiece position. The XYZ 4-point method and XYZ reference method are commonly used for finding the origin of the tool and ABC world method is used to find the orientation.

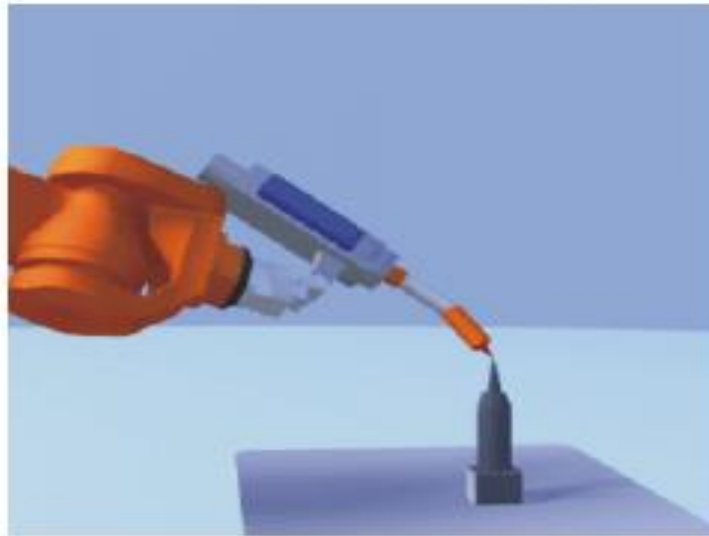


Figure 3-5: Tool calibration layout Kuka (2010)

Base calibration

The Base calibration is used for finding the reference point on the workpiece from which the other point coordinate data will be saved. In Base coordinate, user mainly assigns Cartesian coordinate system to the base or workpiece which will be used for grinding. The most common method for base calibration is 3-point method and Indirect method which includes manual implementation of coordinates. This is achieved by manipulating the robot trajectory to move to the origin, and two further points, of a new base position for the operation as shown in figure 3-6 below. To ensure the robot remained within the surface of the block, the robot arm is moved

to the datum point at the corner of the block. Then, subsequently moved across in the X-axis in the linear axial direction and in the Y-axis.

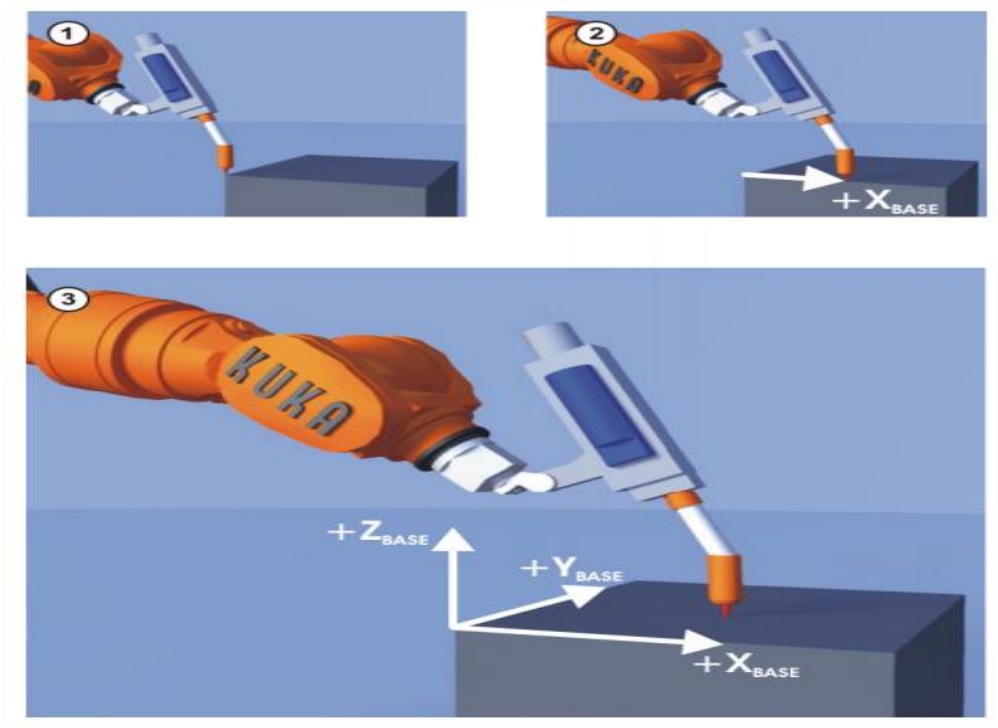


Figure 3-6: Base Calibration Kuka (2010)

3.2.3 Electric Circuit

An electric circuit is constructed and connected to the robot control box to be able to detect the points on the workpiece so that electrical repeatability can be performed. Using an electric circuit allows the robot to communicate with the user so that when the robot tool tip approaches the workpiece it triggers the circuit and send feedback to the controller telling the user contact point is triggered and registered. The schematic diagram below illustrates the simple electric circuit connection.

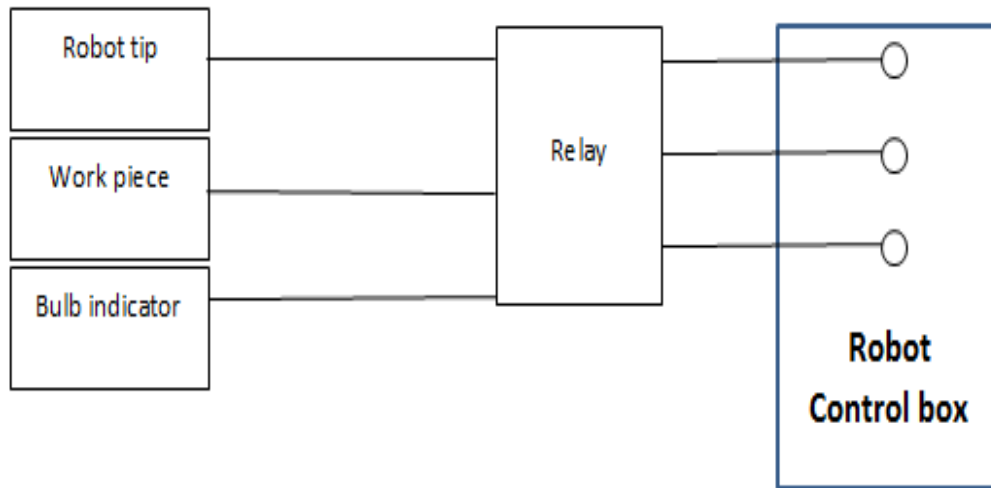


Figure 3-7: Electric circuit Connection

The electric circuit is manually constructed throughout the experimental stage in order to communicate with the robot as the tool engages with workpiece. This increases the accuracy of detection when performing repeatability as its crucial not to damage the component before error modelling for reconstruction and grinding. Therefore, the sensor is built to communicate with the robot when the tip tool contacts the workpiece. The way this works is by integrating the electric circuit with the robot control box, which triggers the input sensor in the robot to visualize the engagement coordinate points. If no detection occurs, the sensor does not trigger and contact must occur between the robot tool and workpiece. Figure 3-8 illustrates a schematic diagram showing this procedure.

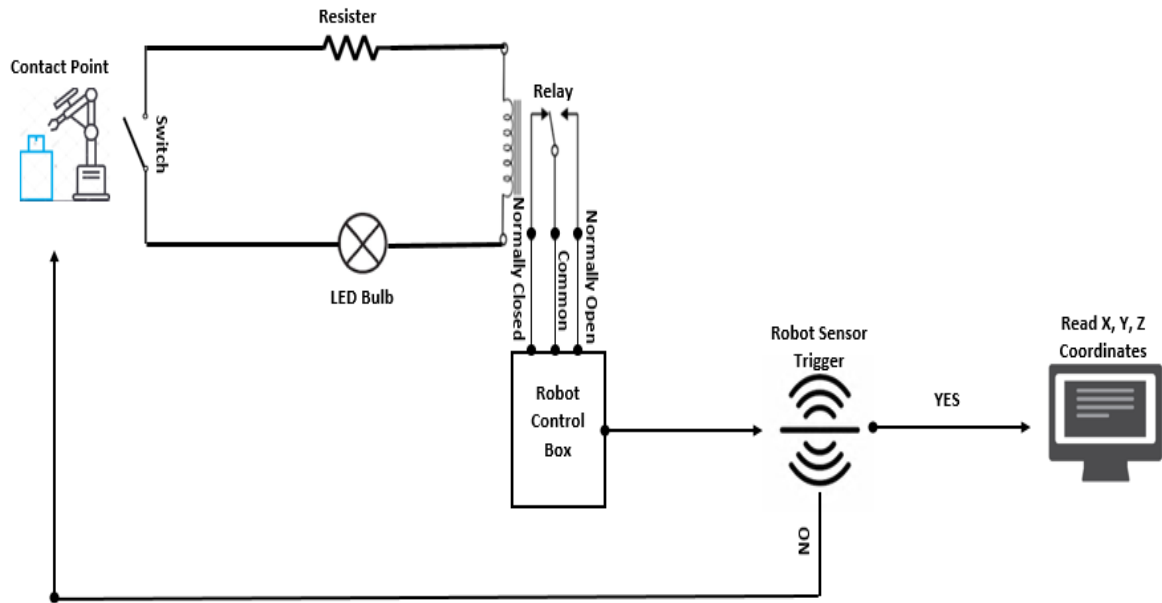


Figure 3-8: Electric Circuit Diagram

Component Function:

- **LED Bulb:** To provide extra indication when detecting the workpiece
- **Relay:** This is used as a switch to control the circuit when the probe come into contact with the workpiece
- **Robot Control Box:** To integrate the external circuit connection to the robot brain
- **Resistor:** To resist current flow in the circuit
- **Sensor:** To indicate the touch contact to allow reading of coordinates

3.2.4 Data accusation log

Data acquisition is a monitoring system used to gives signals such as voltage to give an indication when tool comes into contact with workpiece. The data log is connected to the acoustic emission through electric circuit connected to the robot control box to give signals for so that measurements can be saved once detected.



Figure 3-9: SBC Balance System Model SB-5500

3.2.5 Workpiece

A low carbon steel workpiece component used to in the experiment of this project. Clamps and magnets are used to keep the work piece in place to give a better grip when using the robot to perform grinding. It is important to hold the workpiece in place to avoid any disruption to detecting the component.

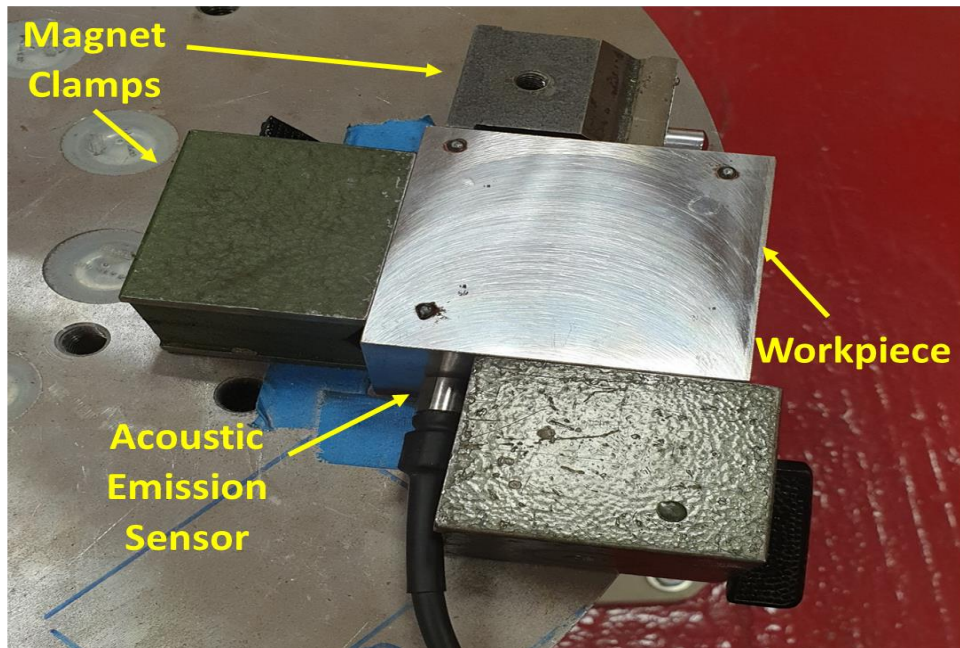


Figure 3-10: Workpiece, Clamps and AE sensor

3.2.6 Single Point Diamond Dresser

A 90-degree diamond dresser is used to dress the grinding wheel after each stage of grinding. The dresser is used to attain the profile accuracy of the grinding tool to perform the grinding, this is done by controlling the robot tool sphere to operate in a semi-circle motion aligned to 180° to the dresser.

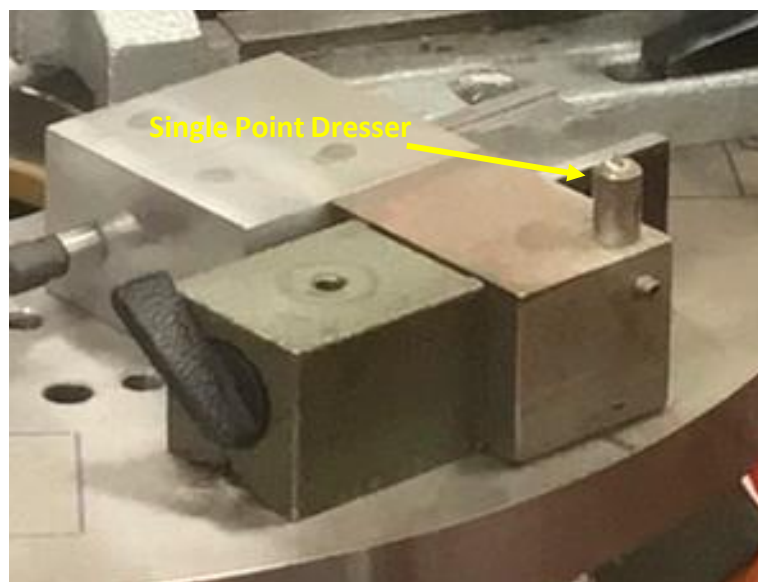


Figure 3-11: Single Point Diamond Dresser

3.2.7 Grinding Tool

A sphere-shaped grinding wheel made out of Aluminium oxide is used as a robot tool in this project. This tool has the ability to stay sharp with minimal material removal and is its abrasives is usually chosen for grinding carbon steel, alloy steel, high speed steel, annealed malleable iron, wrought iron, and bronzes and similar metals.



Figure 3-12: Grinding Wheel

3.2.8 Surface Measurement Machine

A surface measurement machine is used to measure the pockets of the geometry by sensing discrete points on the surface of the object with a probe. The probe is manually controlled by the operator to specify the reference position to allow measurement of the surface. The machine has an accuracy level of less than $3.3\mu\text{m}$ according to the manufacturer website Hobson (2016).

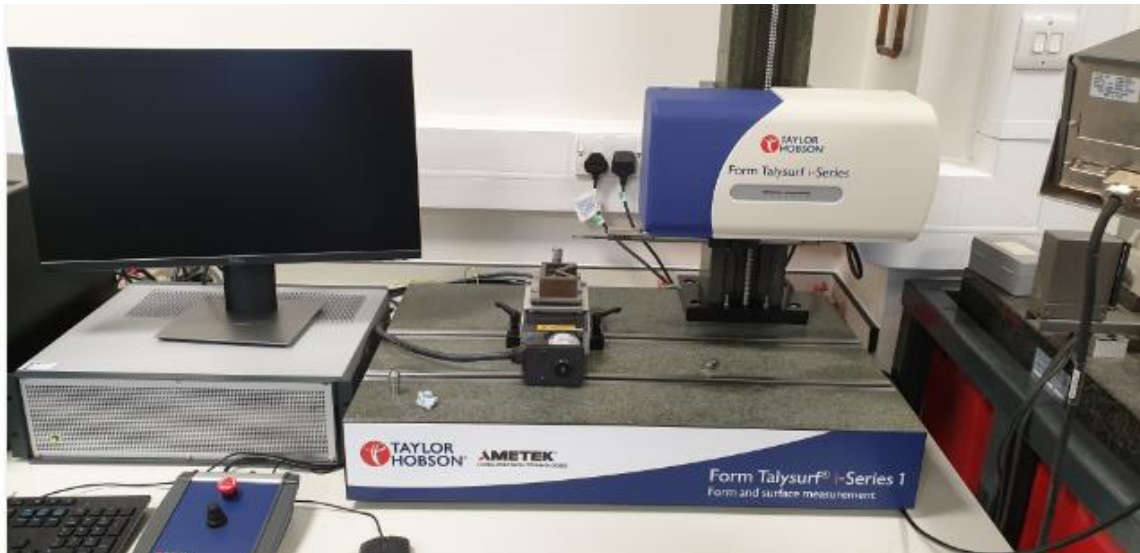


Figure 3-13: i-Series Talysurf Surface Machine

3.2.9 Bruker machine (Microscope)

A surface roughness microscope (Bruker) has been used in this experiment to verify the feasibility of the depth of cut. The machine is designed to measure spots sizes down to $100\mu\text{m}$ level according to its specifications. The machine creates a profile that is connected to the computer software to produce the required outcome results



Figure 3-14: Bruker Machine

3.2.10 3D Scanner

The scanner function is to capture the structure of the workpiece in 3D form of millions of point. The resulting data is called point cloud and is captured in real time. The 3D scanner is used to scan the weld material added onto the workpiece in order to create point cloud data of the component so that it can be implemented in the robot Mastercam software to design the tool path required to carry out the grinding process.



Figure 3-15: Romer 3D scanner

Chapter Four. Geometrical Error Analysis

Aiming to improve accuracy, this chapter illustrates a geometrical error analysis to visualize the performance by repeatability as well as developing a mathematical model for analysing and compensating machining errors in relation to position and system deflection. At first, repeatability is crucial in order to visualize how well the robot responds to its programmed position in defining a workpiece datum in the robot system. After that, a datum setting method is established to assess the datum alignment of the workpiece with the robot tool to support the process monitoring and control strategy to provide a reliable and accurate grinding movement. Based on repeatability measurements of the relative position between workpiece and robot datum a mathematical model is developed to predict the datum reference point and then can be modified accordingly to the robot tool position.

However, a set of experiments is performed with three different methods, (1) Mechanical dial gauge, (2) Electrical circuit probe, (3) Acoustic Emission Sensing to determine the best repeatability accuracy and establishing the geometrical relationship between reference datum and probe point. The accuracy level of datum is assessed based on the repeatability of defined measuring points and a mathematical model is constructed and developed based on the collected data and transformed to the coordinate system.

4.1. Repeatability Tests

Focusing on prober location and error, repeatability test is firstly preformed to see how well robot responds to the programmed positions and detection accuracy. The procedure of detecting the contact points on workpiece is shown in figure 4-1. The variation of the contact point coordinates can represent the repeatability of the robot measured by each method. With the most suitable probing measuring method, a mathematical model is constructed and the accuracy level of datum is assessed based on the repeatability and defined measurement.

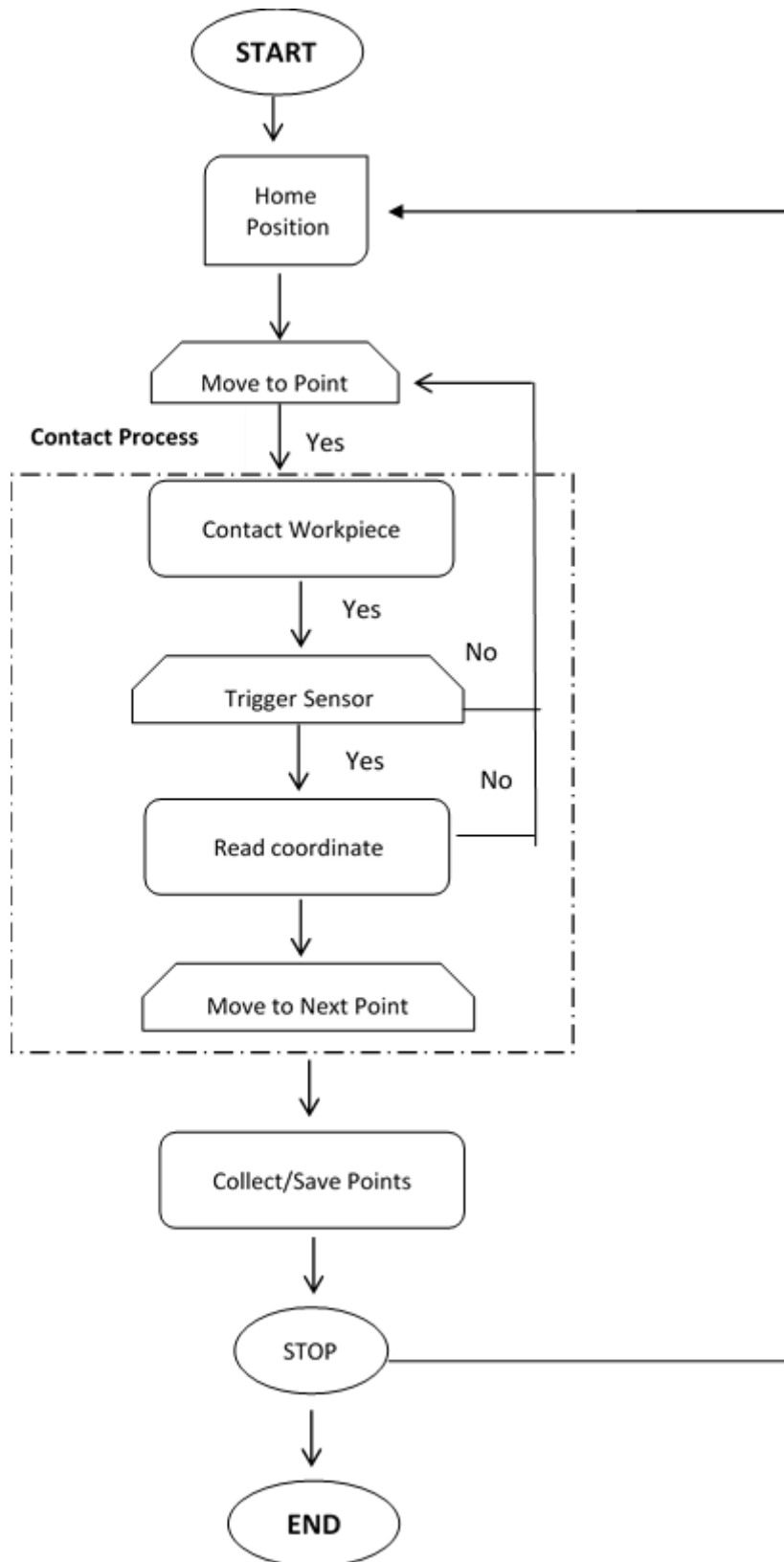


Figure 4 - 1: Point Detection Flow Chart

4.1.2 Mechanical Method

In the mechanical test, a gauge indicator with 0.05mm accuracy was used to measure the repeatability at the required positions on the workpiece. The indicator is securely mounted on the robot arm at the end joint to ease the measurement procedure and to ensure accuracy. The measurement is taken from each plane of the block at different positions. The repeatability process is based on four different positions on the robot table and 3 planes at (XY, YZ, ZX) as shown in figure 4-2. For each run the robot controller adjusts the motion and meets the conditions adapted in the robot and a single algorithm was created to run the robot with a speed of 10% (0.1m/s) and 30% (0.3m/s) of the robot infeed speed 1m/s and 100mm distance offset from each surface. The calibration method is done by setting the dial gauge indicator to zero and positioning the robot arm on the surface of the block, as soon as the dial gauge taps the block the dial indicator reading is taken to determine that it is functioning properly to check for smooth and easy movement to ensure accuracy on the robot.



Figure 4 - 2: Mechanical Method detection points

The robot is programmed to stop after it had repeatedly detected the measurements on the surface of the block for 15 times. After each trail, robot speed is modified to include the second operational speed and then reinitialized to the start from the beginning as indicated in the flow chart in figure 4-1. However, the data collected from the experiment is shown in a graphical in Appendix 1 and the best outcome results of the positions is show in this section, collected data results are shown in Appendix 1. Based on the test under 0.3m/s speed, the repeatability shows high variations in all positions. The maximum variation can reach 2.5mm in x direction, 2mm in YZ direction and 1.5mm in ZX direction. However, looking at the results under the 10% of

the speed, the errors become smaller. The kinematics of the robot often effects the position and orientation of detecting each joints, this has obviously affected the repeatability results because it reduces the stability position when detecting each point. The maximum variations are all smaller than 1.5mm under the minimal speed. Therefore, this obviously indicates that the slower the approaching speed the better repeatability. Considering the situation 0.3m/s speed, the variations at position 1 for the three Cartesian coordinates is approximately 20% higher than position 2. Position 3 and 4 also share a similarity, this variation is due to the position of the robot were the stiffness of robot joints affected the repeatable momentum when measuring the points at different positions, offset distance also plays a major role in which it causes deviations of the end effector position on the robot.

The results from position 2, 3 and 4 show a similar variation in terms of expected readings at 100mm offset and 0.1m/s speed. Depending on the workpiece position, results show there is significant differences in all positions. For example, on plane XY position 3 and 1 the accuracy error level is about 1.4mm and 1.1mm whereas position 2 and 4 are 0.8mm and 0.9mm. This indicates that the repeatability at position 2 at this point is good because the variation in reading is close to the zero point according to the gauge. Coordinates of ZX and YZ at position 2 also indicate an error level of 0.5mm and 0.8mm. All other positions are above 1mm error which are considered not ideal for further analyses in terms of repeatable error accuracy. In another hand, planes YZ and ZX in all positions have high error levels in the which was expected due to the changes of locations of the block in the work table causing high variations in these results. To conclude, position 2 at 0.1m/s speed is best position to undertake further analyses because the accuracy level is (0.7mm – 700micorn) which is the lowest comparing to the rest of the positions (see figure 4-3 and 4-4). The accuracy level achieved in this mechanical method is very high therefore; further action is taken under the electrical method.

Mechanical Repeatability Measurement

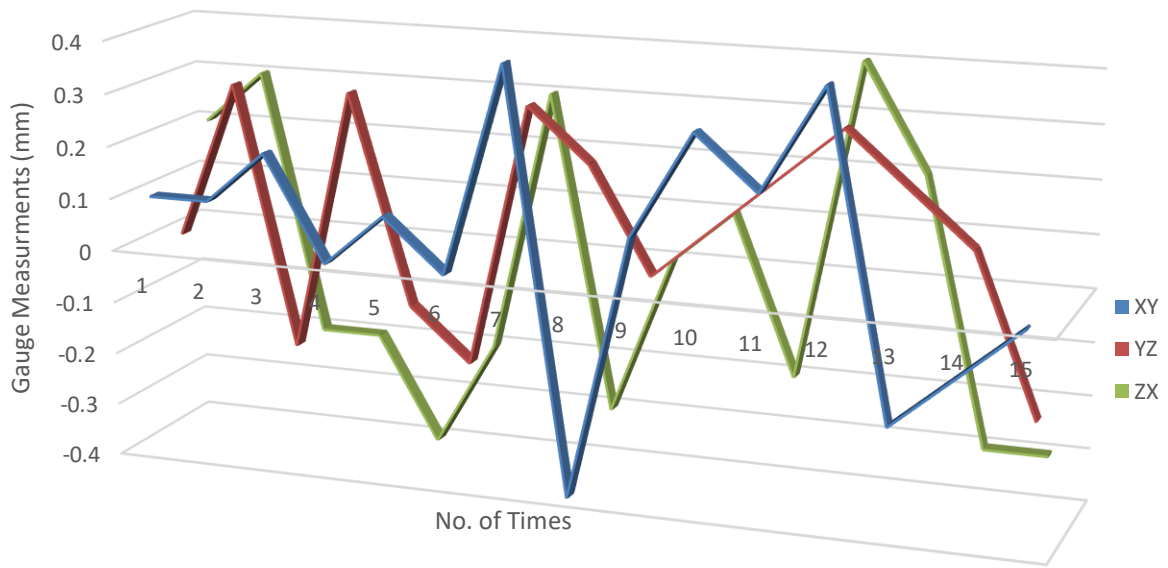


Figure 4 - 3: Position 2 Repeatability Measurement for 0.3m/s

Mechanical Repeatability Data

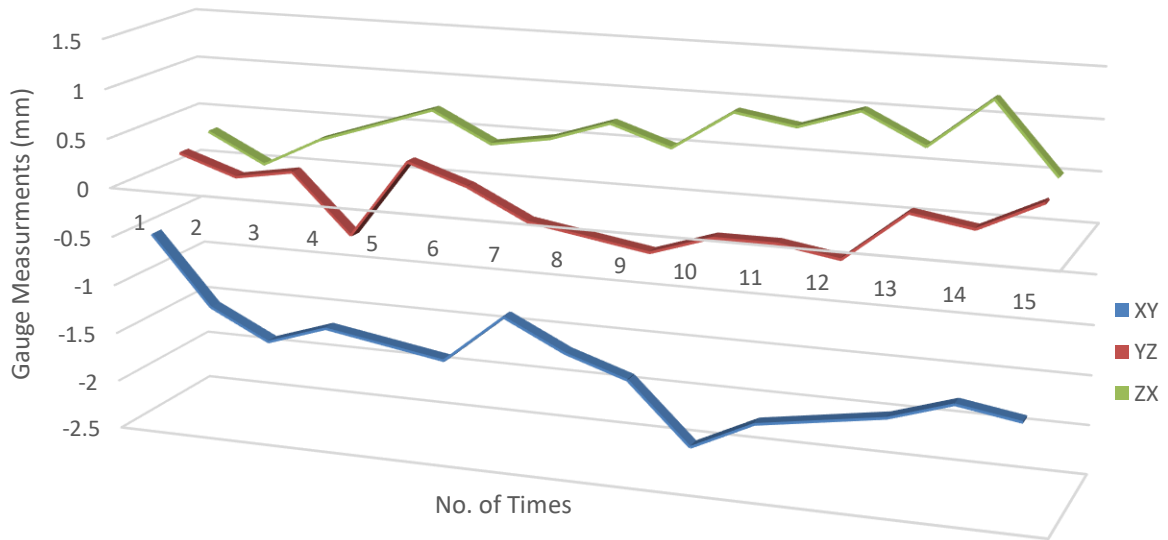


Figure 4 - 4: Position 2 Repeatability Measurement for 0.1m/s

4.1.2 Electrical Method

Another way to verify the performance of repeatability is by constructing another repeatability based on electrical circuit detection method. The aim of this procedure is to reduce the accuracy error to a minimum level as possible. The electric circuit is manually constructed throughout the experimental stage, shown in the facility setup section in chapter 3, in order to communicate with the robot. This electrical method is actually useful because it allows the robot to directly register points accordingly as the probe engages with the workpiece. By integrating the electric circuit, the probe engages with the workpiece and triggers the input sensor in the robot so that contact positions is registered providing real time response to the data collected. If no detection occurs, the sensor does not trigger and contact must occur between the robot tool and workpiece. The electrical method repeatability test is based on much slower infeed speed 0.01m/s (1% of 1m/s). Speed and offset distance (100mm) were chosen at this particular rate to give the robot the ability and flexibility to move without any restrictions to its joint or overall movements. The measurements collected from the results is shown in table 4 below:

Data Measurements and Results

Table 4: Electrical Repeatability Results

No. of Detection Times	Measurement of coordinates		
	Plane XY	Plane YZ	Plane ZX
1	974.3596	529.9383	798.5589
2	974.2318	529.9474	798.4896
3	974.3255	529.8953	798.4458
4	974.3534	529.954	798.4985
5	974.4272	529.9258	798.5023
6	974.3105	529.912	798.5563
7	974.3205	529.9189	798.5534
8	974.3172	529.956	798.5685
9	974.3744	529.785	798.551
10	974.328	529.8953	798.4856

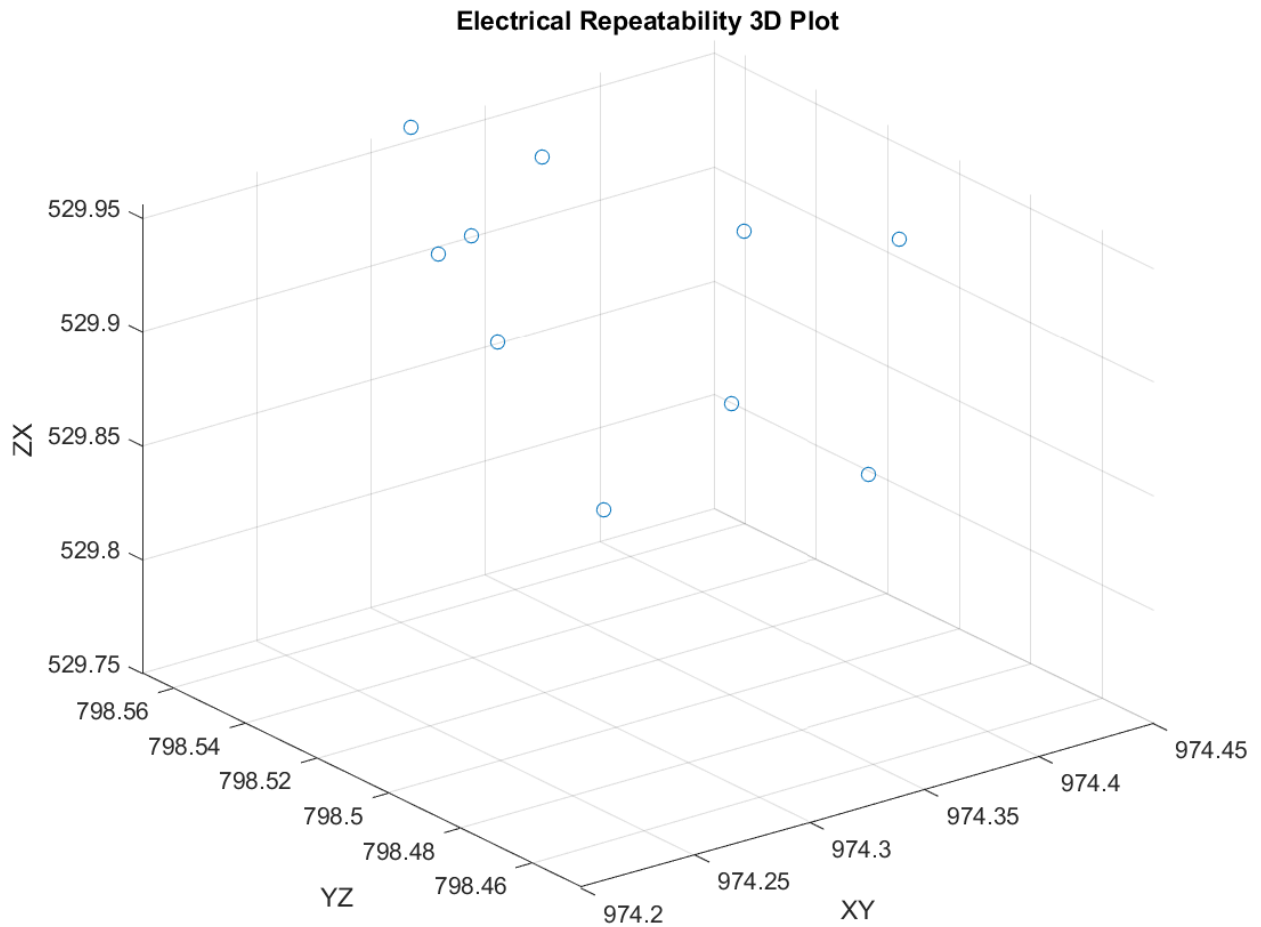


Figure 4 - 5: Electrical Repeatability Measurements

As can be seen from the data gathered table 4 and figure 4-5 the variations are similar when comparing the XY, YZ and ZX surfaces on the block. All planes on the block demonstrate a small level variation from the values recorded. From the measurements, the accuracy error level at the XY surface is about 0.195mm, YZ is 0.171mm and ZX is about 0.122mm which gives an average of 0.163mm (163micron) repeatability accuracy error. Even though the error level has been reduced by changing the repeatability method from mechanical to electrical, this accuracy level is still considered to be high because in grinding level the minimum achievable error should be less the 50micron in accuracy according to literature. The disadvantage of this method is that it does not directly engage the robot tool on the workpiece. Therefore, to achieve better accuracy the robot tool will be used as a probe to contact the workpiece and this will be monitored by using acoustic emission sensor to assist the robot accordingly when engaging with the workpiece.

4.1.3 Acoustic Emission Probing Method

Acoustic Emissions (AE) is used to generate digital signals, which were registered within the control panel interface of the robot program in order to aid the control and monitoring of detecting points. Acoustic emissions generally occur at frequency from 100 kHz to 2 MHz which is well above the most structural natural frequencies. This makes it one of the most promising processes for detection and monitoring methods, therefore, acoustic emission is ideal for characterizing the material removal activity. The acoustic emission voltage spectrum is used as indicators in this method to detect the tool as it engages with the workpiece. This method is constructed in a similar way the electric circuit is constructed, where the sensor is mounted on the block acting as a relay circuit switch. As the robot tool moves to the contact proximity of the block, the electronic circuit is triggered, registering the point of contact in the robot program. At the point of contact, a signal appears to provide the operator with a visual reference of the tool contacting the surface of the workpiece. At this stage, the interrupt is declared and measurement points are saved in the robot software interface. The AE sensor is capable of generating feedback by sensing the position of the workpiece in relation to the tip of the robot tool. A graphical illustration of an example AE sensory system, that contains a similar configuration to the assembly used in this project, is given in Figure 4-6 below:

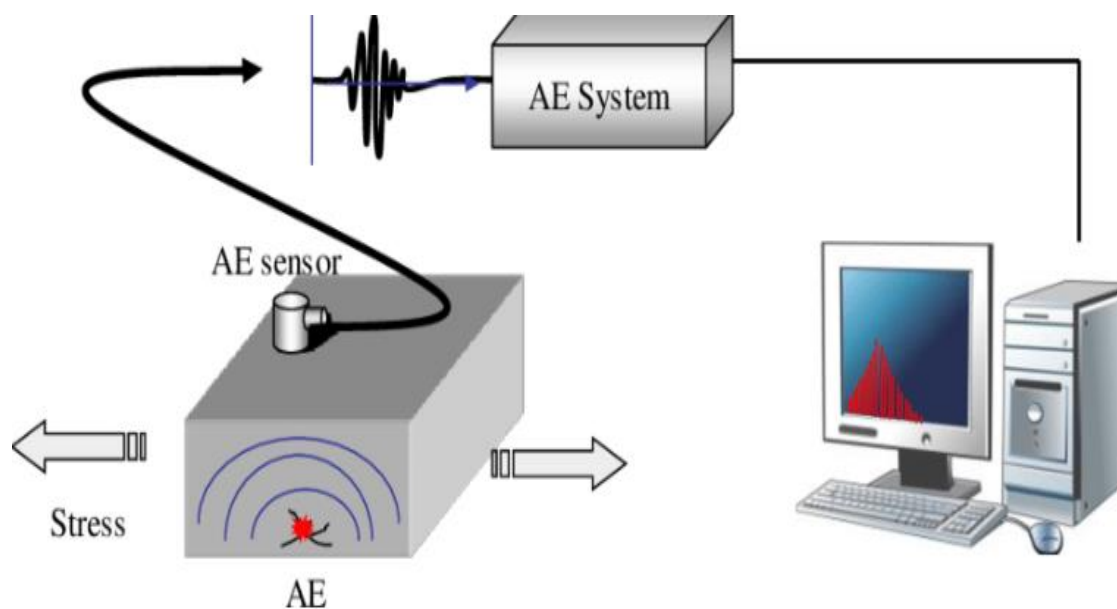
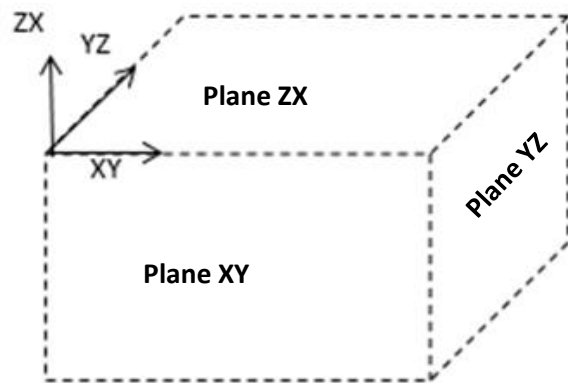


Figure 4 - 6: Acoustic Emissions sensory system Li.et.al (2018)

The use of AE sensor is to measure points by directly engaging grinding wheel to the workpiece to eliminate the effect of error between the tool and the workpiece. This is done by registering multiple points in each surface of the block under the same operational speed as the electrical method 0.01m/s (1% of 1m/s). After that, accuracy error have been improved by reducing the speed of the robot to its minimum achievable infeed speed 0.005m/s (1% of 0.5m/s).

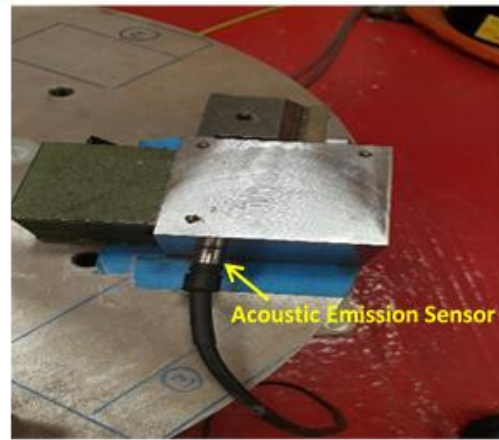
In order to avoid the tool damaging the workpiece, an interrupt command is built into the robot programme file. The interrupt command (see Appendix 2) is a function of the robot operation that provides a signal that acts to inform the robot arm to retract from the workpiece as it comes into contact and subsequently progress to the next detection point Noda et.al (2003). The measurements derived from the detection analysis were performed with the grinding ball mill as the robot tool. The tool sphere is operated at a 45° angle to the material due to the fact that the grinding ball mill was metal tipped. Resultantly, detecting at acute an angle approximately below 45° to the surface would culminate in the abrasion of the metal tip against the workpiece surface. The processing action of metal on metal contact would cause significant damage to both the material specimen and the tool. Consequently, for the stability of results and standardisation across the process due to the orientation of the robot and layout of the workspace, no angle exceeding 180° was possible and by the process of elimination 45° was the only viable option. Figure 4-7 below shows a general overview of the set up.



(b) Workpiece Coordinates



(a) Workpiece Location on Worktable



(c) Acoustic Emission Sensor illustration

Figure 4 - 7: Overview Set Up of Acoustic Emission method

Data Measurements & Discussions

Table 5: AE Repeatability Results uner 0.01m/s

No. of Detection Times	Measurement of coordinates under 0.01m/s		
	Plane XY	Plane YZ	Plane ZX
1	-10.89361	-13.39375	-12.52279
2	-10.90271	-13.39154	-12.47864
3	-10.8525	-13.31482	-12.48037
4	-10.80291	-13.35384	-12.48574
5	-10.83113	-13.31399	-12.55578
6	-10.88352	-13.357548	-12.51432
7	-10.85952	-13.347558	-12.51432
8	-10.85952	-13.357548	-12.50432
9	-10.88552	-13.337948	-12.50532
10	-10.87589	-13.37848	-12.50532

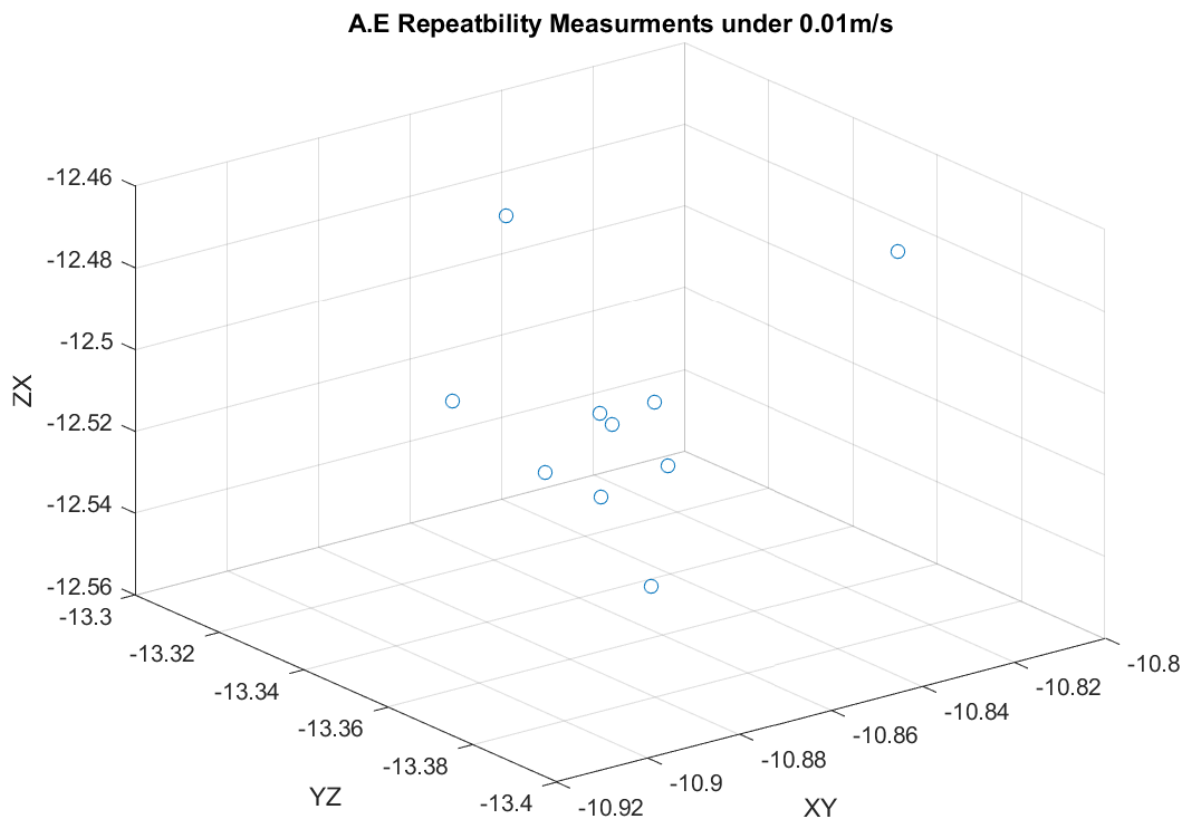


Figure 4 - 8: Acoustic Emission Repeatability Measurements under 0.01m/s

Table 6: AE Repeatability Results uner 0.005m/s

No. of Detection Times	Measurement of coordinates under 0.01m/s		
	Plane XY	Plane YZ	Plane ZX
1	-10.84361	-13.3375	-12.5153
2	-10.85271	-13.35154	-12.5264
3	-10.8525	-13.35482	-12.5157
4	-10.85291	-13.35384	-12.51574
5	-10.85113	-13.34399	-12.5161
6	-10.88352	-13.347548	-12.51432
7	-10.85952	-13.347558	-12.5145
8	-10.85952	-13.357548	-12.5148
9	-10.88552	-13.357948	-12.5151
10	-10.87589	-13.35848	-12.5149

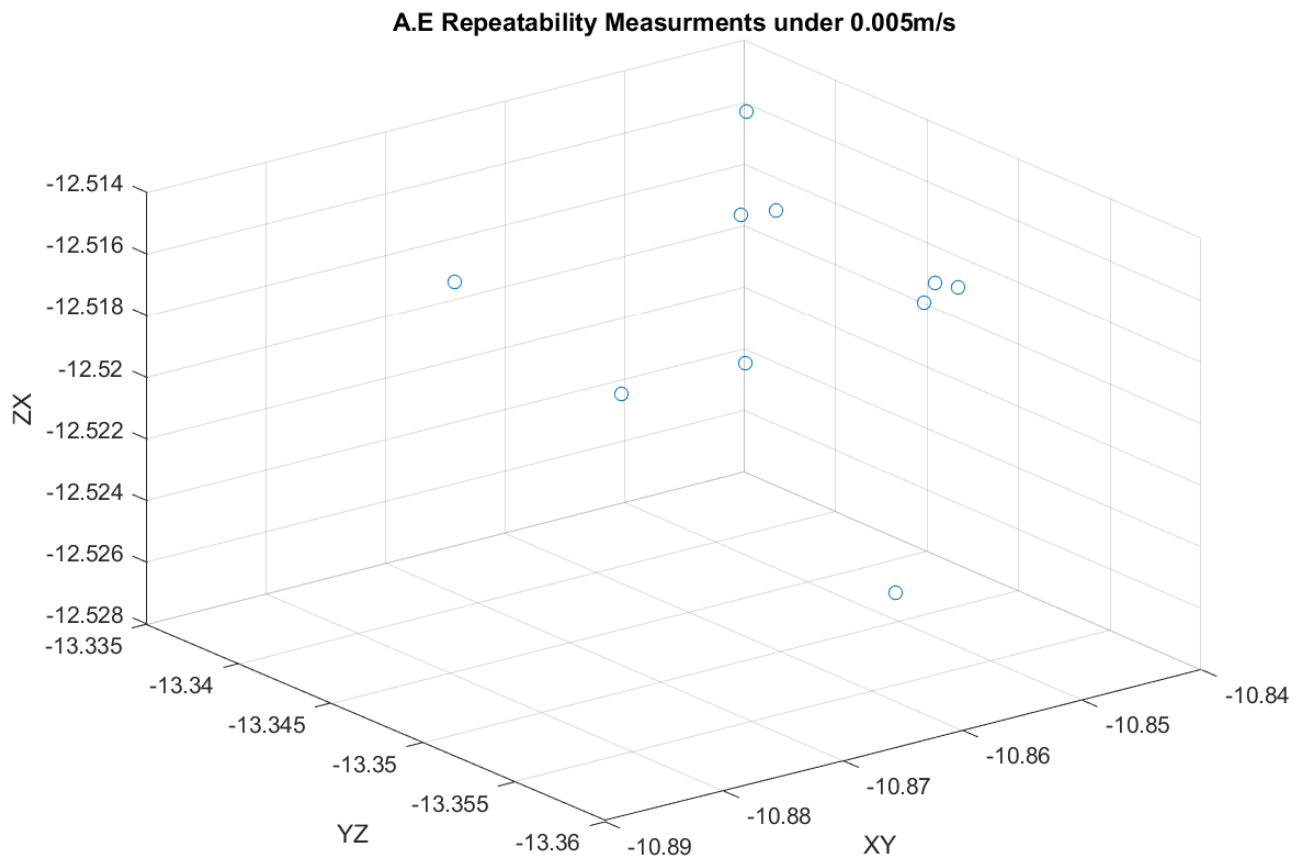


Figure 4 - 9: Acoustic Emission Repeatability Measurements under 0.05m/s

The result above show the relationship of all points have high similarity within number of repeatable times which indicates that the use of acoustic emission sensor was useful for accuracy detection purposes. Figure 4-8 to 4-9 show the measurements the speed of 0.01m/s and 0.005m/s. The average error accuracy achieved is 85micorn on all planes. Comparing to the electrical method, it has decreased by 48%, which proves the reliability and compatibility of the acoustic emission sensor when using it as an indication for the probe by directly engaging the tool into the workpiece. Although the error accuracy has been reduced by high percentage comparing to the electrical method, it was possible to further improve the error accuracy by reducing the infeed speed to its minimum level of 0.005m/s. The error accuracy have been improved to an average of 25micron, which is much more better than the electrical method. It was also noticed from all results that there is the distribution in measurements in XZ and YZ planes due to the position of the workpiece on the worktable, which sometimes effects the position and orientation of the joints of the arm of the robot. Plane XZ has the highest distribution due to the limitations the robot can achieve at this particular plane, which reduces the stability position when detecting the point. Plane XY has the best results due to the comfortable positions the robot can operate when detecting those points.

Finally, to verify the feasibility of the accuracy error achieved the depth of cut have been measured to see how much material been removed once the tool been in a contact with the workpiece during the contact measurements. The depth of cut in the figures below shows how much material is been taken of each surface plane during acoustic emission monitoring.

Depth of cut results from 0.005m/s – Average error of 25micron

Plane XY

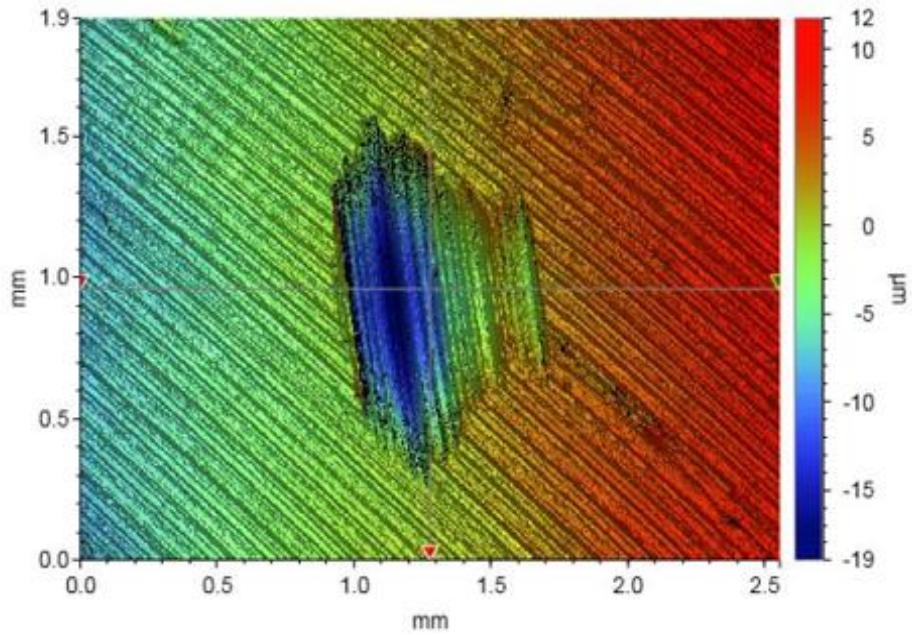


Figure 4 - 10: XY depth of cut

Plane YZ

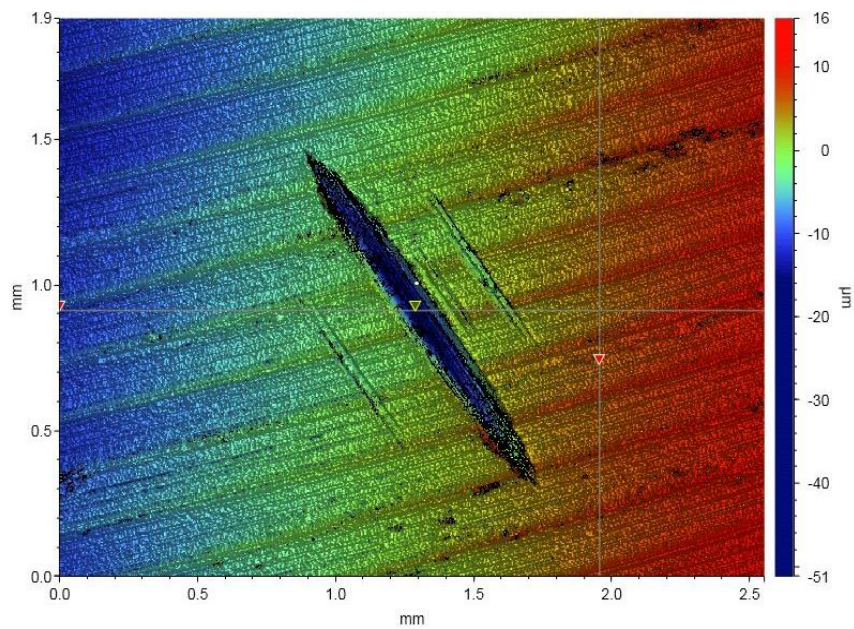


Figure 4 - 11: YZ depth of cut

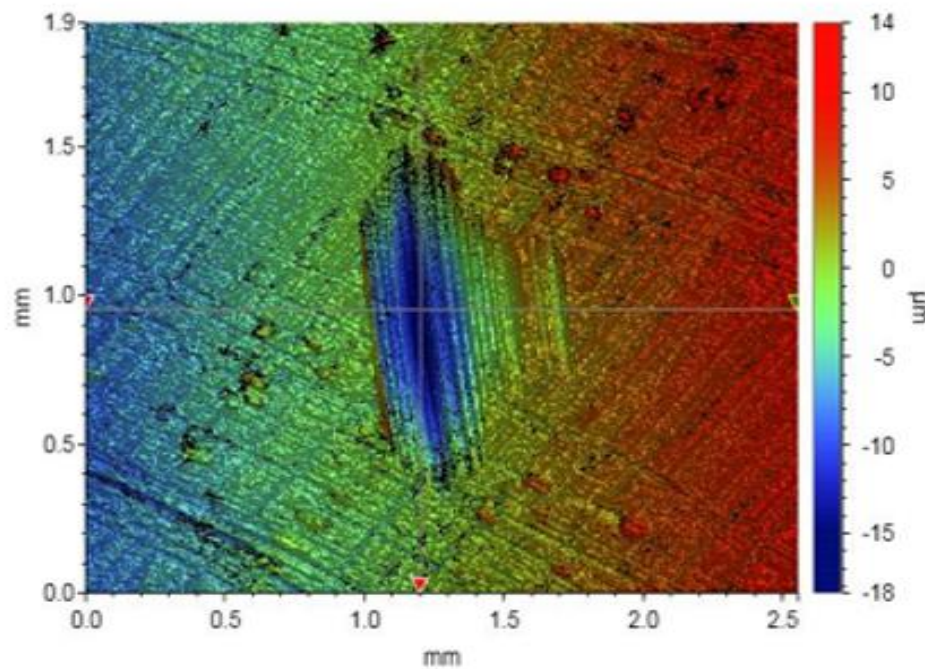
Plane ZX

Figure 4 - 12: XZ depth of cut

Figure 4-10 to 4-12 above illustrates how much material is being removed of each surface plane from the 0.005m/s once detection has been taken place by directly engaging the tool and the workpiece. To validate the accuracy error, achieved when applying A.E sensor all planes have less than 30micron material being removed from the surface of the workpiece. This suggests that the use of acoustic emission have been very effective for repeatability because it is very sensitive that signals communicate with the robot when wheel touch the workpiece making a small number of grains to be removed from the wheel which minimizes the effect of error between the tool and the workpiece.

Maintaining precision grinding to control the depth of cut is important, therefore limiting the material removal by using acoustic emission sensor that provides feedback to the robot machine to give better accuracy. The results below show the depth of cuts results for the higher robot speed operated using the acoustic emission sensor.

Depth of cut results from 1% of 1m/s – Average error of 85microm

Plane XY

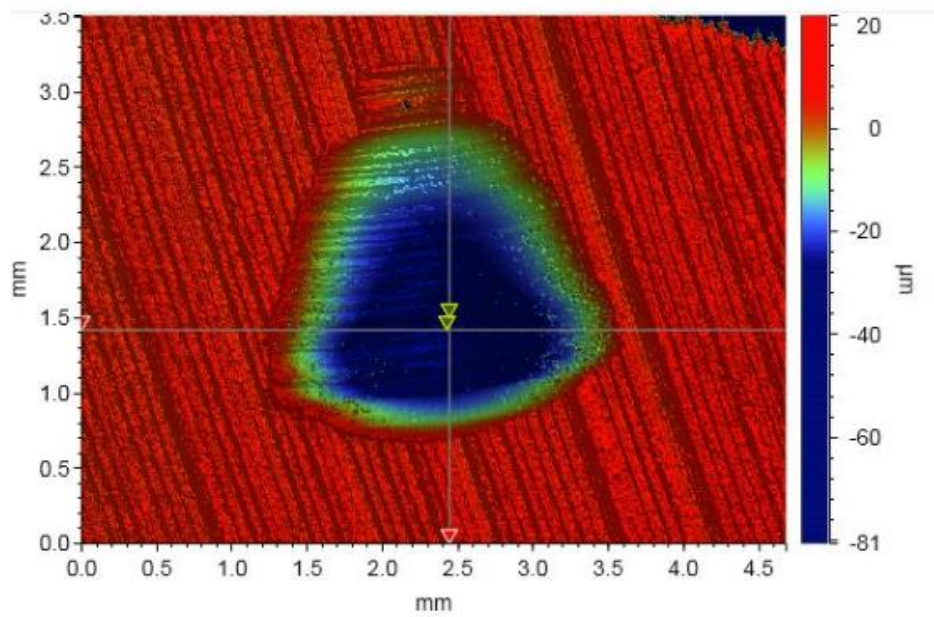


Figure 4 - 13: XY depth of cut

Plane YZ

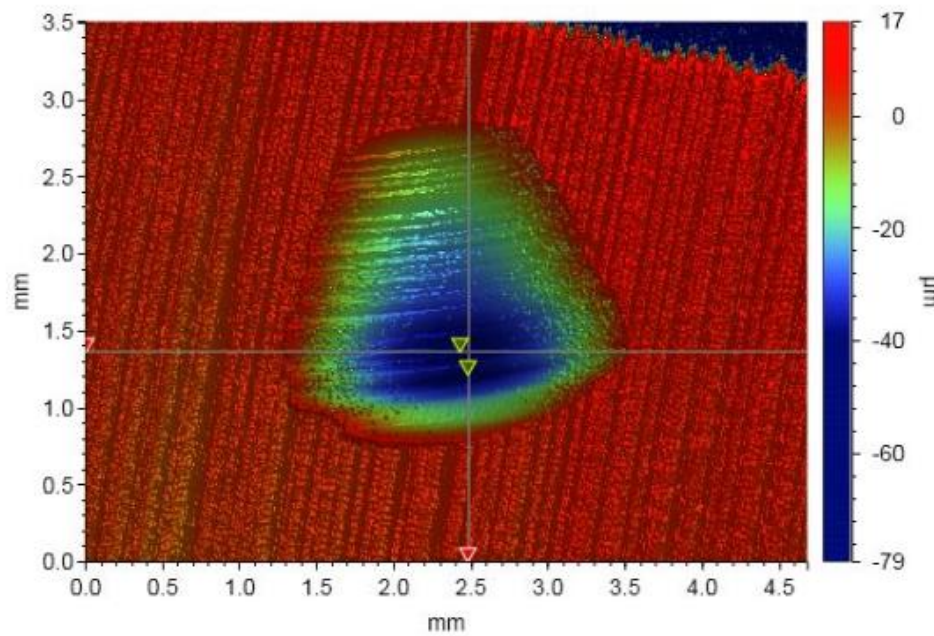


Figure 4 - 14: YZ depth of cut

Plane ZX

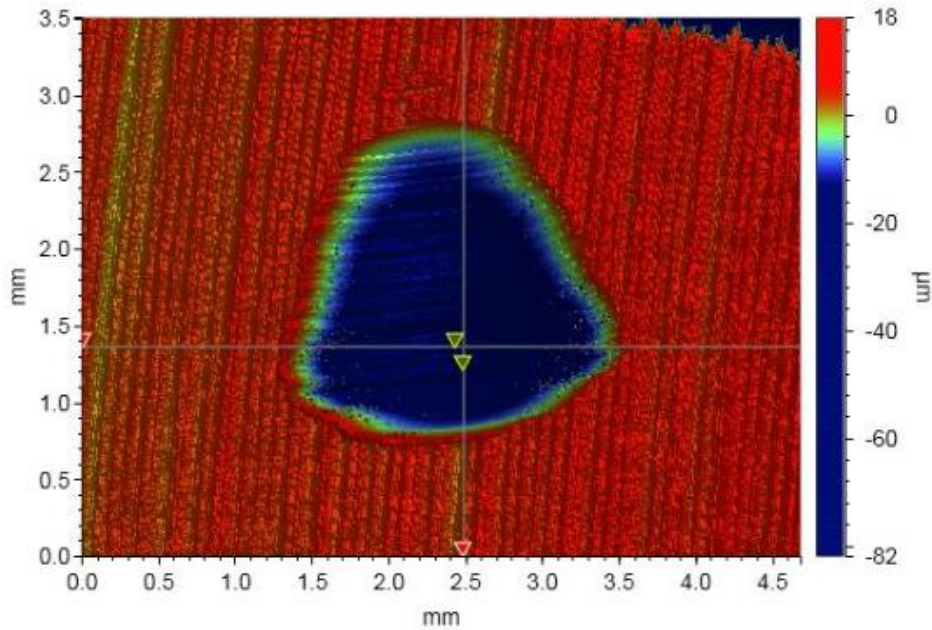


Figure 4 - 15: ZX depth of cut

4.1.4 Accuracy Error Comparison

The motivation in developing three different repeatability methods is that to see which will give the best accuracy level in order to position the workpiece accurately to the robot when performing grinding. According to repeatability, the less infeed speeds the more stable the robot and the better results is achieved. Acoustic emission results give the best accuracy error level because it allows the operator to control wheel as it comes into contact with the workpiece. It also uses the cutter tool as a probe so that positional error between the tool and sensor can be eliminated. The table below summarizes the accuracy error achievements from all methods

Table 7: Repeatability Comparison Results

Repeatability Error Accuracy Results			
Mechanical Method	Electrical Method	Acoustic Emission	Acoustic Emission
0.1m/s	0.01m/s	0.01m/s	0.005m/s
700µm	163 µm	85 µm	25 µm

4.2. Mathematical Model for Error analysis

To be able to confirm the accuracy achieved through repeatability test, a theoretical model based on repeatability measurement is established to define the datum. The actual datum position of the workpiece can be estimated based on multiple points collected from the original datum surface of the workpiece to be able to control the accuracy using the robot. After that, the trajectory datum point is established through vector model to compensate the error correlation between the real datum surface and nominal datum surface of the workpiece to improve the accuracy of the grinding process. Through this model, the actual position of the workpiece is estimated and error could be compensated by applying suitable machining strategy.

4.2.1 Position Modelling

The mathematical model proposed does not need to rely on kinematic parameters because there is no modification to the robot control system. The error is compensated by modifying the position coordinates taken of multiple measurements on the workpiece to estimate the error correlation between the real datum surface (RD) and the nominal datum surface (ND) of the workpiece. Figure 4-16 shows an overview of the proposed real and nominal surface geometry on the workpiece.

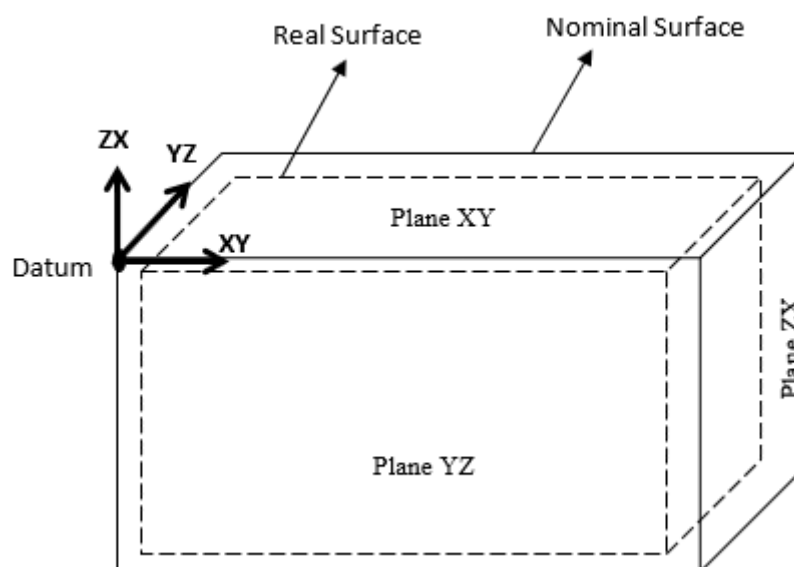


Figure 4 - 16: Overview of the geometric surface error of on the workpiece

The compensation of error is performed by modifying the positional coordinate based on multiple measurements for each plane (XY, YZ and XZ). The aim of this approach is to eliminate the influence of all sorts of errors on the geometrical accuracy which is the key for controlling the robot to conduct grinding. By establishing the geometrical relationship between the nominal surface and the collected measured points, the datum error could be assessed by multiple regression mathematical model. It is a statistical technique that allows us to determine the correlation between a continuous dependent variable and two or more independent variables. It can be used for a variety of purposes such as analyzing of experimental, ordinal, or categorical data. For example, Reddy et.al (2008) used multiple regression to predict surface roughness based on all cutting parameters such as feed rates, depth of cut and cutting speed in a turning operation. In this experiment, a multiple regression model is performed towards the data collected from the measurement with minimum estimation errors.

A common formula of a plane in space can be presented as:

$$\mathbf{aX} + \mathbf{bY} + \mathbf{cZ} + \mathbf{d} = \mathbf{0}$$

4- 1

As for variables **X**, **Y** and **Z** are coordinates taken from the different point of the surface of the plane on the block, **a**, **b**, **c** and **d** are constants that defines the plane position, and ϵ_i is the geometrical error. For all planes on block, the formulas are rearranged in the multiple regression because of the potentially large number of predictors, it is more efficient to use matrices to define the regression model and the subsequent analyses. By doing so, we can observe that the multiple regression and matrices calculation gives an adequate answer to each other. Here, we review the mathematical model.

All points coordinate on the plane should satisfy the equation 4-1

$$\mathbf{aX}_i + \mathbf{bY}_i + \mathbf{cZ}_i + \mathbf{d} = \epsilon_i \quad \text{for } i, \dots, n$$

4- 2

Considering the measurement errors ϵ , the measured points on plane XY should satisfy:

$$\mathbf{Z}_i = \mathbf{b}_0 + \mathbf{b}_1\mathbf{X}_i + \mathbf{b}_2\mathbf{Y}_i + \epsilon_i \quad \text{for } i, \dots, n$$

4- 3

where $b_0 = -d/c$, $b_1 = -a/c$ and $b_2 = -b/c$. By defining $\mathbf{Z} = (Z_1, Z_2, \dots, Z_n)'$, $\mathbf{B} = (b_1, b_2, \dots, b_n)'$,

$\boldsymbol{\varepsilon} = (\varepsilon_1, \varepsilon_2, \dots, \varepsilon_n)'$ and

$$\mathbf{X} = \begin{pmatrix} 1 & X_1 & Y_1 \\ 1 & X_2 & Y_2 \\ \vdots & \vdots & \vdots \\ 1 & X_n & Y_n \end{pmatrix}$$

Then, the regression function becomes

$$\mathbf{Z} = \mathbf{X} \mathbf{B} + \boldsymbol{\varepsilon}$$

4- 4

On modelling point of view, multiple regressions provide wider and broad problems to solve compare to simple linear regression such as joint effect, account interactions, estimate the effect of a variables and so on. However, having established the repeatability error in each plane by constructing the regression model, each axis equation can be derived for the outer, middle, and Inner square of each surface to give full inspection of the plane (see figure 4-16). Three linear equations shown below must be solved simultaneously to determine the experimental datum coordinates X_0, Y_0, Z_0 . For example, Equation 4-5 below reflects the surface equation for the XY plane of the points detected, as shown below.

$$Z = d + (aX) + (bY)$$

4- 5

Note that the plane value, XY in the above case, is now reflective of any given point within the total plane. Consequently, transposition of the surface equation above, to find the constant 'd', yields the axis equation for the square. As shown in Equation 4-6:

$$d = (aX) + (bY) - Z$$

4- 6

Applying the same principle to for all other planes,

$$d = (aX) + (cZ) - Y$$

$$d = (bY) + (cZ) - X$$

4-7

Presenting the 3 linear equations with 3 unknowns, from Equations 4-6 and 4-7

$$d_1 = (aX) + (bY) - Z$$

$$d_2 = (aX) + (cZ) - Y$$

$$d_3 = (bY) + (cZ) - X$$

4-8

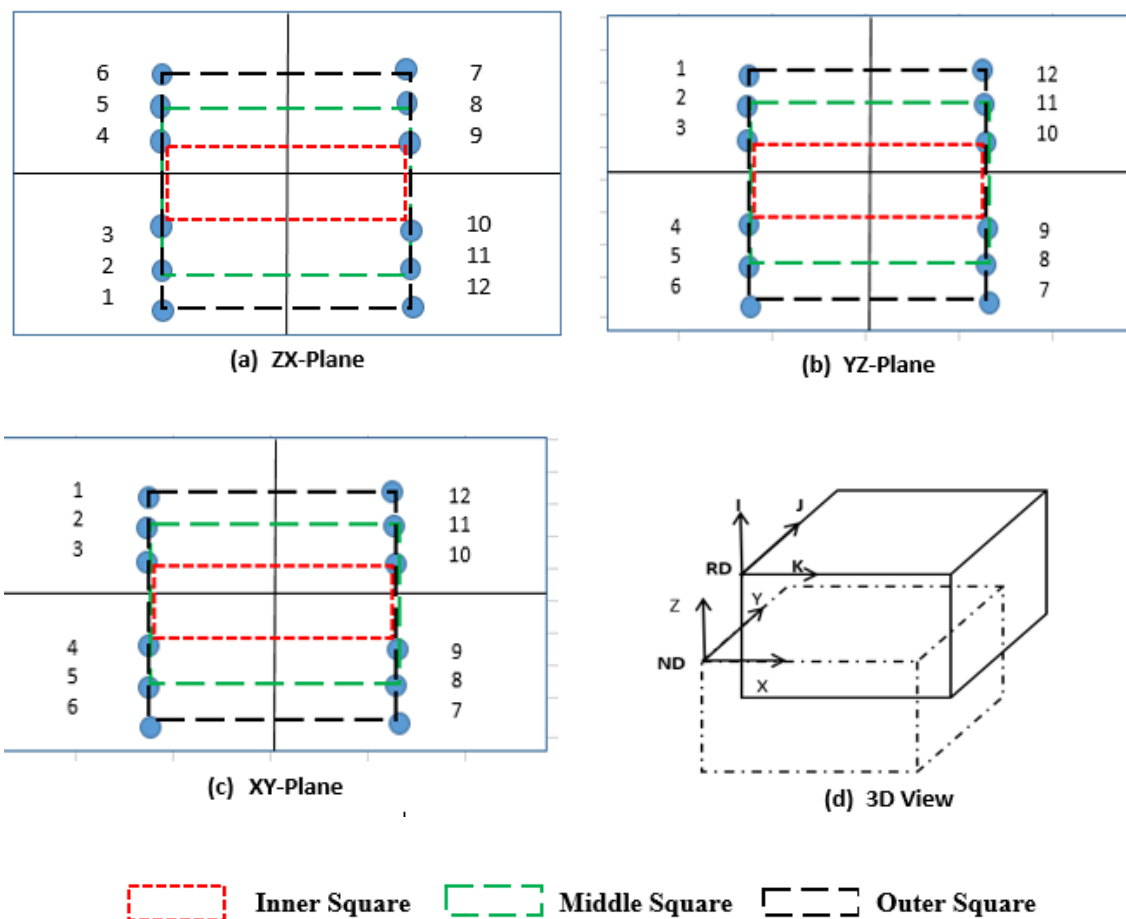


Figure 4 - 17: (a) ZX Plane squares, (b) YZ Plane squares, (c) XY Plane squares, (d) Overall 3d view

The 3 linear equations stated previously must be solved simultaneously to determine the datum coordinates: X_0 , Y_0 , & Z_0 . In three-dimensional space and integration of the variables and constants specified for each plane, the formula for the datum point of the robot work envelope can be established as shown below

$$aX + bY + cZ + d = 0$$

4- 9

Therefore,

$$\begin{pmatrix} X_0 \\ Y_0 \\ Z_0 \end{pmatrix} = \begin{pmatrix} a_1X + b_1Y + c_1Z = 0 \\ a_2X + b_2Y + c_2Z = 0 \\ a_3X + b_3Y + c_3Z = 0 \end{pmatrix}$$

4- 10

Having established the initial datum point on the robot work envelope, the mathematical model can be converted to a matrix form and be arranged accordingly to determine the error values in each plane as shown equation 4-11 below;

$$[\mathbf{E}] = [\mathbf{A}_0] + [\mathbf{A}][\boldsymbol{\alpha}]$$

4- 11

Where:

The error model, $[\mathbf{E}]$, represents the error in each plane:

∴

$$[\mathbf{E}] = \begin{bmatrix} \varepsilon_X \\ \varepsilon_Y \\ \varepsilon_Z \end{bmatrix}$$

4- 12

$[\mathbf{A}_0]$ Denotes the origin points as in;

$$[\mathbf{A}_0] = \begin{bmatrix} a_0 \\ b_0 \\ c_0 \end{bmatrix} = 0$$

4- 13

[**A**] Represents the points developed from the axial equations and solved simultaneously:

$$[\mathbf{A}] = \begin{bmatrix} a_1 & a_2 & a_3 \\ b_1 & b_2 & b_3 \\ c_1 & c_2 & c_3 \end{bmatrix}$$

4- 14

The matrix [**α**] is symbolises the standard deviation of the results generated in the repeatability testing for each plane:

$$[\boldsymbol{\alpha}] = \begin{bmatrix} \alpha_X \\ \alpha_Y \\ \alpha_Z \end{bmatrix}$$

4- 15

Hence, the error model presented as:

$$[\mathbf{E}] = [\mathbf{A}][\boldsymbol{\alpha}] = \begin{bmatrix} \varepsilon_X \\ \varepsilon_Y \\ \varepsilon_Z \end{bmatrix}$$

4- 16

Developing error values by implementing vector system for each axis, the resultant vector (I, J, K) shown in figure 4-18 below can be programmed into the robot to perform grinding. The error vectors for each plane is to be assumed perpendicular to one another (Khodaygan, 2014). The error can be corrected through vector models to compensate the error correlation between the real surface and nominal surface of the workpiece. Through this way the actual position of the workpiece can be estimated and implemented into the robot.

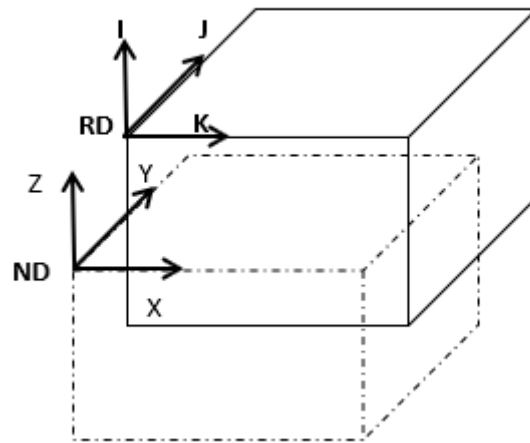


Figure 4 - 18: Illustration of Real and Nominal Datum

In order to create the required vector to compensate the error trajectory for each plane, it is firstly essential to establish the denoted planes which correspond to each vector, as demonstrated in figure 4-19 below:

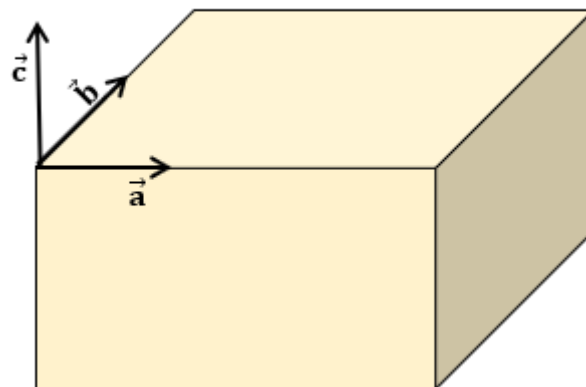


Figure 4 - 19: Vectors Attributed to each plane of the block.

The vectors of each plane in the workpiece can be expressed as shown in the equations below.

$$\vec{a} = a_1 i + a_2 j + a_3 k$$

$$\vec{b} = b_1 i + b_2 j + b_3 k$$

$$\vec{c} = c_1 i + c_2 j + c_3 k$$

4- 17

Expanding each vector component for equation;

$$a_1 i = X_1 - X_0$$

$$a_2 j = Y_1 - Y_0$$

$$a_3 k = Z_1 - Z_0$$

4- 18

Identically, applying the same process to other forms,

$$b_1 i = X_1 - X_0$$

$$b_2 j = Y_1 - Y_0$$

$$b_3 k = Z_1 - Z_0$$

$$c_1 i = X_1 - X_0$$

$$c_2 j = Y_1 - Y_0$$

$$c_3 k = Z_1 - Z_0$$

4- 19

Where, X_0 , Y_0 and Z_0 , are the datum coordinates established through solving the simultaneous equations associated with each set square for the given surface. The datum values are determined by, firstly combining the matrix of the constants associated with each given plane, and then multiplying the inverse matrix of the point values found. Finally, correcting the transitional angles for each vector coordinate as shown figure 4-20 below

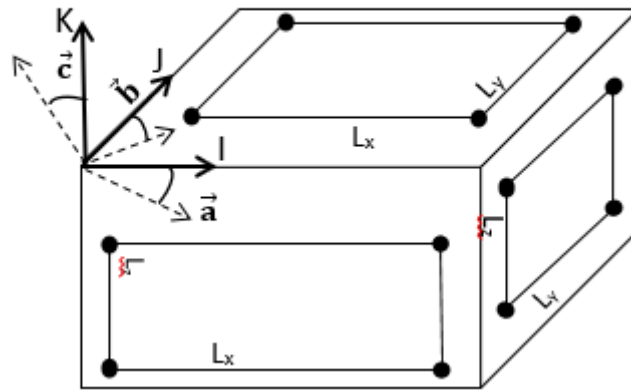


Figure 4 - 20: Transition Angle Correction

$$\text{Transition Angle } \vec{a} = \pm \left(\tan^{-1} \left(\frac{\Delta Y}{L_x} \right) + \tan^{-1} \left(\frac{\Delta Z}{L_x} \right) \right)$$

$$\text{Transition Angle } \vec{b} = \pm \left(\tan^{-1} \left(\frac{\Delta X}{L_y} \right) + \tan^{-1} \left(\frac{\Delta Z}{L_y} \right) \right)$$

$$\text{Transition Angle } \vec{c} = \pm \left(\tan^{-1} \left(\frac{\Delta Y}{L_z} \right) + \tan^{-1} \left(\frac{\Delta X}{L_z} \right) \right)$$

4- 20

Where:

$\Delta X, \Delta Y, \Delta Z$ = Repeatability Values

L_x, L_y, L_z = Distance between each detection point.

4.2.2 Model Establishment Implementation

The influence of measuring error in repeatability must be eliminated on the geometrical accuracy in order to set a datum for grinding purposes. The identified workpiece datum will act as the reference point to perform grinding operation. For correct implementation of the model, first a full inspection of the plane is carried out by detecting nine points on each surface plane to see the accuracy error level. After that, based on the best square location on the surface plane further analyses is carried out to calculate the datum point. After that, the error level is calculated to increase the accuracy of the grinding process. Finally, the trajectory datum point

is corrected through vector model to compensate the error correlation between the real surface and nominal surface of the workpiece.

The model is implemented by using acoustic emission sensor to help detect multiple points at XZ, YZ and XY planes. As the robot tool tip come into contact with the workpiece, the sensor is triggered in the robot system and data were registered directly into the robot. A number of 12 points is detected on each plane to make up a full plane regression equation, each point detected is based on equal distance from each sides of the plane of the workpiece to allow an approximate full detection of the whole plane. For example, looking at plane XY the robot travels at only x or y coordinate directions to the next detection point while remains constant at z direction. In this way, coordinates were collected as shown in Table 8, 9 and 10 which presents measurement data for all planes.

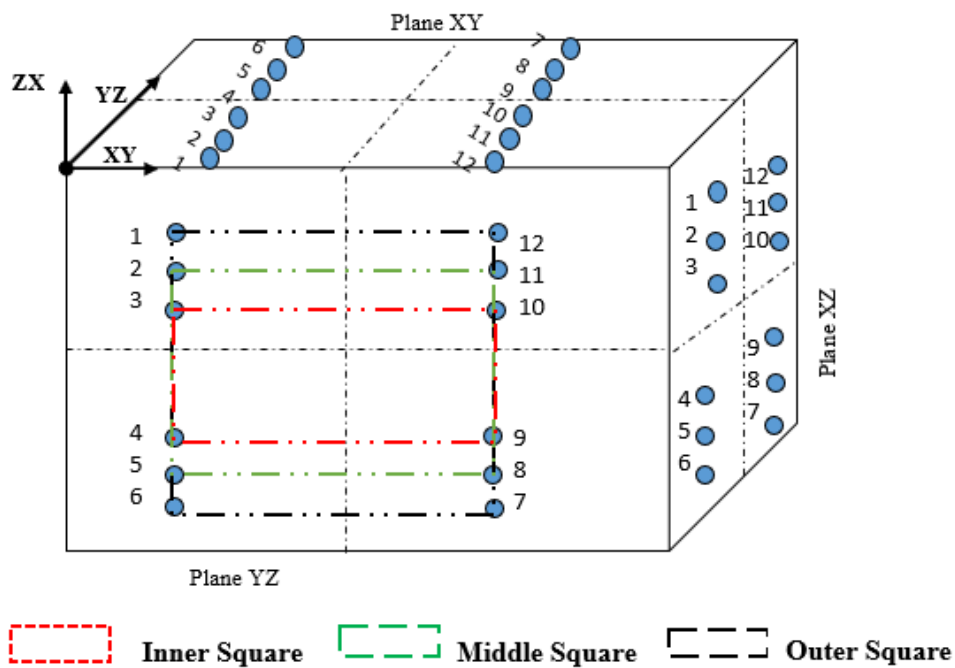


Figure 4 - 21: Point detection on surface planes

Measurement Results

Table 8: Measurement Results of XY Plane

<i>Plane XZ</i>				
	Point1	point6	point 7	point 12
x	60.295460	60.29092	20.28898	20.28729
y	13.2364	63.2265	63.22607	13.2261
z	-12.3864	-12.2679	-12.3238	-12.3917
	Point 2	point 5	point 8	point 11
x	60.29613	60.9007	20.28846	20.28848
y	20.24124	56.22882	56.22425	20.15967
z	-12.3889	-12.2407	-12.2733	-12.3420
	Point 3	point 4	point 9	point 10
x	60.29283	60.29274	20.28628	20.28562
y	27.23311	49.23095	49.2251	27.22685
z	-12.3879	-12.2901	-12.3506	-12.3824

Table 9: Measurement Results of YZ Plane

<i>Plane YZ</i>				
	Point1	point6	point 9	point 10
x	59.73283	59.72475	26.72356	26.72593
y	-13.0609	-13.1378	-13.6475	-13.5406
z	4.28394	37.27139	37.27094	4.26587
	Point 2	point 5	point 8	point 11
x	59.73188	59.72728	26.72447	26.72588
y	-13.0361	-13.0876	-13.6530	-13.5592
z	9.28046	32.27143	32.27114	9.26449
	Point 3	point 4	point 7	point 12
x	59.73029	59.72874	26.72418	26.72455
y	-13.0376	-13.1147	-13.6294	-13.5808
z	14.27766	27.27610	27.27153	14.26890

Table 10: Measurement Results of XZ Plane

<i>Plane ZX</i>				
	Point1	point6	point 9	point 10
x	19.12889	54.10206	53.99452	19.01110
y	-12.3685	-11.9852	-11.7611	-12.3925
z	-3.03946	-3.18400	-33.2526	-33.2073
	Point 2	point 5	point 8	point 11
x	19.12888	54.11262	54.00875	18.99360
y	-12.3685	-11.9658	-11.9228	-12.3843
z	-8.08076	-8.10593	-28.2543	-28.2557
	Point 3	point 4	point 7	point 12
x	19.12916	54.11277	54.05620	18.98845
y	-12.3921	-11.9787	-11.9291	-12.3689
z	-13.1104	-13.1318	-23.1883	-23.2207

A regression is performed to estimate the error correlation. All data points are collected based on global coordinate system movement of the robot. This movement usually consists of a point coordinate (x, y, z) and may include additional information such as velocity, or angular velocity. For illustration purposes only, the error analyses results shown in this section is based on the robot moving speed of 0.01 m/s (1% of 1m/s) which was according to the first acoustic emission repeatability test. The theoretical method in the mathematical model section defines a set of matrices is used integrate data to for each plane to visualize the error correlation.

Plane ZX Calculated values
Table 11: Error Correlation of palne ZX

Regression Values -0.0076x - 0.0018y - Z + 12.44463= 0			
	Z (mm) Measurements	Z (mm) Theoretical	Error (mm)
Point 1	-12.38643	-12.37378644	0.012643
Point 6	-12.26792	-12.28056553	-0.012645
Point 7	-12.32383	-12.31118697	0.0126430
Point 12	-12.39179	-12.40443106	-0.0126410

Regression Values -0.0068x - 0.00204y - Z + 12.43444			
	Z (mm) Measurements	Z (mm) Theoretical	Error (mm)
Point 2	-12.38895	-12.35165168	0.037298
Point 5	-12.24077	-12.27751307	-0.036743
Point 8	-12.34202	-12.30535664	0.036663
Point 11	-12.34202	-12.37923862	-0.037218

Regression Values -0.00068x - 0.00294y - Z + 12.4930			
	Z (mm) Measurements	Z (mm) Theoretical	Error (mm)
Point 3	-12.38798	-12.37147207	0.016507
Point 4	-12.29016	-12.30666824	-0.016508
Point 9	-12.35065	-12.33414207	0.016507
Point 10	-12.38244	-12.39894762	-0.016507

A standard deviation has been calculated to statistically measure the dispersion of the data related to the calculated error values. See table below

Table 12: Standard deviation of calculated error

Standard Deviation (mm)	
Point 1, 6, 7, 12	0.014599218
Point 2, 5, 8, 11	0.042703029
Point 3, 4, 9, 10	0.019061716

Plane YZ Calculated values
Table 13: Error Correlation of palne YZ

Regression Values $0.0149x - 0.0027z - Y + 13.9369 = 0$			
	Y (mm) Measurements	Y (mm) Theoretical	Error (mm)
Point 1	-13.06096	-13.00517531	0.05578
Point 6	-13.13784	-13.0050825	0.13276
Point 7	-13.64757	-13.4983607	0.14921
Point 12	-13.54066	-13.49862268	0.04204

Regression Values $-13.981 = 0.0164x - 0.00315z - Y + 13.981$			
	Y (mm) Measurements	Y (mm) Theoretical	Error (mm)
Point 2	-13.03617	-12.95514418	0.081025822
Point 5	-13.08764	-12.95505758	0.132582421
Point 8	-13.65306	-13.49752625	0.155533751
Point 11	-13.55926	-13.49779906	0.061460936

Regression Values $-13.932 = 0.0160x - 0.0048z - Y + 13.932 = 0$			
	Y (mm) Measurements	Y (mm) Theoretical	Error (mm)
Point 3	-13.03762	-12.91260901	0.12501
Point 4	-13.11479	-12.91226053	0.20253
Point 9	-13.62945	-13.43871382	0.19074
Point 10	-13.5808	-13.43894324	0.141856

A standard deviation has been calculated to statistically measure the dispersion of the data related to the calculated error values. See table below

Table 14: Standard deviation of calculated error

Standard Deviation (mm)	
Point 1, 6, 7, 12	0.05387
Point 2, 5, 8, 11	0.04381
Point 3, 4, 9, 10	0.03744

Plane XY Calculated values
Table 15: Error Correlation of palne XZ

Regression Values -0.0141y - 0.00247z - X + 10.472 = 0			
	X (mm) Measurements	X (mm) Theoretical	Error (mm)
Point 1	-10.68789	-10.67865365	0.00924
Point 6	-10.74352	-10.7527554	-0.00924
Point 7	-11.22754	-11.21830931	0.00923
Point 12	-11.13489	-11.14412164	-0.00923

Regression Values -0.0136y - 0.0044z -X + 10.4454 = 0			
	X (mm) Measurements	X (mm) Theoretical	Error (mm)
Point 2	-10.66394	-10.67288845	-0.00895
Point 5	-10.77060	-10.76165317	0.00895
Point 8	-11.20401	-11.21295356	-0.00894
Point 11	-11.13302	-11.12407483	0.00895
Regression Values -0.0137y - 0.0036z -X + 10.4598 = 0			
	X (mm) Measurements	X (mm) Theoretical	Error (mm)
Point 3	-10.69066	-10.69798442	-0.00732
Point 4	-10.74226	-10.73493625	0.00732
Point 7	-11.18107	-11.18839028	-0.00732
Point 12	-11.15870	-11.15137904	0.00732

A standard deviation has been calculated to statistically measure the dispersion of the data related to the calculated error values. See table below

Table 16: Standard deviation of calculated error

Standard Deviation (mm)	
Point 1, 6, 7, 12	0.01066
Point 2, 5, 8, 11	0.01032
Point 3, 4, 9, 10	0.00845

The data taken from the detection of points shown in tables 11, 13 and 15 provides useful assessment of robots responses. The multiple regression method estimates the parameters of workpiece datum planes and provides a response model to assess robot performance. From the regression results the predicted dependent variable known as **x**, **y** and **z** from aforementioned

equations were identified. The error is estimated by taking the average difference between the experimental values and the calculated theoretical values for each plane. For example, from tables 10, 12 and 14 plane XY the independent variable (Z) from regression is calculated for each point. It can be seen that the error becomes approximately less than 50µm in all surface planes which corresponds effectively with the acoustic emission error accuracy under the same infeed speed. Based on this evidence and in conjunction with the support of results across both the Matlab and Excel software packages, the mathematical modelling is valid for further use in this project. The exact same procedure, as performed for a sample calculation for the **XY** and **YZ** planes is recorded in **Appendix 3**. A sample calculation is presented in the next section

Taking ZX-plane at point 1, 6, 7 and 12 as an example

$$Z_{\text{Theoretical}} = D + (aX) + (bY)$$

4- 21

The estimated point can be regressed for, by the equation for the Z plane in three-dimensional space. Note that no Z component is presented, as Z is the subject of the operation. Thus, the point is found by the relationship between the two other corresponding points, in this case X and Y, and the regression constants, D, a, and b. This is true for all regression calculations and the corresponding points are determined by the plane under consideration (Draper & Harry, 1998). However, to quantify the constants that define the plane under inspection, it was necessary to run the desired equations through the Matlab software (See Appendix 3). Regressed values from software are represented in the table below:

Table 17: Regressed Values calculated from software

Known:	Value:	Found by:
a	0.000765	Matlab
b	0.001865	Matlab
D	-12.4445	Matlab
X	60.29546 mm	Practical Experimentation
Y	13.23640 mm	Practical Experimentation

Hence, inserting the values stated in Table 17 gives:

$$Z_{\text{Theoretical}} = -12.4446 + (0.000765 \times 60.29546 \text{ mm}) + (0.001865 \times 13.23640 \text{ mm})$$

4- 22

Therefore,

$$Z_{\text{Theoretical}} = -12.37378 \text{ mm}$$

From the point detection experiments, the actual value of Z is shown below:

$$Z_{\text{Experimental}} = -12.38643 \text{ mm}$$

Using the theoretical and experimental plane values stated, the error in the plane can be found as shown below:

$$\text{Plane}_{\text{Theoretical}} - \text{Plane}_{\text{Experimental}} = \Delta_{\text{Plane}}$$

4- 23

Inserting the values established for the Z plane:

$$Z_{\text{Theoretical}} - Z_{\text{Experimental}} = \Delta_Z$$

∴

$$-12.37378 \text{ mm} + 12.38643 \text{ mm} = \Delta_Z$$

$$\Delta_Z = 12.64 \mu\text{m}$$

4- 24

Theoretical accuracy error in each plane is shown in the table below.

Having established the repeatability error in each plane by constructing the regression model, each axis equation can be derived for the outer, middle, and Inner square of the each surface to give full inspection of the surface plane. Three linear equations must be solved simultaneously to determine the datum coordinates of the workpiece X_0 , Y_0 , Z_0 as shown in equation 4-5 to 4-8. Demonstration of the solution to the three linear equations is best achieved by sample calculations. For example, squares of each outer surface (see figure 4-17) on the block is demonstrated in equation 4-25

$$-12.44463 = (-0.0076 X) - (0.0018 Y) - Z$$

$$-13.9369 = (0.0149 X) - Y - (0.0027 Z)$$

$$-10.472 = -X(-0.0141 Y) - (0.00247 Z)$$

4- 25

Writing in matrix form,

$$\begin{bmatrix} -1 & -0.0076 & -0.0018 \\ 0.0149 & -1 & -0.0027 \\ -0.00247 & -0.00141 & -1 \end{bmatrix} \begin{bmatrix} -124463 \\ -13.9369 \\ -10.472 \end{bmatrix}$$

∴

Solving simultaneously

$$\begin{pmatrix} X_0 \\ Y_0 \\ Z_0 \end{pmatrix} = [M^{-1}][C] = \begin{matrix} 10.2433 \\ 14.0562 \\ 12.3431 \end{matrix}$$

4- 26

Having established the experimental datum coordinates X_0 , Y_0 , Z_0 , the error values in each plane can be calculated in matrix form as shown below:

$$[E] = [A][\alpha]$$

4- 27

Where:

[A] Represents the points derived from the simultaneous equations for each plane

[α] is symbolises the standard deviation of repeatability testing for each plane:

$$[A] = \begin{bmatrix} -1 & -0.0141 & -0.0024 \\ 0.0149 & -1 & -0.0027 \\ -0.0076 & -0.0018 & -1 \end{bmatrix}$$

$$[\alpha] = \begin{bmatrix} 0.041 \\ 0.065 \\ 0.041 \end{bmatrix}$$

Therefore,

$$[\mathbf{E}] = [\mathbf{A}][\boldsymbol{\alpha}] = \begin{bmatrix} \varepsilon_X \\ \varepsilon_Y \\ \varepsilon_Z \end{bmatrix}$$

∴

$$\begin{bmatrix} -1 & -0.0141 & -0.0024 \\ 0.0149 & -1 & -0.0027 \\ -0.0076 & -0.0018 & -1 \end{bmatrix} \times \begin{bmatrix} 0.041 \\ 0.065 \\ 0.041 \end{bmatrix} = \begin{bmatrix} -0.042 \\ -0.064 \\ -0.041 \end{bmatrix}$$

$$\therefore \begin{bmatrix} \varepsilon_X \\ \varepsilon_Y \\ \varepsilon_Z \end{bmatrix} = \begin{bmatrix} -0.042 \\ -0.063 \\ -0.041 \end{bmatrix}$$

Note: All values are in (mm)

Average Error in each set of square is shown below.

Table 18: Datum Error for each set of square.

Outer Square	Middle Square	Inner Square
$\begin{bmatrix} \varepsilon_X \\ \varepsilon_Y \\ \varepsilon_Z \end{bmatrix} = \begin{bmatrix} -0.0424 \\ -0.0643 \\ -0.0412 \end{bmatrix}$	$\begin{bmatrix} \varepsilon_X \\ \varepsilon_Y \\ \varepsilon_Z \end{bmatrix} = \begin{bmatrix} -0.0428 \\ -0.0645 \\ -0.0417 \end{bmatrix}$	$\begin{bmatrix} \varepsilon_X \\ \varepsilon_Y \\ \varepsilon_Z \end{bmatrix} = \begin{bmatrix} -0.0426 \\ -0.0649 \\ -0.0415 \end{bmatrix}$

The table above illustrates the datum error for each surface plane on the block. The motivation in developing 3 set squares in each surface of the plane is to be able to see the error coloration by taking into account the majority of the overall surface of the workpiece. It can be seen that the error becomes smaller as the full outer surface is detected (see figure 4-17), this is because the robot tool becomes less stiff and more orientated when detecting the outer points. For that reason, the outer square is best considered to calculate the trajectory correction of the datum point. According to repeatability, the less operational speed the more stable the robot and the better Acoustic Emission response signals can be detected. Finally, the generation of vector models enables the subsequent correction of the trajectory datum point, which aims to increase the accuracy of the grinding processes using the robot.

To create the required vector plane, it is firstly essential to establish the denoted planes which correspond to each vector as demonstrated in Figure 4-20 shown in the error modelling section. Combining the vectors of each experimental plane is shown below,

$$\vec{a} = a_1 i + a_2 j + a_3 k$$

$$\vec{b} = b_1 i + b_2 j + b_3 k$$

$$\vec{c} = c_1 i + c_2 j + c_3 k$$

4- 28

Where:

$$a_1 i = X_1 - X_0, b_1 i = X_1 - X_0 \text{ and } c_1 i = X_1 - X_0$$

$$a_2 j = Y_1 - Y_0, b_2 j = Y_1 - Y_0 \text{ and } c_2 j = Y_1 - Y_0$$

$$a_3 k = Z_1 - Z_0, b_3 k = Z_1 - Z_0 \text{ and } c_3 k = Z_1 - Z_0$$

4- 29

Vector \vec{a}

Calculating \vec{a} based on equations found for \vec{b} and \vec{c} in *Set 1*:

$$\dot{b} = -13.9369 = (0.0149 X_1) - (0.0027 Z_1) - Y_1$$

$$\dot{c} = -12.44463 = (-0.0076 X_1) - (0.0018 Y_1) - Z_1$$

Solving these equations requires the elimination of one unknown, by applying an arbitrary to X_1 for the plane i:

$$X_1 = X_0 + 1 = 10.24332 + 1 = 11.24332 \text{ mm}$$

Inserting the value of X_1 in to the equations for \vec{b} and \vec{c} :

$$\dot{b} = -13.9369 = (0.0149 \times 11.24332) - (0.0027 Z_1) - Y_1$$

$$\dot{c} = -12.44463 = (-0.0076 \times 11.24332) - (0.0018 Y_1) - Z_1$$

∴

$$\begin{aligned}\dot{b} &= -13.9369 = (0.16748) - (0.0027 Z_1) - Y_1 \\ \dot{c} &= -12.44463 = -(0.08542) - (0.0018 Y_1) - Z_1 \\ &\vdots\end{aligned}$$

By transposing the equation to isolate the unknowns, and solving:

$$\begin{aligned}\dot{b} &= -13.9369 - (0.16748) = -(0.0027 Z_1) - Y_1 \\ \dot{c} &= -12.44463 + (0.08542) = -(0.0018 Y_1) - Z_1 \\ &\vdots\end{aligned}$$

$$\dot{b} = -14.097 = -(0.0027 Z_1) - Y_1$$

$$\dot{c} = -12.3546 + (0.08542) = -(0.0018 Y_1) - Z_1$$

Thus, the vector components have been reduced to two equations with two unknowns. The equations developed can be solved simultaneously in a matrix form:

$$\begin{bmatrix} Y_1 \\ Z_1 \end{bmatrix} = [M^{-1}][C]$$

4- 30

$$\begin{bmatrix} -0.0027 & -1 \\ -1 & -0.0018 \end{bmatrix} \begin{bmatrix} -14.097 \\ -12.3546 \end{bmatrix}$$

$$Y_1 = 14.06371 \text{ mm}$$

$$Z_1 = 12.32929 \text{ mm}$$

Implementing the established values in to the vector equation for \vec{a}

$$a_1 i = 11.24332 - 10.24332 = i$$

$$a_2 j = 14.06371 - 14.0562 = 0.00751 j$$

$$a_3 k = 12.32929 - 12.34315 = -0.01212 k$$

Combining each vector component:

$$\vec{a} = i + 0.00751 j - 0.01212 k$$

Performing the precise same operations for the \vec{b} and \vec{c} vectors in *Set 1* finds:

$$\vec{b} = -0.01398 i + j - 0.00224 k$$

$$\vec{c} = -0.00342i + 0.0693 j + k$$

Recalling that the workpiece vector for the X plane is represented by \vec{a} , as expanded below:

$$\vec{a} = i + 0.00751 j - 0.01212 k$$

Finally, calculating transitional angle error for each vector coordinate as shown in figure 4-22.

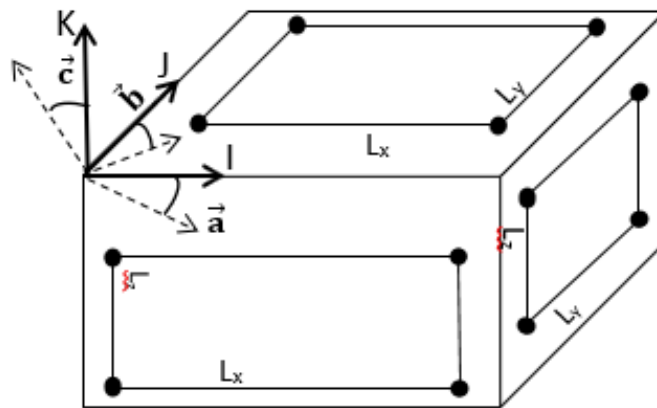


Figure 4 - 22: Illustration of transitional angle error

$$\text{Angle } \vec{a} = \pm \left(\tan^{-1} \left(\frac{\Delta Y}{L_x} \right) + \tan^{-1} \left(\frac{\Delta Z}{L_x} \right) \right)$$

$$\text{Angle } \vec{b} = \pm \left(\tan^{-1} \left(\frac{\Delta X}{L_y} \right) + \tan^{-1} \left(\frac{\Delta Z}{L_y} \right) \right)$$

$$\text{Angle } \vec{c} = \pm \left(\tan^{-1} \left(\frac{\Delta Y}{L_z} \right) + \tan^{-1} \left(\frac{\Delta X}{L_z} \right) \right)$$

Where:

$\Delta X, \Delta Y, \Delta Z$ = Repeatability values

L_x, L_y, L_z = Distance between each detection point.

&

$\Delta X = 0.0408\text{mm}$

$\Delta Y = 0.0650\text{mm}$

$\Delta Z = 0.0413\text{mm}$

$$\text{Angle } \vec{\mathbf{a}} = \pm \left(\tan^{-1} \left(\frac{0.0650}{32} \right) + \tan^{-1} \left(\frac{0.0413}{32} \right) \right)$$

$$\text{Angle } \vec{\mathbf{a}} = \pm 0.190^\circ$$

$$\text{Angle } \vec{\mathbf{b}} = \pm \left(\tan^{-1} \left(\frac{0.0408}{33} \right) + \tan^{-1} \left(\frac{0.0413}{33} \right) \right)$$

$$\text{Angle } \vec{\mathbf{b}} = \pm 0.143^\circ$$

$$\text{Angle } \vec{\mathbf{c}} = \pm \left(\tan^{-1} \left(\frac{0.0650}{30} \right) + \tan^{-1} \left(\frac{0.0408}{30} \right) \right)$$

$$\text{Angle } \vec{\mathbf{c}} = \pm 0.202^\circ$$

The matrix formation of calculating error help to derive a relationship between the workpiece original datum point position and real datum point position. Locating error based on repeatability have been considered in this mathematical model. Consequently, the values determined have been combined to produce an error vector relative of the given plane. The generation of this vector enables the subsequent correction of the datum transitional angle, and by extension fulfils the project aim of increasing the accuracy of the robotic grinding process.

4.2.3 Error Comparison

By considering the effect of datum error and repeatability error values from section 4.1.4, it was considered to reduce the speed to 0.005m/s (1% of 0.5m/s) to achieve a better accuracy level and minimal datum error. Therefore, by following the same mathematical concept the detection process have been demonstrated and the outcome results are presented in the table below. (see **Appendix 4** for readings)

Table 19: Overall outcome results of two different speeds

Speed (m/s) 0.01 m/s (1% of 1m/s)	Speed (m/s) 0.005 m/s (1% of 0.5m/s)
Workpiece Datum Coordinates (mm)	
$X_0 = 10.2433$ $Y_0 = 14.0562$ $Z_0 = 12.3431$	$X_0 = 12.7302$ $Y_0 = 13.2228$ $Z_0 = 13.6362$
Error Value (mm)	
$\begin{bmatrix} \varepsilon_X \\ \varepsilon_Y \\ \varepsilon_Z \end{bmatrix} = \begin{bmatrix} -0.0424 \\ -0.0646 \\ -0.0412 \end{bmatrix}$	$\begin{bmatrix} \varepsilon_X \\ \varepsilon_Y \\ \varepsilon_Z \end{bmatrix} = \begin{bmatrix} -0.01834 \\ -0.02072 \\ -0.01597 \end{bmatrix}$
Error Correction Trajectory	
$\vec{a} = i + 0.00751j - 0.01212k$ $\vec{b} = 0.01364i - j - 0.00294k$ $\vec{c} = -0.00353i - 0.00486j + k$ Angle $\vec{a} = \pm 0.190^\circ$ Angle $\vec{b} = \pm 0.143^\circ$ Angle $\vec{c} = \pm 0.202^\circ$	$\vec{a} = i + 0.01432j + 0.00397k$ $\vec{b} = -0.01230i + j + 0.00201k$ $\vec{c} = -0.01054i + 0.008401j + k$ Angle $\vec{a} = \pm 0.066^\circ$ Angle $\vec{b} = \pm 0.059^\circ$ Angle $\vec{c} = \pm 0.053^\circ$

As can be seen from table 19 the slower the operational speed the less the error is achieved. Positional error of x and y axis are 18 and 20 microns while the z axis is around 16 microns, the difference could be due to the base frame constructed by the robot was more accurate on the z axis than that on the x and y axis. On the other hand, the values showed that the positional error is in the range of 20µm on the lower operational speed (0.005m/s) whereas on the higher speed (0.01m/s) the error range is in 60µm to 40µm.

Remarks

Throughout the investigation procedure and applying the mathematical model, some errors have affected the outcome of the results. The type of error is due to the compliance of robot structures and this can be divided into two categories, 1) Geometrical error, 2) Non-Geometrical error. Geometrical error arises from various machining tolerances of robot components. These errors are mainly caused by improper robot link geometry. Non-Geometrical error are related to the dynamic behavior of the robot, they occur from structural deformations, stiffness and robot compliance.

4.3. Summary

Geometrical error analysis was carried out in this chapter to derive a general relationship between the workpiece and the cutting tool to eliminate the error. This is done by visualizing the performance of robot repeatability and deriving a mathematical model for error compensation to locate the geometry datum points. The proposed method provided an efficient way to calibrate the robot to create the required tool path and produce grinding efficiently. It is a competent method that incorporates an error level less than $30\mu\text{m}$ for locating the datum accuracy in order to start grinding. However, a repeatability tests under three different probing methods have been constructed to visualise the repeatability error accuracy of the measurements. All methods showed different error levels (see section 4.1.4).

According to results, acoustic emission under the minimum speed demonstrated the best accuracy of less than **$30\mu\text{m}$** . Based on repeatability measurements of the relative positions between workpiece and robot datum, a mathematical model is developed to predict the estimated datum. It was observed that the datum error achieved is less also than **$30\mu\text{m}$** which corresponds to the accuracy error found from repeatability. Finally, error correction form transitional angles were established to assess the alignment of the workpiece with the robot coordinate system to support the process monitoring and control strategy that provide a reliable and accurate grinding movement.

Chapter Five. System Compliance Model

Grinding is a process used to remove material from a part in order to acquire the size and form with required surface finish. The grinding interaction between the wheel and the workpiece depends in a number of applied parameters such as depth of cuts, spindle speed, in feed speed and material removal as this will eventually affect the grinding quality. Generally, higher material removal rate means faster production and higher wear rate increases wheel cost (Jin, et al., 2002). In this chapter, an empirical model experiment is designed to obtain a clear and appropriate method to perform grinding for reconstruction of the surface. The goal is to have a maximum workpiece quality, minimum machining time and economic efficiency by making a selective adaptation strategy and chosen parameter. The model will allow grinding cycle to achieve a decent finish level on the surface on the workpiece for reconstruction after weld is applied.

The selection of the optimum grinding cycle parameters depends on the knowledge of grinding process and compliance performance of the robot. In order to compensate the effect of deflections during grinding, it is essential to observe the robot compliance performance in relation to robot grinding infeed and sparking within the cycle. As the magnitude of the grinding force changes with material removal rate and grinding wheel surface condition, it is often necessary to set a conservative operation conditions to perform grinding (Allanson, et al., 1997). This means that most grinding cycles are not optimised for minimum cycle time and take longer time than required. To improve grinding performance, a better understanding of grinding system should be available, the system time constant is a good measure of compliance of the grinding system. The time constant is the combined effect of the system compliance and the grinding forces during deflection between the machine and workpiece Allanson et.al (1997). The compliance represents the rate of deflection per unit force which depends on the geometrical factors of the workpiece as well as the grinding wheel and material properties.

However, a model is required to demonstrate the system performance in relation to the time constant. In the case of cylindrical plunge grinding, the compliance of the system depends on the geometrical factors of the workpiece, such as length and cylindrical diameter from one position to another. The sparking time of grinding cycle is often decided by the time constant Allanson et.al (1997). In case of surface grinding, it is a discrete cutting process system,

therefore the time constant concept is borrowed from cylindrical plunge grinding to enable to work out the number of spark out passes. The proposed model will give a clear insight to build up a reliable method to eliminate the residual error when performing robot abrasive grinding.

5.1. Influential Factors for Robotic Grinding

This chapter demonstrates a build up a strategy to perform robotic grinding for reconstruction of the surface. The procedure involves dressing under two different conditions fine and coarse to observe the best cutting ability based on multiple grinding cuts. After that, grinding is constructed to explore the influence of the time constant on the workpiece material under multiple grinding speeds. This will ease the build up for a strategy to perform grinding in the final model. Influential factors such as the ideal dressing condition and best feed speed is discussed in this chapter to get better understanding of the grinding system.

5.1.1 Dressing

Dressing is a process where the surface of the grinding wheel grains are sharpened to carry out cutting, it is crucial stages of any grinding procedure. In this experiment, the grinding tool is dressed at different speeds rates to observe the best dressing strategy to perform the final grinding model. A single point dresser was used to dress the tool, the reason this particular dresser is used because it is highly effective for 25mm diameter tool and cope with dressing action. Also, gives the robot the flexibility of movement to its joint without any restrictions that may be caused of it arm stiffness. However, the speed of wheel speed is set to 12000rpm, which considered being a normal speed to ensure material does not run out and avoid vibration in the robotic machine. In most common dressing situations, vibration sensors are normally placed at various positions on the machine to check for frequency levels. For this robot, sensors could not be fit for safety purposes.

However, dressing is performed under coarse and fine conditions in order to observe the best conditions to be applied in the final grinding strategy. Both conditions are applied under same depth of cuts but different wheel speeds to observe the effect of the wheel condition. The dressing is performed in a way where a single dress is carried out, and after that a single cut is completed on the workpiece (see figure 5-1). Then the depth of cut is measured to give a clear insight on the effectiveness of the dressing condition. The dressing parameters are as follows:

Fine Dressing (3% of 2m/s) equivalent to 0.06m/s

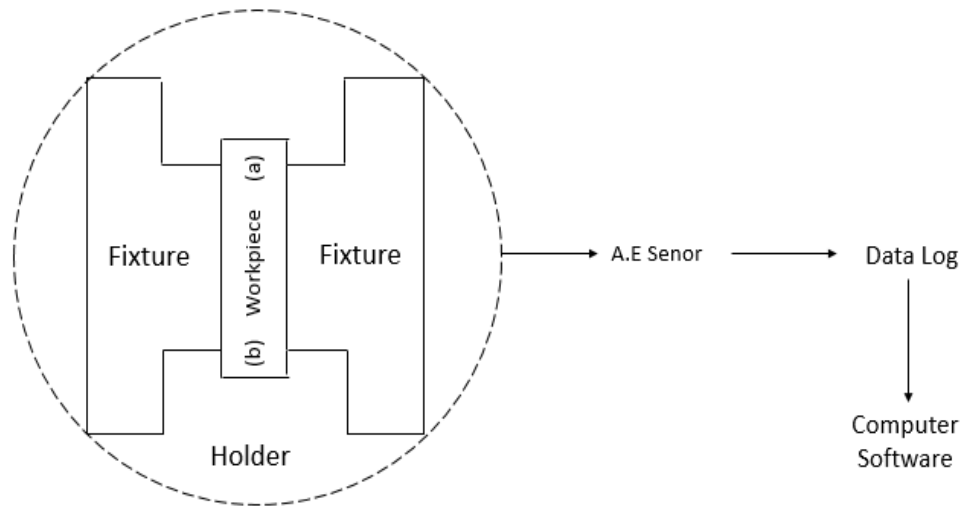
- Grinding Speed
 - 3% of 2m/s equivalent to 0.06m/s
 - 10% of 2m/s equivalent to 0.2m/s
- Robot Wheel Speed - 12000 rpm
- Depth of cut of 0.1mm,0.2mm and 0.3mm

Coarse Dressing (10% of 2m/s) equivalent to 0.2m/s

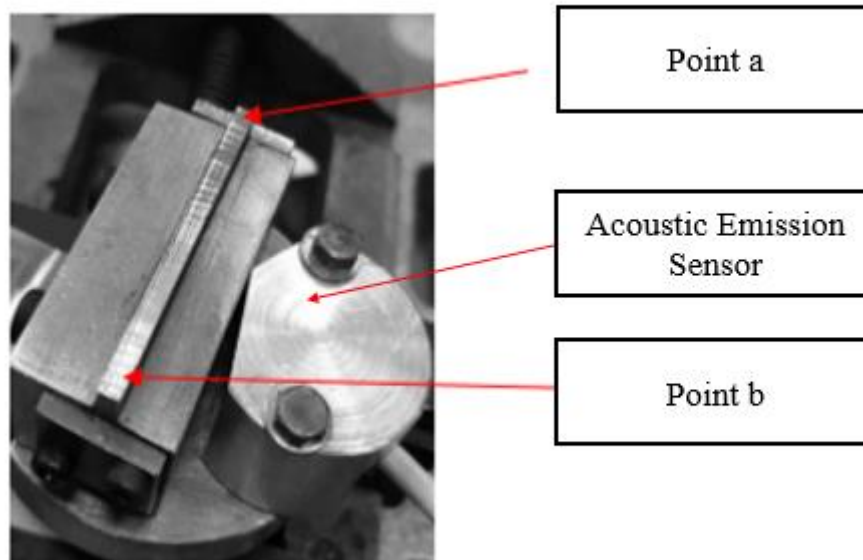
- Grinding speed
 - 3% of 2m/s equivalent to 0.06m/s
 - 10% of 2m/s equivalent to 0.2m/s
- Robot Wheel Speed - 12000 rpm
- Depth of cut of 0.1mm,0.2mm and 0.3mm

5.1.2 Grinding

Grinding is performed under two different speeds, feeds and depth of cuts in order to observe the influence of grinding conditions and estimate time constant to build a reliable model for the repair grinding strategy. For that to be done, the workpiece is clamped in place on the workbench with a sensor connected to it. A force sensor is connected to a computer and Labview6.1Vi and is used to show and record the data whilst wheel and workpiece come into contact with each other, the sensor gives signals to indicate the start of grinding. The robot is fixed in its location and is set so that the arm moves the wheel along the workpiece path from **a** to **b** as shown figure 5-1 below.



(a)



(b)

Figure 5-1: (a) Schematic Diagram for Experimental Setup, (b) Grinding Locations and Sensor illustration

The robot arm moves over from point **a** to point **b** of the workpiece to ensure grinding is taking place correctly, the tool path is constructed manually to ensure the work piece is covered whilst making the cuts. The process as follows:

- Spark out the workpiece once or twice to make sure the surface has no debris
- Measure the thickness of the workpiece using the digital Vernier at points a. and b.
- Complete cuts at 0.3mm depth of cut to ensure material is taken off.
- Record depth of cuts
- Re-measure depth of cut after each cut
- Repeat steps until reach the nominal depth of cut
- Change work speed
- Repeat grinding and spark-outs

The table below shows the overall experimental parameters

Table 20: Experimental parameters of grinding

Experiment Parameters

Grinding Mode	Surface Grinding
Grinding Wheel Material	Aluminium Oxide
Robot Machine	Kuka KR16
Robot Wheel Speed (V_c)	24000 rpm
Grinding Speed (V_w)	2m/s and 1m/s (1%, 3% and 10%)
Depth of Cut (a)	0.3 mm = 300 μ m
Coolant	Dry
Workpiece material	Alloy Steel
Workpiece size	60mm x 6.45mm
Dresser Type	Single Point Tip Dresser
Dressing depth	0.1mm = 100 μ m
Dressing Speed	12000 rpm

5.1.3 Tool Path Generation

Tool path has been created to determine the path that guide the robot cutter to perform grinding. The tool path is generated by referring to the workpiece space cartesian coordinate system using direct teaching on contact points between the tool and the workpiece. The contact points are manually selected as teaching points to feature the shape of the workpiece, the way this is constructed is by creating a zigzag contour over the workpiece and considering the z-height as a cutting plane. This is done by offsetting the boundary by the radius of the cutting tool to give the required offset before material removal as shown below.

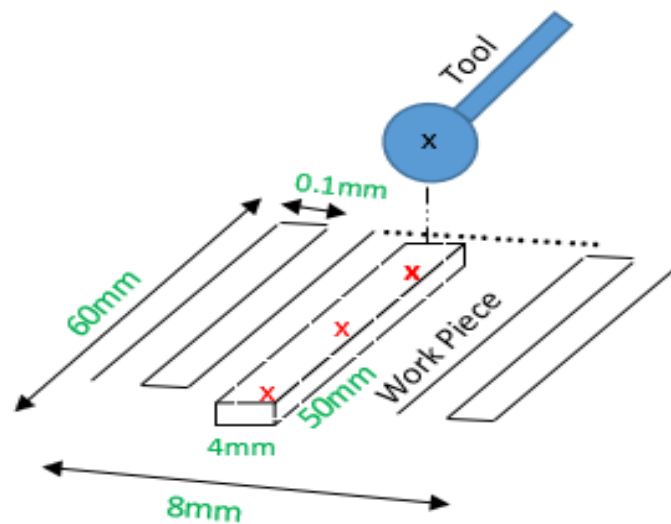


Figure 5-2: Schematic of tool path generation

5.2. Results & Discussions

This section discusses the results gained from the collected data of both experimental procedures. Dressing results is firstly presented in this section to discuss the best dressing condition, then grinding is demonstrated and discussed under different depth of cuts and speeds to build a strategy upon. Table 21 and 22 below illustrates the dressing measurements under both fine and coarse conditions.

Dressing Results

Table 21: Fine Dressing Results

Fine Dressing					
Nominal Depth of Cut (mm)	Initial Depth of cut (mm)	Final Depth of cut (mm)	Real Depth of cut (mm)	Wheel Speed (rpm)	Grinding speed (m/s)
0.1	4.995	4.985	0.01	1200	0.06
0.2	4.985	4.85	0.14	1200	0.06
0.3	4.85	4.61	0.24	1200	0.06
0.1	4.61	4.592	0.02	1200	0.2
0.2	4.592	4.48	0.11	1200	0.2
0.3	4.48	4.3	0.18	1200	0.2

Table 22: Coarse Dressing Results

Coarse Dressing					
Nominal Depth of Cut (mm)	Initial Depth of cut (mm)	Final Depth of cut (mm)	Real Depth of cut (mm)	Wheel Speed (rpm)	Grinding speed (m/s)
0.1	4.31	4.245	0.065	1200	0.06
0.2	4.245	4.085	0.16	1200	0.06
0.3	4.085	4.095	0.01	1200	0.06
0.1	4.61	4.57	0.04	1200	0.2
0.2	4.57	4.42	0.15	1200	0.2
0.3	4.42	4.31	0.11	1200	0.2

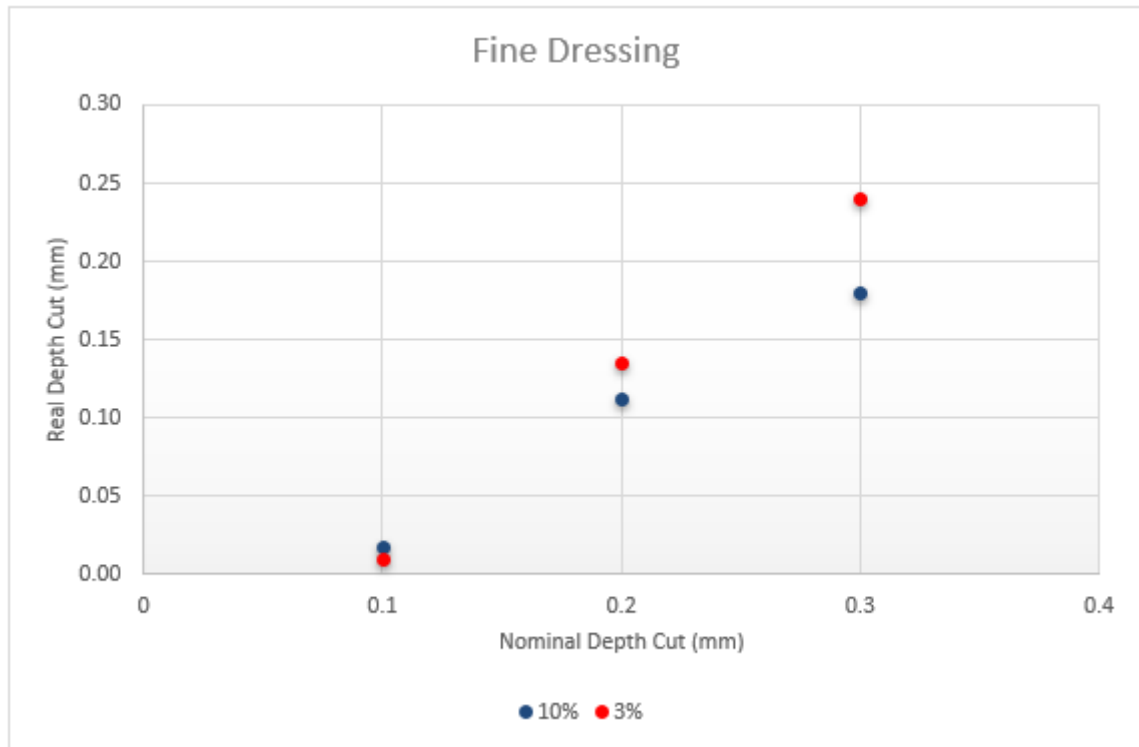


Figure 5-3: Fine Dressing Results

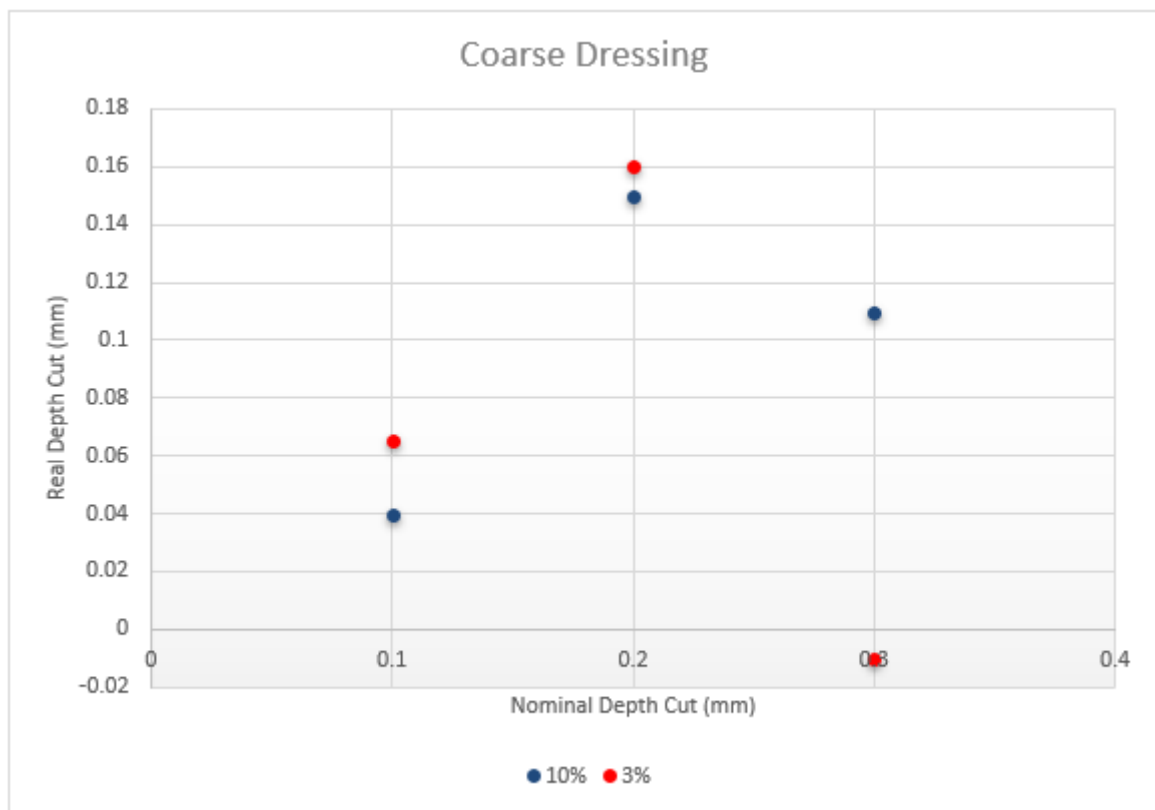


Figure 5-4: Coarse Dressing Results

The results above show both fine and coarse dressing results based on the real and nominal depth of cut when grinding the workpiece. The dressing have been done under three nominal depth cuts 0.1mm,0.2mm,0.3mm were 0.1mm is the limitation of the robot can achieve. Each dressing procedure is performed at two dressings speeds 0.06m/s, 0.2m/s and a wheel speed of 12000rpm to illustrate the effect of both fine and coarse dressing on the results.

Looking at table 21 from fine dressing, the real depth of cut results indicate that material taking off the workpiece is gradually increasing at low increments under both grinding speeds whereas in coarse dressing the material taking off in both conditions is un-stable. For example, figure 5-3 in fine dressing under the speed of 0.06m/s shows the real depth of cut is gradually increasing from 0.01mm to 0.24 under the nominal cut set in the robot. At higher grinding speeds, the real depth of cut demonstrates slower gradual increase then expected, this could be due to the fact that the dressing was taking place before the speed change and the touch point of the workpiece must have affected the real depth of cut.

In another hand, the coarse dressing seems to be unstable whist looking at the real depth of cut results shown in figure 5-4. It can be seen that both grinding speeds, the real and nominal depth of cuts have a 35 % to 65 % variation. This could be because the wheel grain must have been worn out were grains are not removing the intended material from the workpiece after making couple of passes during the grinding procedure. Also, rough dressing causes big wheel wear, which produces high chatter and making it unstable.

The outcome of the results shows that the amount of material taking of the workpiece is much less under coarse dressing than fine dressing. The concept is the higher dressing speed, the less density of cutting edges on the wheel surface which then causes the wheel grains to be removed faster during grinding. The density of the cutting edges increases in fine dressing due to the stability of the grains on the wheel making them less likely to be broken from the surface and being more active when grinding the workpiece. Conversely, in coarse dressing the grains on the wheel are more likely to be broken from the surface of the wheel which makes it weak to cut the material. Therefore, from figure 5-3, fine dressing shows faster gradual increase under 0.06m/s (3% of 2m/s) speed will be carried out for the proposed strategy because of the good level of wheel stability.

Grinding Results

Table 23: Experimental grinding results

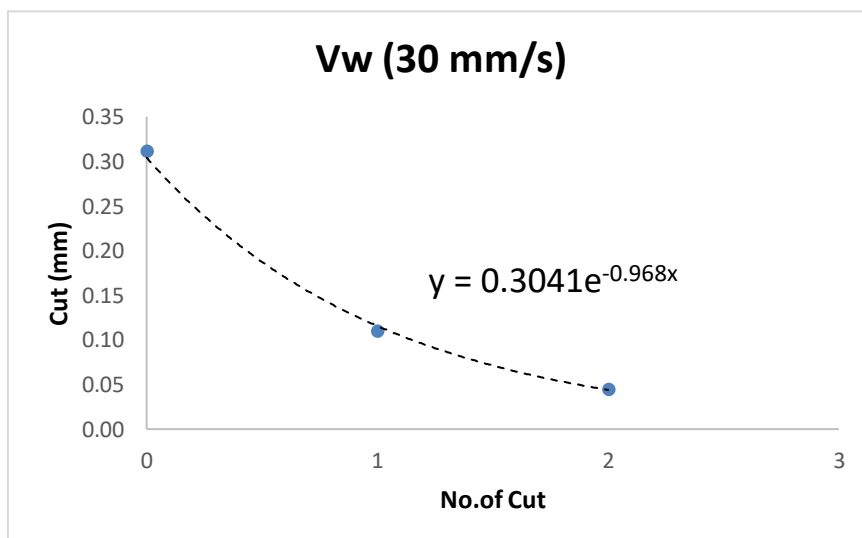
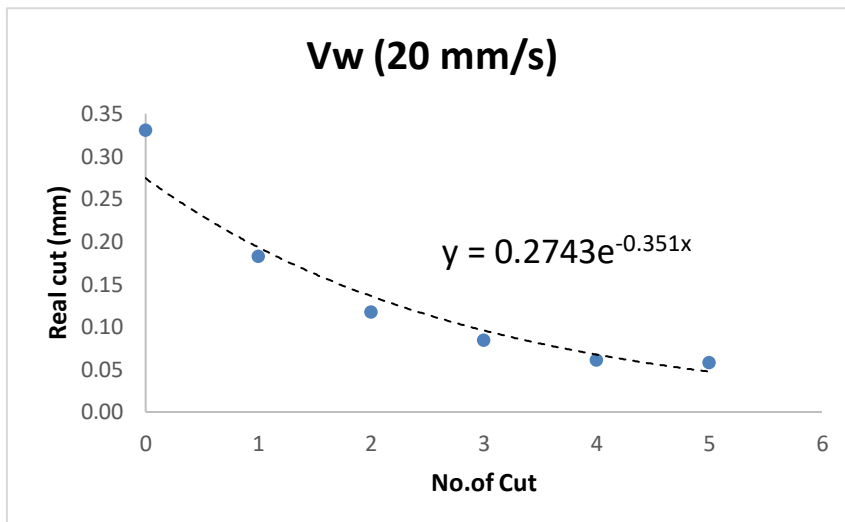
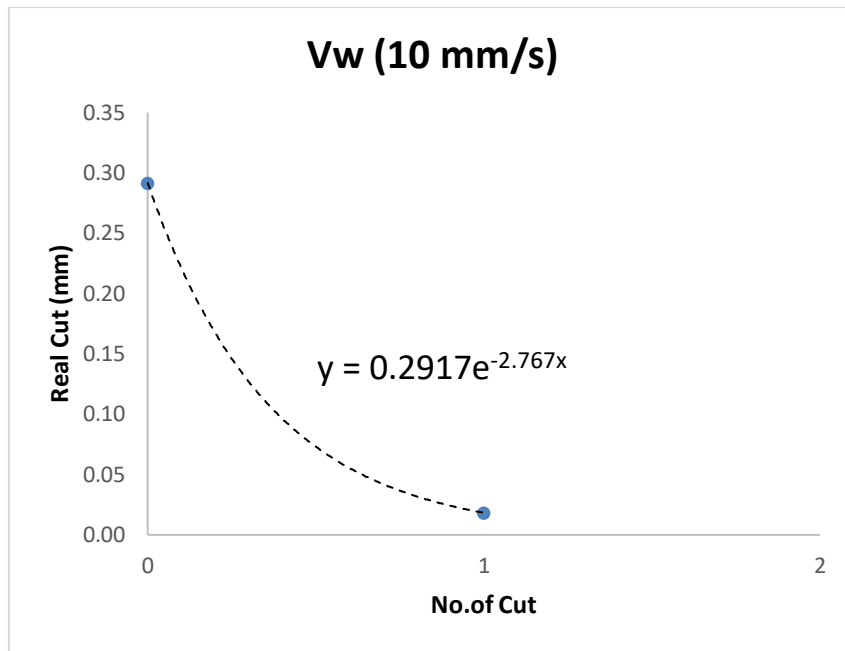
Feed Speed V_w	No. of Spark Cuts	Experimental Depth of cut (mm)	Real Depth of Cut (mm)	Nominal Depth cut (mm)
20mm/s	0	4.07	0.33	3.74
	1	3.92	0.18	3.74
	2	3.86	0.12	3.74
	3	3.83	0.09	3.74
	4	3.80	0.06	3.74
	5	3.80	0.06	3.74
60mm/s	0	3.75	0.31	3.44
	1	3.68	0.24	3.44
	2	3.65	0.21	3.44
	3	3.62	0.18	3.44
	4	3.59	0.15	3.44
	5	3.57	0.13	3.44
	6	3.52	0.08	3.44
	7	3.49	0.05	3.44
200mm/s	8	3.49	0.05	3.44
	0	3.47	0.33	3.14
	1	3.46	0.32	3.14
	2	3.41	0.27	3.14
	3	3.37	0.23	3.14
	4	3.32	0.18	3.14
	5	3.29	0.15	3.14
	6	3.27	0.13	3.14
	7	3.26	0.12	3.14
	8	3.25	0.11	3.14
10mm/s	9	3.23	0.09	3.14
	10	3.24	0.10	3.14
	0	3.32	0.3	2.73
30mm/s	1	3.02	0.29	2.73
	2	2.71	0.02	2.73
	0	4.96	0.30	4.35
	1	4.66	0.31	4.35
100mm/s	2	4.46	0.11	4.35
	3	4.31	0.04	4.35
	0	4.82	0.30	4.52
100mm/s	1	4.54	0.02	4.52
	2	4.51	0.01	4.52
	3	4.50	0.01	4.52

During the infeed phase of a grinding cycle the grinding wheel approaches the workpiece surface and makes contact it starts to remove material. The relationship between the actual and the remaining stock can be used to predict the decay of the remaining stock during the spark out period. The exponential decay of depth of cut during spark outs can be approximately presented as an exponential decay. The relationship can be shown in the expression (Cheng, 2008)

$$A = A_0 \cdot e^{-\frac{t}{\tau}}$$

5- 1

Where, **A** being the remaining stock, **A₀** being the initial stock, **t** is the contact time and **τ** is the time constant estimated of the grinding system. Equation 5-1 can be used to produce a predicted depth of cut for different grinding parameters. The above relationship can then be used together with depth of cut data to estimate the system time constant **τ** during the spark outs. In order to proceed further and design a cycle for grinding using the robot, it essential to take into account the number of spark outs of the feed of the cycle. According to equation 5-1 the removal time constant can be calculated based on the collected data to describe the behaviour of the grinding process as a first order system and is identified from the power decay developed from grinding during the number of spark outs. It is used in this experiment to identify the ideal speed which can be used as a reference to perform in the grinding strategy. Figure 5-5 below illustrates the decay charts based on the experimental cuts of grinding for each speed.



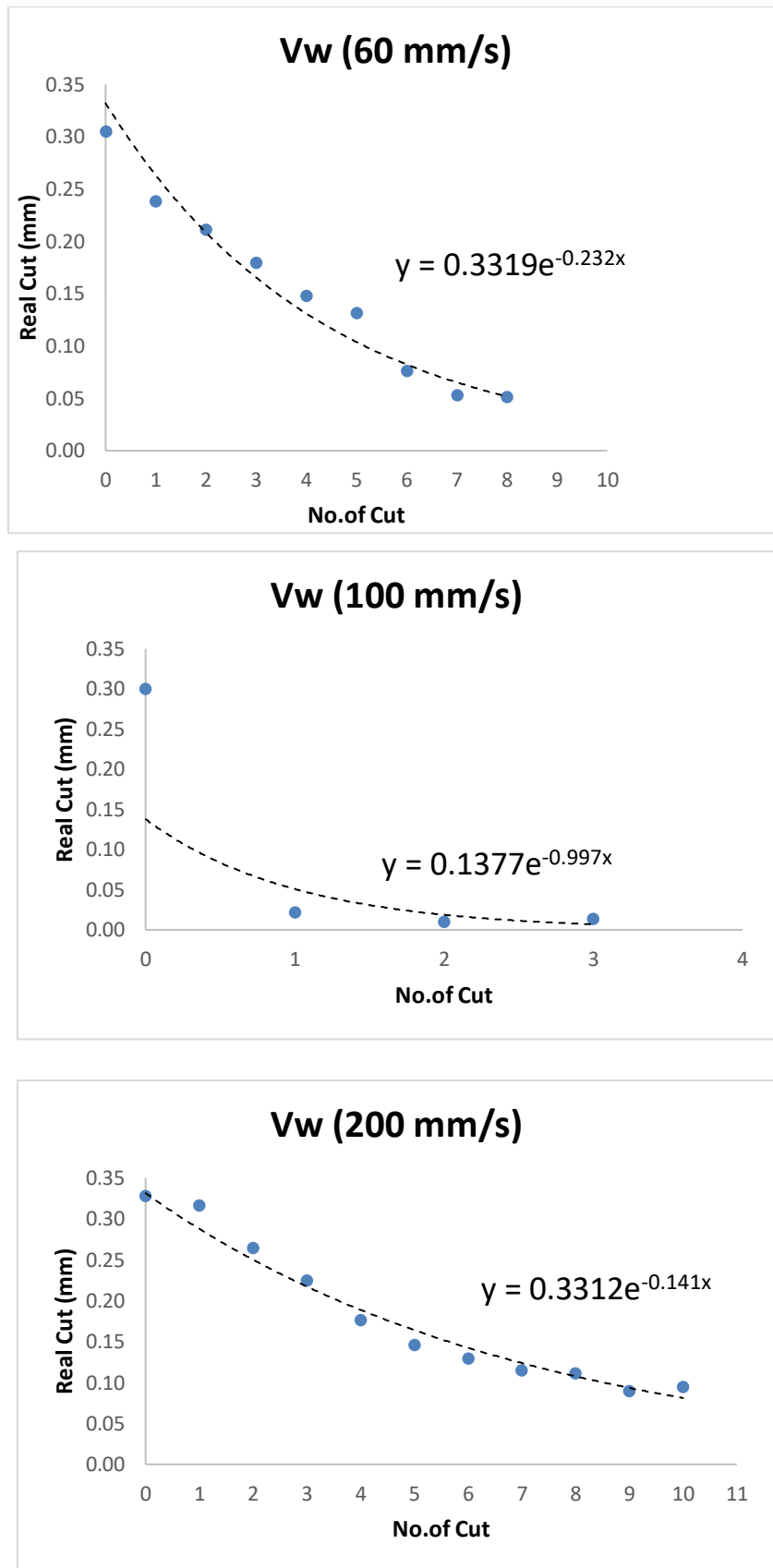


Figure 5-5: Decay Chart for all Selected Speeds

The relationship of the number of cuts and the real depth of cuts during grinding under various speeds is shown in figure 5-5 above. The feed speed and number of cuts obviously have an effect on the material removal during each grinding pass, lower feed speeds take less number of cuts to achieve the nominal depth of cut whereas at higher speeds it takes more time to achieve the nominal depth of cut. For example, at a speed of 20mm/s & 100mm/s, the real cut has been gradually decreasing until reaches stability under 3-5 cuts where nominal cuts have been achieved. Higher speed such as 60mm/s and 200mm/s show stability as it achieves the nominal cut but undertakes more cuts which may not be ideal to choose for time efficiency purposes. Under slower speeds such as 10mm/s, the nominal depth of cut achieved is under 2 cuts which does not show the stability for the wheel in terms of achieving the nominal depth, another reason could be the stiffness of the robot were lower speeds vibrations in the tool tip is more likely to be uncontrolled may cause more material being cut off.

However, the time constant is calculated based on the output of the results of the multiple works speeds and is illustrated in figure 5-6. According to equation 5-1 the removal time constant can be calculated based on the collected data to describe the behaviour of the grinding process as a first order system and is identified from the power decay developed from grinding during the number of spark outs. It can be seen that the time constant demonstrates a good stability of the wheel at speed 20mm/s and 10m/s whereas at 30mm/s, 60mm/s, 100m/s and 200m/s the grinding wheel demonstrates instability to the wheel condition. It becomes very unstable as it reaches 200mm/s work speed where the wheel may have been affected after multiple dressing procedures. The time constant changes due to the condition of the wheel and the wheel sharpness, for that reason higher speeds does not show a good stability of the wheel. Therefore, the ideal grinding speed to be performed in the strategy developed is 20mm/s due to its stability of cutting. Based on these results, a mathematical model developed to estimate the number of a spark outs and number of infeed cycles to reach the minimum residual stock to perform a grinding cycle using the robot.

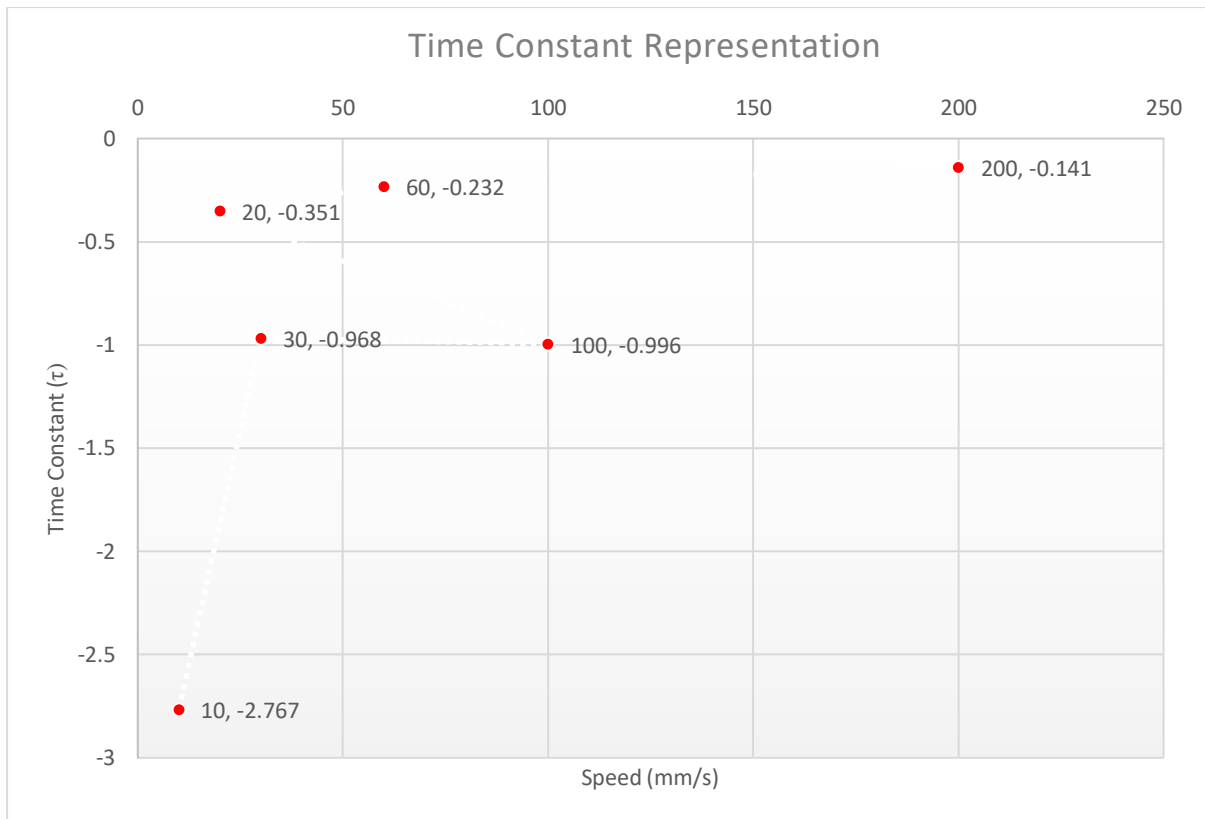


Figure 5-6: Time constant representation graph

5.3. Mathematical Model

To perform a reliable grinding model, it is important to determine the number of infeed and spark outs for each grinding pass. The grinding cycle is strongly affected by main factors affecting the precision of grinding, for example error caused by machining, measurement, reading error due to size shape and positioning accuracy of the workpiece. The selection of the optimum grinding cycle parameters depends on the knowledge of deflections performance of the cycle. Therefore, to compensate the effect of deflections during grinding, it is essential to include a spark out period in the proposed experiment to give us an idea of the infeed rates employed within the cycle as well as the flexibility of the part, grinding wheel and the machine. The time constant characterises the effects of system compliance and the grinding forces. In this experiment, the time constant is used to allow for a more consistent control of spark out time during grinding as shown in section 5.2.

However, during the infeed stage, the wheel is fed into the workpiece at a constant rate due to the deflections reduction of workpiece size lags behind the indicated infeed positions.

Designing the grinding cycle model is firstly started by taking into consideration the infeed stage as the first step, after that spark out cycle is implemented as the residual stock continues to be removed. Figure 5-7 below illustrates the main parameters of the proposed design cycle.

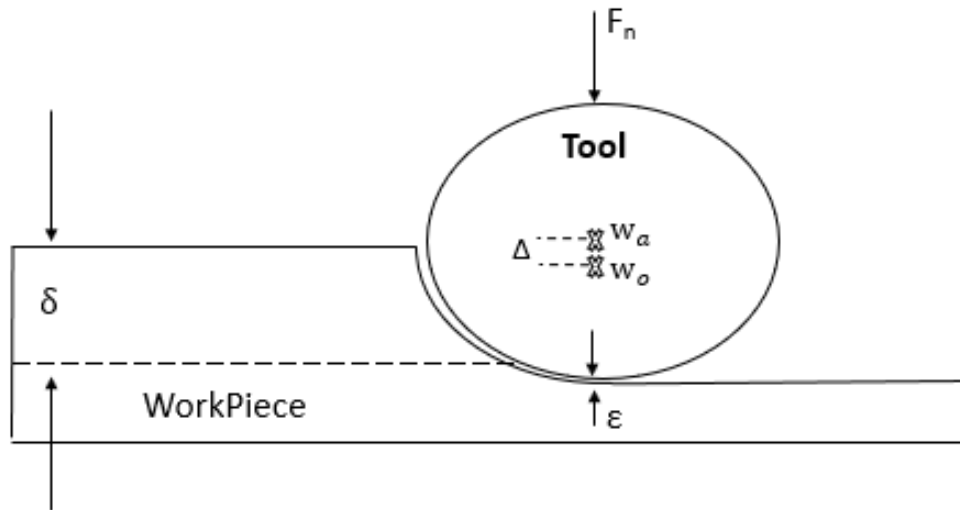


Figure 5-7: Grinding wheel interaction with work piece

Where:

F_n = Normal Force

ϵ = Elastic deformation

δ = Real depth of cut

δ' = Nominal depth of cut

W_a = actual centre of wheel

W_o = Static wheel position

Δ = Static deflection

The amount of deformation is proportional to the normal forces and the real depth of cut during the grinding pass

Where;

$$F_n \propto \delta' \tag{5-2}$$

$$F_n \propto \varepsilon = F_n \propto \delta \tag{5-3}$$

$$\varepsilon \propto \delta \tag{5-4}$$

From hooks law relationship the stiffness (k) is introduced;

$$k\varepsilon \propto \delta \tag{5-5}$$

$$\varepsilon = \frac{1}{k}\delta \tag{5-6}$$

Therefore,

$$\varepsilon = \alpha \delta \tag{5-7}$$

Where α is the coefficient of deformation and $1/k$ is the stiffness. In the spark out stage, the residual stock continues to be removed until the wheel is retracted as shown in figure 5-7 were the grinding wheel is in contact with the workpiece. If the real depth of cut is δ it should theoretically be cut to that position, but due to elastic deformation of the process system, it is elastically deformed due to the tip of the tool and the workpiece and only cuts to δ' . However, the infeed cycle can now be designed by taking into account the number of grinding strokes needed to reach the real depth of cut as shown in the figure below:

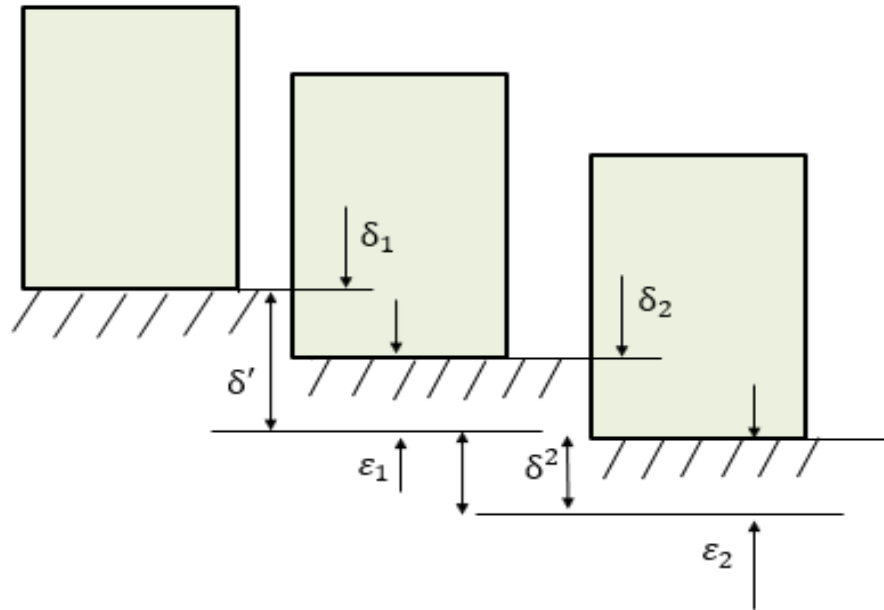


Figure 5-8: Infeed process

If the theoretical depth of cut is δ' , the elastic defamation amount per stroke is $\epsilon_1, \epsilon_2 \dots$ the real depth of cut is as follows:

$$\delta_1 = \delta' - \epsilon_1$$

5- 8

Second stroke

$$\delta_2 = 2\delta' - \delta_1 - \epsilon_2$$

5- 9

Where $\delta_1 = \delta' - \epsilon_1$

$$\delta_2 = 2\delta' - (\delta' - \epsilon_1) - \epsilon_2 = \delta' + \epsilon_1 - \epsilon_2$$

⋮

$$\delta_i = \delta' + \epsilon_{i-1} - \epsilon_i$$

5- 10

Where, i is more number of infeeds in the cycle

Therefore,

$$\varepsilon_1 = \alpha \delta_1 \dots \dots \varepsilon_i = \alpha \delta_i \tag{5-11}$$

$$\delta_1 = \delta' - \alpha \delta_1 \tag{5-12}$$

$$\delta' = \delta_1(1 + \alpha) \tag{5-13}$$

$$\delta_1 = \frac{1}{1 + \alpha} \delta'$$

⋮

Carrying over from previous feed, Therefore,

$$\delta_i = \left[1 - \left(\frac{\alpha}{1 + \alpha} \right)^i \right] \delta' \tag{5-14}$$

Where:

$$\frac{\alpha}{1 + \alpha} = \text{Infeed Ratio}$$

However, the overall actual depth of cut is normally smaller than the total theoretical depth of cut, so the required dimensional accuracy is not achieved. Therefore, it is necessary to carry out the spark out cleaning and gradually eliminate the residual deformation during grinding to achieve the required size as shown in figure 5-9 below.

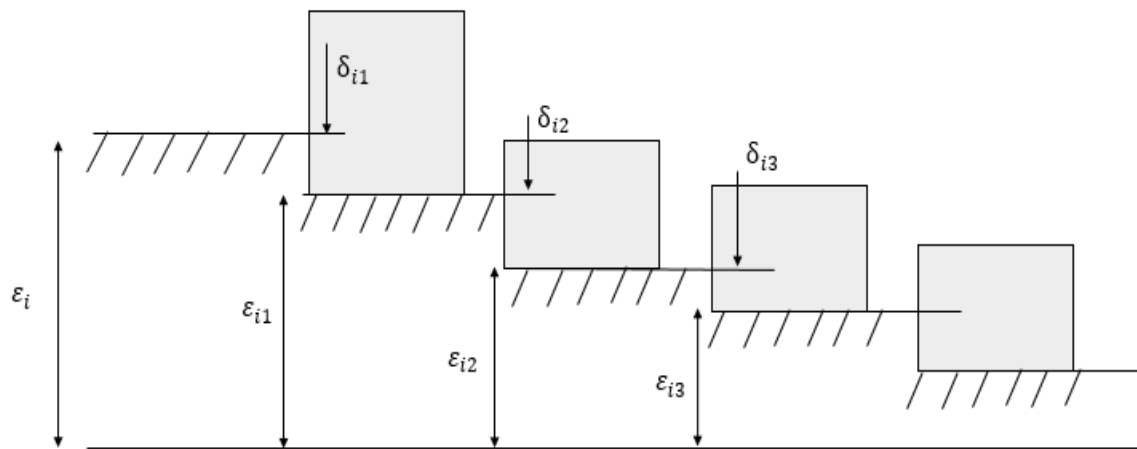


Figure 5-9: Spark-out process

For spark outs cycle design the following model procedure is followed,

First time spark out to achieve the depth of cut;

$$\begin{aligned} \delta_{1i} &= \varepsilon_1 - \varepsilon_{1i} \\ &\vdots \\ &\vdots \\ \delta_{ni} &= \varepsilon_n - \varepsilon_{in(n-1)} \end{aligned}$$

5- 15

Where:

ε_{1i} = first spark out deformation

δ_{1i} = first spark out depth of cut

Where

$$\varepsilon_i = \alpha \delta_i \dots \dots \dots \varepsilon_{in} = \alpha \delta_{in}$$

5- 16

Substituting into Equation 5-12:

$$\delta_{i1} = \frac{\alpha}{1 + \alpha} \delta_1$$

$$\begin{matrix} \cdot \\ \cdot \\ \delta_{in} = \left(\frac{\alpha}{1+\alpha}\right)^n \delta_i \end{matrix}$$

5- 17

Bringing the infeed stroke number from 5-12;

$$\delta_i = \left(\frac{\alpha}{1+\alpha}\right)^n \left[1 - \left(\frac{\alpha}{1+\alpha}\right)^i\right] \delta'$$

5- 18

Note: See appendix 6 for calculations

Remarks

Some source of error may have affected the mathematical calculations developed in this section were the wheel is assumed to be rigid during contact with the workpiece which has an effect on the deflection of the wheel. Another source of error is the robot software used in this experiment does not take into considerations the dynamic feature of the robot, it can only create the robot trajectories from tool path data. Singularity, collision, out of reach, and joint extension the only errors checked when the robot trajectory is generated. Dynamic features are not considered in the calculations which may also have an effect in the results achieved.

5.4. Summary

This chapter demonstrates a compliance model to help design an optimum grinding strategy for reconstruction repair using a robot. The model defines the suitable condition for dressing based on a different work speeds and depth of cuts to observe the effect of wheel condition on multiple passes on workpiece. Results demonstrated that the fine dressing is the ideal condition to be used for grinding because of stability of the wheel condition.

A mathematical model is then developed to build a grinding cycle to define the number of passes required to perform grinding workpiece, the effect of system compliance is compensated by working out the time constant which is used to allow for a more consistent control of spark out time during grinding. It was observed that the best work speed to use for the grinding cycle strategy is 20mm/s because of its stability and time required to achieve the final required depth.

Chapter Six. Grinding Strategy for Repair

Robotic grinding is kind of a manufacturing technique that can effectively contribute towards the manufacturing grinding industry. Despite of the obvious advantages that the robot has such as production flexibility and functional integration. There are still gaps in machining accuracy and surface quality by robotic grinding compared to the CNC machine tools. To further improve the grinding performance capability, this chapter provides a grinding strategy repair that can improve the surface quality of the component. The goal of this chapter is to present a practical method to improve the machining accuracy by compensating the geometrical error to achieve smooth surface finish when performing repair engineering. This chapter illustrates the strategy proposed by discussing each step in detail from creating weld for reconstruction purposes, generation of tool path, contact registration/model alignment to implementation of the theoretical strategy and control followed by the experimentation results and validations.

6.1. Component Repair Strategy Development and Validation

The set up for this experiment is constructed as shown in figure 6-1. At first the process parameter is adjusted where the operational speed is set for the robot arm and tool. Secondly, welding is created on random positions on the surface of the block so that the model can be scanned using a 3D scanner to generate a tool path that can be implemented into the robot to perform grinding. Thirdly, contact registration between the robot arm and the workpiece is constructed using Acoustic Emission sensor for accurately detecting the points to define the datum of the block. After that, the model is aligned to locate the workpiece with the actual tool path profile by compensating the geometrical errors. Finally, grinding is performed and results and validations are illustrated. The following stages is illustrated in the flow chart below;

Grinding Strategy Repair Flowchart

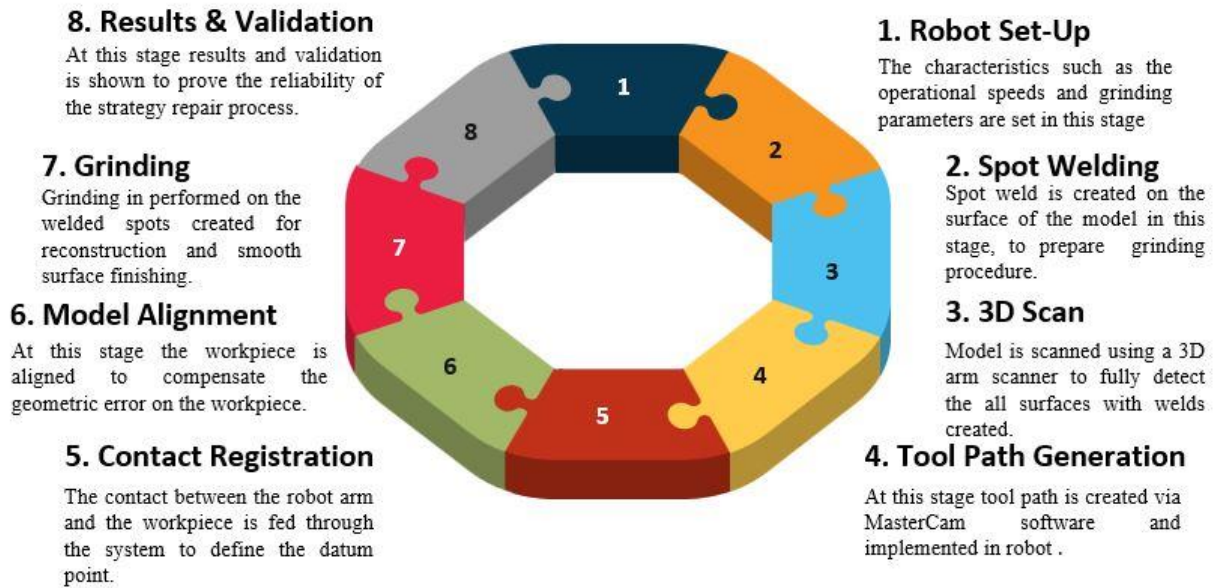


Figure 6-1: Grinding Strategy Flow Chart

6.1.1 Robot setup and grinding parameters

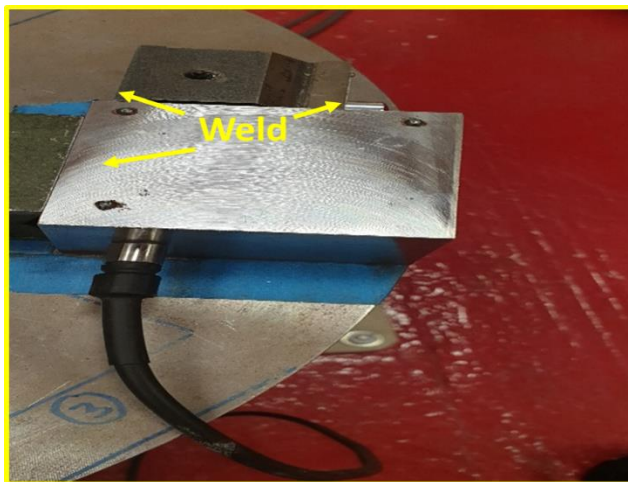
This stage defines the initial set up of the robot such as coordinate system, tool calibration, base calibration and motion specification, see chapter 3 for more details. It also defines the parameters which sets the conditions of the experiment. These physical parameters were chosen based on the working knowledge of the robot by the faculty. The control variables such as speed, depth of cut and dressing type is based on the outcome results shown in chapter 5. Table 24 illustrates the parameters for this repair strategy.

Table 24:Grinding Strategy Experimental Parameters

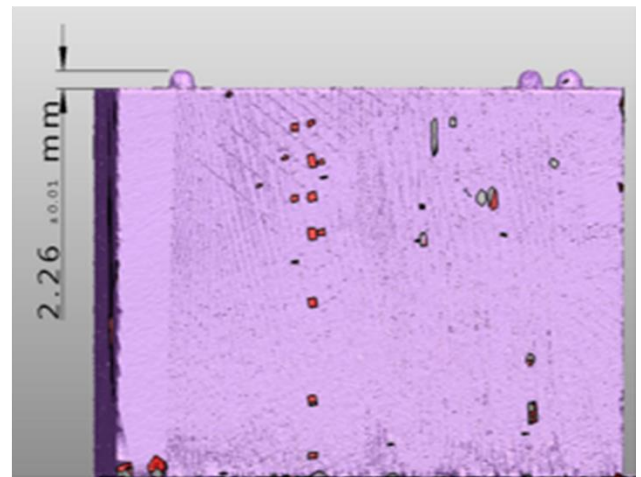
Grinding Mode	Surface Grinding
Grinding Wheel Material	Aluminium Oxide
Robot Machine	Kuka KR16
Robot Wheel Speed (V_c)	24000 rpm
Wheel Radius	12.5mm
Feed rate (V_w)	20mm/s
Depth Cut	0.3 mm
Coolant	Dry
Dressing Condition	Fine Dress

6.1.2 Spot weld & 3D scan

A weld at random positions of the workpiece is created at this stage, so that the model can be scanned using a 3D scanner to generate a tool path that can be implemented in the robot to perform the grinding operation. This is a general way to perform repair engineering where small welding in small zones on the block is welded on the workpiece to ease grinding and return to its original shape. Figure 6-2 below shows the weld positions created on the block with the 3D model scan as well as the size of the weld created



(a)



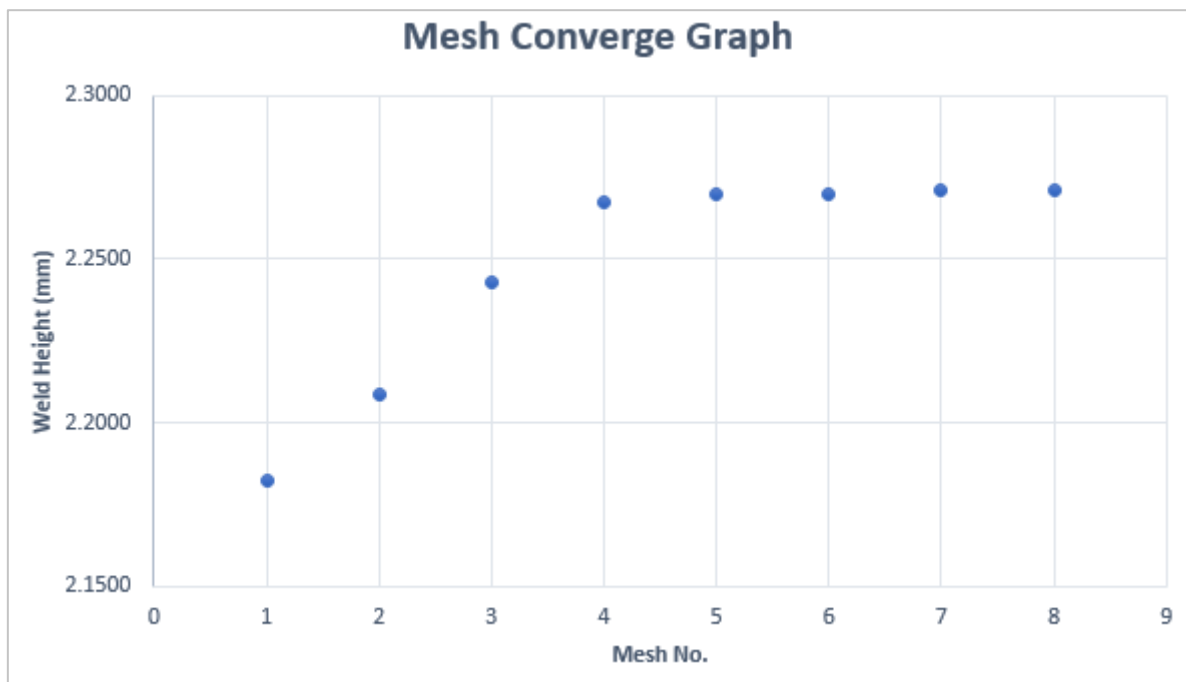
(b)

Figure 6-2: (a) Weld view of the block, (b) weld size measurement

Mesh generation is important in order to achieve a good set of results. Meshing the top surface of the model is significant in order to detect the welds created and provide accurate results. Therefore, some considerable skill is required to generate a suitable shape of grid by specifying the number of points in the X, Y and Z direction of surface domain. The increase in memory sizes and processing speed of computers has enabled finer and finer mesh to be generated. Due to time and memory size of the computer used for the current model the maximum number of cells were made up to 1,000,000 points on the top surface and relatively less number of points in all sides. Mesh converge graph is made in order to determine the best type of mesh to be used to detect the weld. The height of the weld is greatly affected by convergence to provide accurate results. The density of the mesh only needs to be increased on areas where weld is created, where weld is not generated only a few points are required. The process is repeated until the solution is not changing from run to run. The table below illustrates the overall mesh results along with the mesh converge graph that gives the best results for accuracy purposes.

Table 25: Mesh convergence results

Mesh No.	No. of Points	Weld Height (mm)	Approximate Time
1	120,000	2.1823	20 Sec
2	201,600	2.2088	40 Sec
3	427,392	2.2432	1 Min
4	683,827	2.2671	3 Min
5	943,682	2.2699	9 Min
6	1,009,739	2.2700	13 Min
7	1,132,418	2.2711	15 Min
8	1,358,901	2.2726	20 Min

**Figure 6-3: Mesh Converge Graph**

From the figure above it can be seen that by increasing the density of each mesh the height of the weld increases to a point where it becomes steady. Mesh 6 is the most appropriate mesh to use due to the CPU time and space. Mesh 6 resulted to a maximum height of 2.2700 comparing to mesh 7 and 8 which gave a similar result but took a longer time to run and more space was used. In this way, the accuracy of the mesh is verified so that the tool path can be generated to be implemented to the robot software.

6.1.3 Toolpath setup

Tool path generation is a significant step in robot grinding. The trajectory tool path in robots robotic is based on the relationship of tool location and workpiece interface. Creating the tool path data exists using Robot Master CAMs software package which is linked to the robot used. Accurate tool paths produce a machined surface within the tolerance zone resulting to good surface finish. Inaccurate tool paths result to undercutting (i.e. beyond the tolerance limit) or overcutting (i.e. more than the allowable limit) or both. Therefore, efficiency is measured based on time spent on tool path generation and actual machining time.

To accomplish these goals, the generation of tool path system should possess the ability to increment the tool across the design surface correctly and efficiently. Individual tool positions must be at a level where its free from both overcuts and undercuts. Therefore, when the optimal tool path is to be obtained, various specific constraints must be observed such as stock level, step over, offset surface is critical to be designed. Table 24 below illustrates the tool path details constructed in this experiment. See **Appendix 5** for tool path program

Table 26: Tool path setup parameters

Tool Parameters				Cut Parameters				
Type of Path	Dia. (mm)	Height (mm)	Stock Size	Spindle speed rpm	Step over mm	Depth of cut mm	Retract default	Clearance default
Zigzag	26.12	40	Same as weld size	3500 rpm	0.4 mm	0.3 mm	25 default	25 default

One of the fundamental parameters in tool path generation is the **step-over**. This parameter is the offset between each path created and is the most important parameter in determining the quality of the finished part. Once tool path is generated, an important factor to take into account is the step-over (the stock left over between the offsets) as shown in the figure 6-4 below.

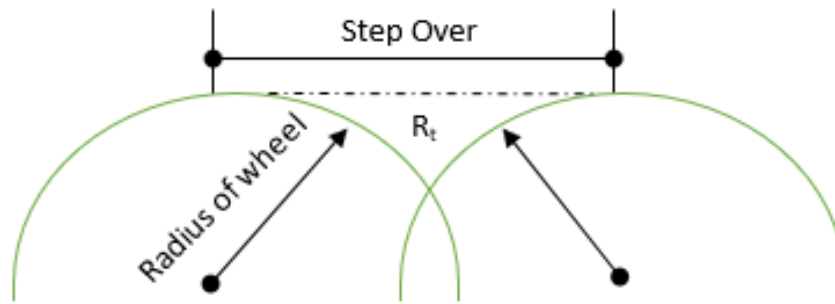


Figure 6-4: Stepover schematic

Where R_t is maximum step of over calculated

The residual stock is an illustration of the stock left over called scallop. Many efforts have been spent to develop a tool path algorithm to minimise the scallop and avoid stock leftovers. According to literature, one of the effective ways to minimize stock level is by creating a step-over between $1/3$ and $1/5$ of the tool diameter depending how well the material can hold details (mach, 2011). For a given step over, the larger the tool and smaller the scallop which means you get a better surface finish and less stock level built. Obviously, this will work very well if a bigger tool was fit into the whole geometry, which is very rear in robot grinding. However, in this experimental work a 26.12mm lollipop ball mill tool is used to fit into robot chuck. Considering the cutting time, material, geometrical error, kinematic error and machining process error the toolpath step over is calculated to a controllable factor so that it does not become a major influence on results achieved. The maximum achievable error is calculated by taking into consideration $1/3$ of the maximum achievable geometrical error. calculation of step over of is as follows:

Radius - 13.06mm

Maximum achievable geometrical error - $20\mu m$

Step over level - $\frac{1}{3}$ of tool diameter

$$\frac{1}{3} \times 20\mu m = 0.007 \text{ mm}$$

$$\sqrt{13.06^2 - (13.06 - 0.007)^2} = 0.417\text{mm}$$

The calculated step over is approximately 0.8mm. Therefore, it is important to consider other machining errors such as kinematic error and process error. For conservative reasons the step over is reduced to 0.4mm through the grinding process.

6.1.4 Contact Registration and Model Alignment using Acoustic Emission

This section focuses on prober location and model alignment. The procedure is assessed based on repeatability of acoustic emission were points is detected on each surface of the model to work out the geometric error and datum reference as shown in chapter 4. Hence, the error model based on repeatability is developed towards the collected data to observe closely the error correlation when setting up a datum. After that, the model is aligned directly to the robot which aims to increase the accuracy of the grinding processes using the robot. See chapter 4 for details.

6.1.5 Theoretical Grinding Analyses

One of the several common types of grinding is surface grinding which has been widely adopted in today's industry. Surface grinding is commonly used as a final finishing operation, its performance has the most significant effect on the overall productivity. The selection of the grinding cycle parameters depends on the knowledge of deflection performance of the grinding cycle. Therefore, a theoretical model is designed to obtain a clear and appropriate grinding cycle to perform grinding for reconstruction of the surface to achieve a smooth surface finish using the robot (see chapter 5.3). The goal is to have the maximum work piece quality, minimum machining time and economic efficiency by making a selective adaptation strategy and chosen parameter selection.

The optimum grinding cycle behaviour is affected by the deflections between the grinding wheel and the workpiece resulting from the grinding force and system stiffness. Therefore, to compensate the effect of deflections during grinding, it is essential to observe the number of in-feeds and spark outs within the cycle. As a key variable in the proposed grinding cycle, the time constant is estimated first for monitoring the material removal of the workpiece, according to equation 5-1. The removal time constant was calculated based on the collected data to indicate the ideal infeed speed. The ideal speed used is 20mm/s for the current strategy cycle. The grinding cycle is proposed in a way where a weld is created at a random position on the

block. After that, the workpiece is located based on multiple point contact registration were tool path is generated.

The cycle is demonstrated where the roughing, finishing and sparkout stages is observed (see figure 6-5). In the roughing stage, the initial contact between the workpiece and the grinding wheel removes the actual material from the workpiece until it becomes steady. During this process, the operating parameters such as spindle speed, feed rate were kept constant and depth of cut is set to 0.3mm. Within the finishing process the depth of cut of 0.1mm is set to minimal to avoid damaging the component. During these stages, the material continues to be removed from the workpiece and monitored by the acoustic emission sensor to give feedback to the operator of material removal. The theoretical model developed to predict the material removal in roughing, finishing and sparking process to achieve high accuracy level. The cycle has been divided into three main stages 1) roughing 2) finishing and 3) Sparking as shown below.

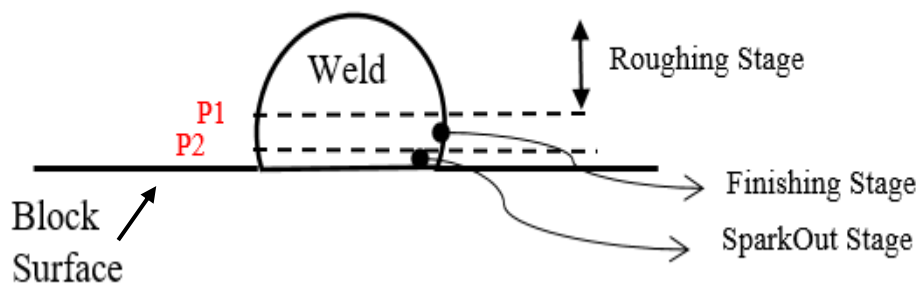


Figure 6-5: Schematic view of weld and block surface.

Grinding Cycle Control

The principle of the grinding cycle is to observe a control strategy based on the weld created to perform grinding. The numerical model developed in chapter 5.3 give a clear indication of the strategy with reference to the geometry and the weld created to reconstruct the surface of the workpiece. Figure 6- 6 below shows a schematic diagram of the expected location at which the depth of cut removes the material. The weld created at the surface of the block is 2.27mm according to the measurement from the 3D scan. During the roughing stage, the influence of the depth of cut at the first path has been used to calculate the coefficient of deformation in the system, which is proportional to the normal forces and the real depth of cut. The theoretical

model suggests that the roughing stage requires a seven number of cuts, two finishing cuts and two number of spark outs to achieve the target of a smooth surface level with minimum residual. These need to be controlled in a way were the weld is completely removed from the surface of the block without making any damage. The diagram illustrates a schematic diagram of the expected locations during each stage based on the theoretical model.

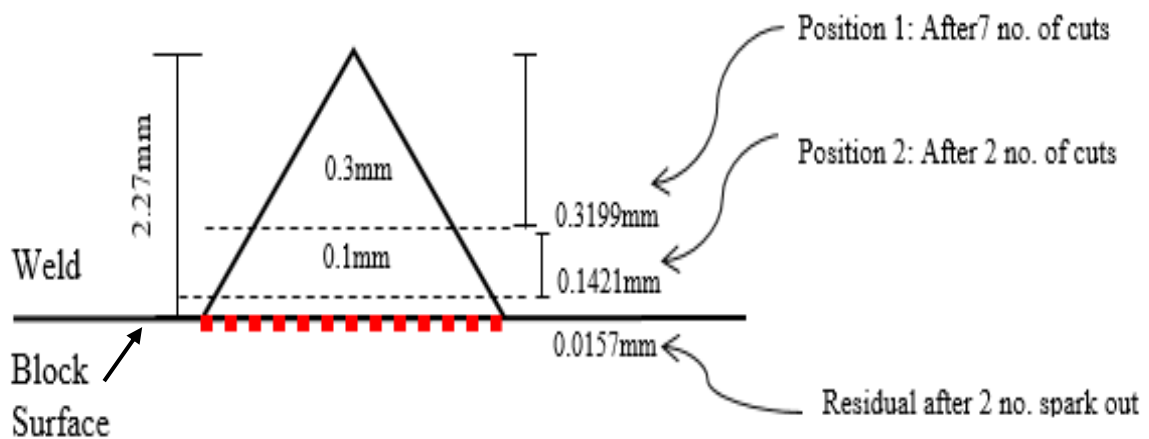


Figure 6-6 – Theoretical schematic view of material removal depth of cut

The calculations demonstrate the theoretical procedure of defining the roughing, finishing and sparking process in the developed grinding cycle. Figure 6-7 and 6-8 below demonstrates the results of the theoretical calculations from the roughing and finishing stages. Refer to **Appendix 5** to see full calculations.

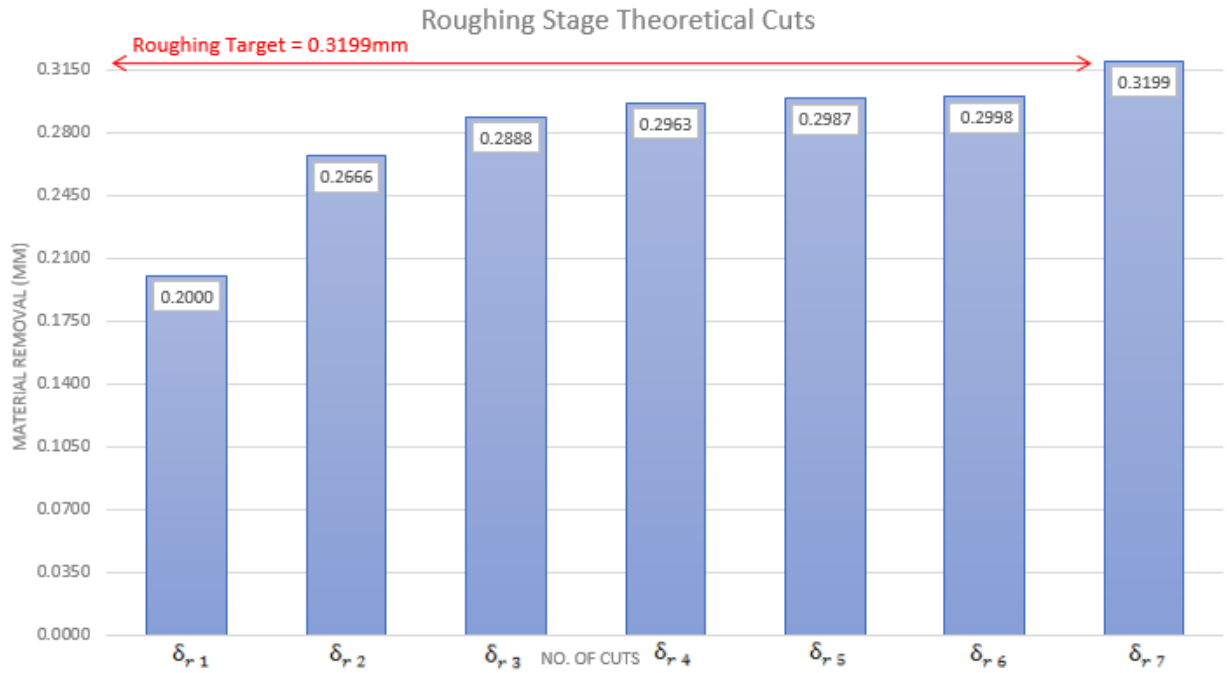


Figure 6-7: Roughing Stage Theoretical Cuts

According to roughing stage, a seven number of roughing cuts is required. Therefore, Position at which roughing ends is as follows:

$$\delta_{r_1} = 0.200, \delta_{r_2} = 0.2666, \delta_{r_3} = 0.2888, \delta_{r_4} = 0.2963, \delta_{r_5} = 0.2987, \delta_{r_6} = 0.2998, \delta_{r_7} = 0.3199$$

Therefore,

$$2.27 - 0.200 - 0.2666 - 0.2888 - 0.2963 - 0.2987 - 0.2998 = \mathbf{0.3199}$$

Where **2.27mm** is the height of the weld form the surface of the block.

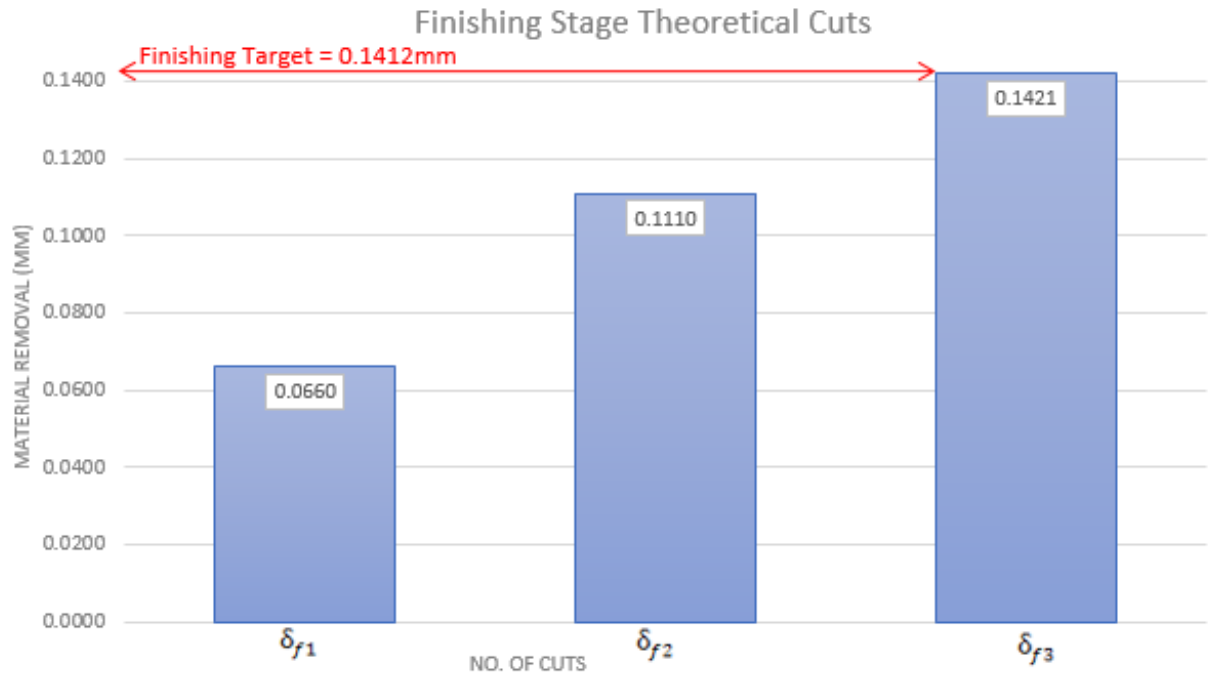


Figure 6-8: Finishing Stage Theoretical Cuts

According to finishing stage, a two number of finishing is required. Therefore, Position at which finishing ends is as follows:

$$\delta_{f1} = 0.066, \delta_{f2} = 0.111$$

Therefore;

$$0.3199 - 0.066 - 0.111 = \mathbf{0.1421}$$

Where **0.1421mm** is the amount of residual left on the surface. This needs a couple of spark outs to achieve the final finish

Finally, the spark out stage is used to approach the final dimension after the infeed stages. On the last finishing stage a few additional passes is made until no sparks is visual and minimum residual is achieved.

Where;

$$\delta_{i1} = 0.0473, \delta_{i2} = 0.0157$$

The information regarding to the number of infeed and spark out required is validated experimentally in the next section

6.1.6 Experimental Results & Validations

This stage verifies the theoretical cycle experimentally to confirm the reliability of the model. Throughout the roughing stage, a seven number of cuts has been established according to the theoretical model; in each stage, the robot tool cuts the material at a controlled depth of cut of 0.3mm to ensure the removal of the weld. As can be seen from the results in table 27 below, the real depth of cut in the roughing stage is ultimately increasing from 0.1967 mm to 0.2933mm. This is due to the influence on the abrasive grains on the wheel in the contact area on the wheel due to the high forces affecting the wheel from stiffness of the joint. However, as the roughing stage proceeds the material is been cut as expected for each roughing stage. The table below illustrates the results collected from the experimental results.

Table 27: Experimental Roughing Results

Roughing Stage					
<i>Speed (mm/s)</i>	20				
<i>Block Size (mm)</i>	49.44				
<i>Weld size (mm)</i>	2.27				
<i>Overall height of block and weld (mm)</i>	51.69				
<i>Nominal Depth of cut (mm)</i>	0.3				
No. Cuts	Readings			Average	Real Cut
0	51.69	51.7	51.74	51.71	0.00
1	51.50	51.51	51.53	51.51	0.1967
2	51.31	51.32	51.31	51.31	0.2000
3	51.00	51.01	51.00	51.00	0.3100
4	50.71	50.70	50.71	50.71	0.2967
5	50.41	50.42	50.39	50.41	0.3000
6	50.14	50.12	50.11	50.12	0.2833
7	49.83	49.83	49.84	49.83	0.2933
Position 1 – The end of roughing stage					0.4030

Finishing Stage					
Speed (mm/s)	20				
Block Size (mm)	49.44				
Weld size (mm)	2.27				
Overall height (mm)	51.71				
Nominal Depth of cut (mm)	0.1				
No. Cuts	Readings			Average	Real Cut
1	50.03	49.99	50.03	50.03	0.090
2	49.92	49.93	49.93	49.93	0.110
Position 2 – The end of finishing stage					0.2130

After the roughing stage have been completed, the finishing stage is performed in order to remove the remaining residual and improve the surface finish the workpiece geometry. This is achieved by removing a thin layer of weld left on the workpiece. In this stage, the depth of cut is set as 0.1mm to carry out the finishing cuts which is the minimum infeed capability of the robot can demonstrate. The material is removed at approximately 0.1mm as expected during the three finishing cuts reaching 0.2130mm of residual stock. In grinding nature, the residual stock is formed due to the deformation of grinding forces in grinding wheels and deterioration of machining accuracy. Figure 6-9 below shows a schematic diagram of the results obtained from the experimental results.

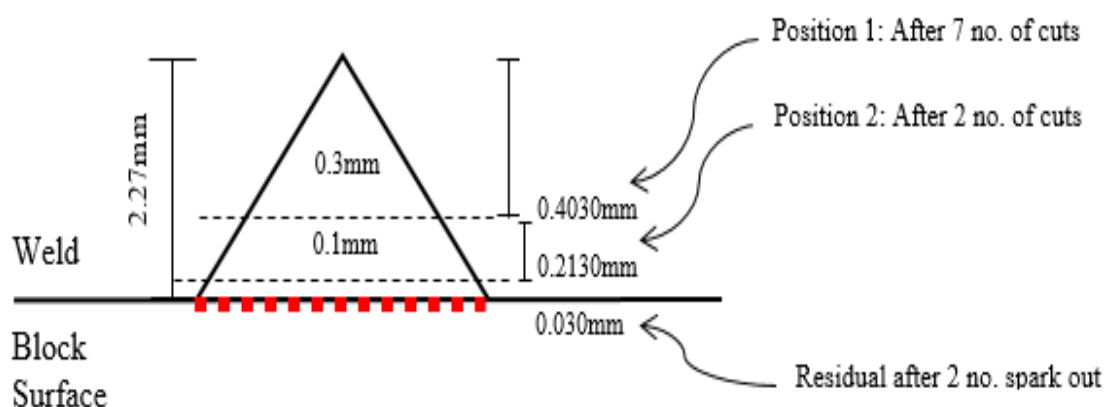


Figure 6-9: Experimental schematic view of material removal depth of cut

Table 28 below illustrates a comparison between both experimental and theoretical values obtained in this strategy.

Table 28: Experimental results comparisons

Roughing Theoretical Real Cut							
1	2	3	4	5	6	7	Position 1
0.200	0.2666	0.2888	0.2963	0.2987	0.2995	0.2998	0.3199
Roughing Experimental Real Cut							
1	2	3	4	5	6	7	Position 1
0.1967	0.2000	0.3100	0.2967	0.3000	0.2833	0.2933	0.4030
Finishing Theoretical Real Cut							
1	2	Position 2					
0.0666	0.1111	0.1421					
Finishing Experimental Real Cut							
1	2	Position 2					
0.090	0.1100	0.2130					

Roughing Stage Theoretical/Experimental Cuts

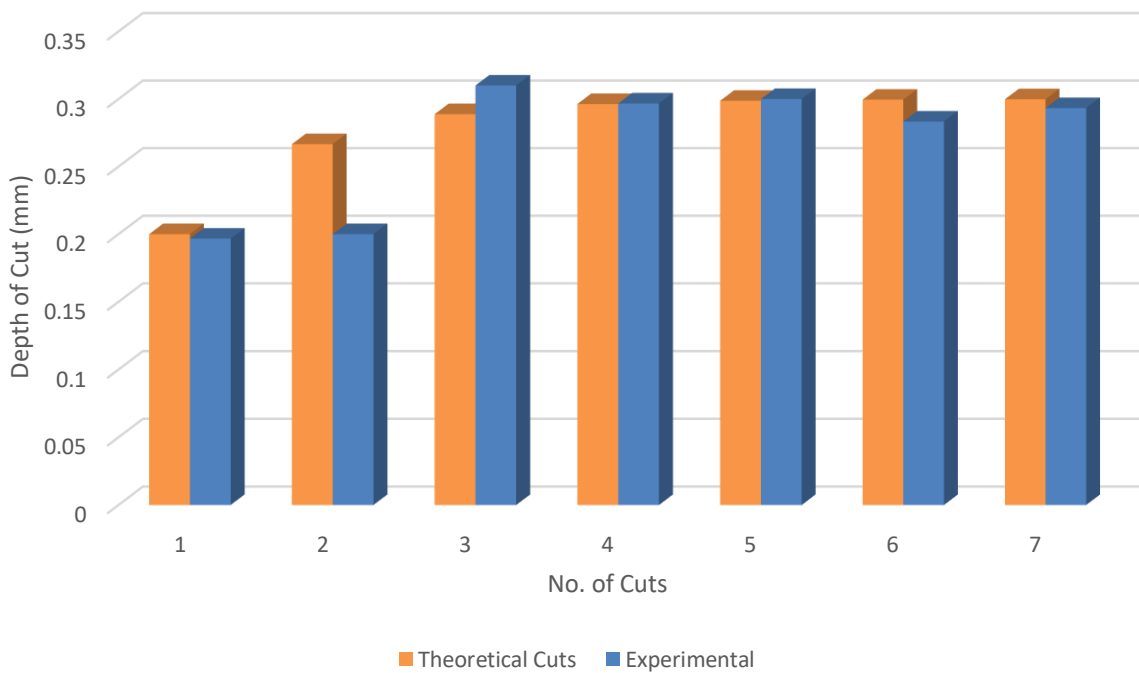


Figure 6-10: Roughing Stage Comparison

Finishing Stage Theoretical/Experimental Cuts

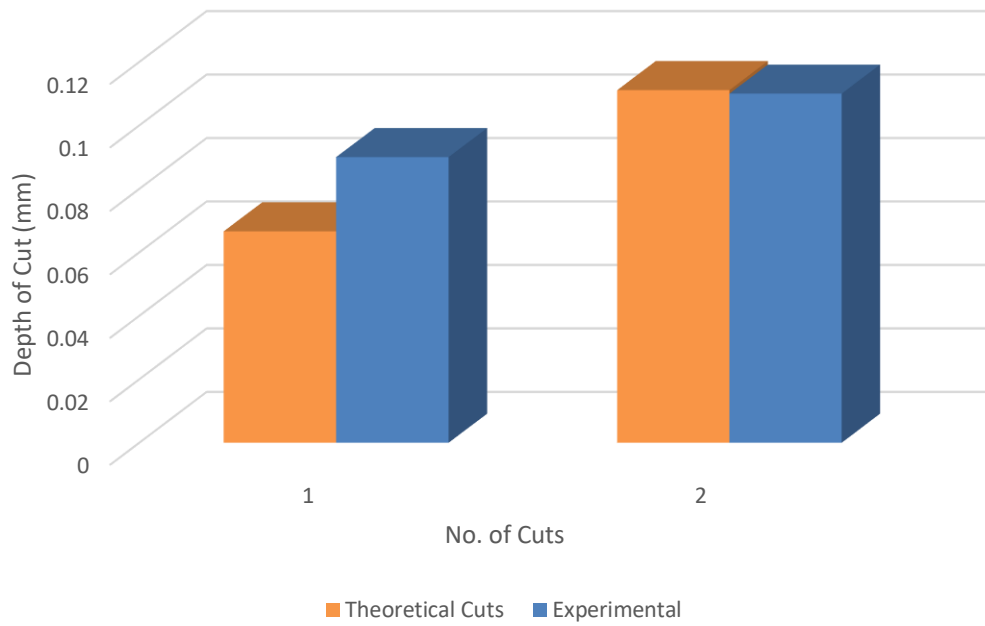


Figure 6-11: Finishing Stage Comparison

Achieved Position Chart

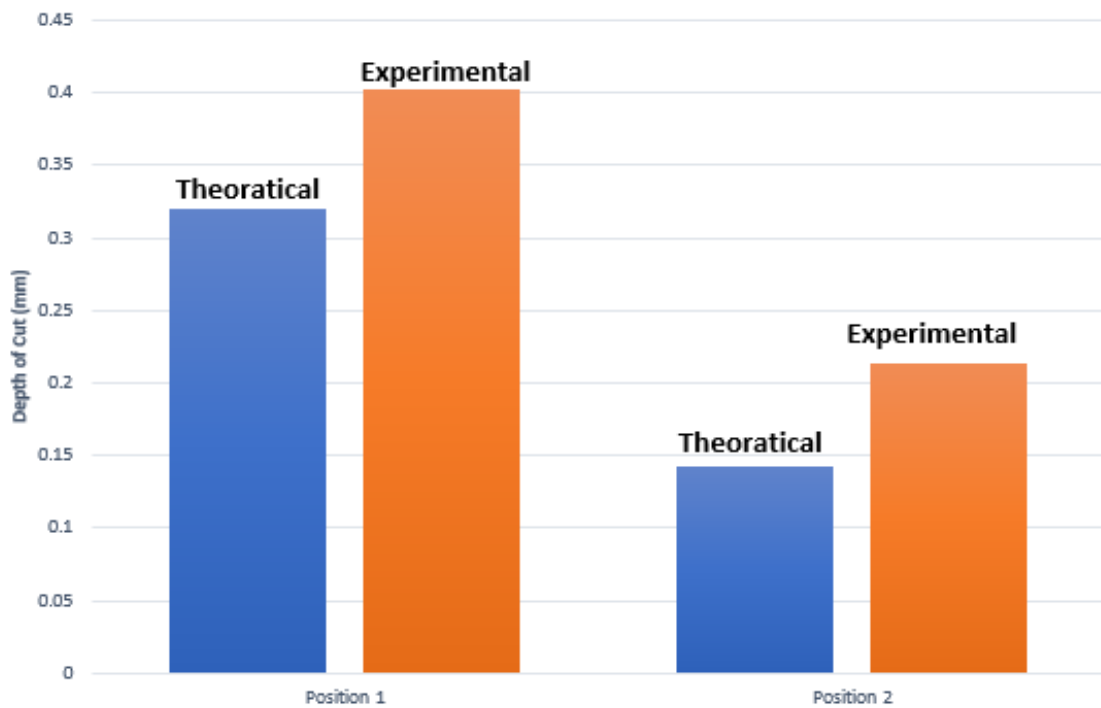


Figure 6-12: Final achieved positions

It can be seen from figure 6-10 to 6-12 and table 28 that there are some minor discrepancies on each cutting depth of cuts, during grinding operation the grinding wheel is deformed by the grinding forces causing the stock removal of the workpiece. This residual stock removal of the workpiece causes low machining efficiency and deterioration of machining accuracy. Due to the robot rigidity at a small area, the coefficient of deformation α value calculated had an effect of the results because it was only calculated through the first cut. Also, the abrasive grains and the contact area were not taken into account in the calculations which affects the contact stiffness of grinding wheel which is normally supported by the stiffness of single abrasive grain as well as the contact area between grinding wheel and workpiece. It is known that the higher the surface roughness the lower the residual of workpiece and the higher the contact stiffness of grinding wheel (Yamada, et al., 2013). From such a viewpoint, this project aims to investigate the total grinding accuracy in order to perform grinding and not the effect of stiffness during grinding. Therefore, grinding operation was carried using a single grinding wheel and residual stock removal of the workpiece was measured based on the depth of cut and calculations performed.

However, at the position at which the finishing stage ends, a number of spark outs have to be carried out to ensure material is completely removed to smoothen up the surface. The advantages of sparking outs is to provide closer tolerances by removing the remaining stock, therefore a number of two spark outs have been made according to the theoretical strategy and a stylus machine is used to measure the area to observe how much residual material left. The machine allows to capture the contour profiles of the boundary using a single probe to observe how much material is been removed from the surface of the block as shown the figure 6-13 below.

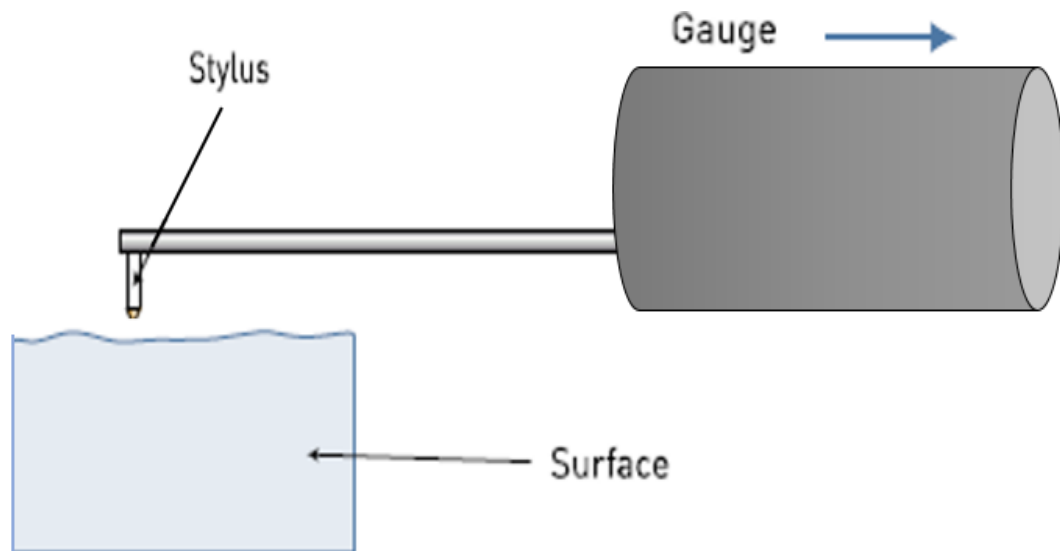


Figure 6-13 – physical profile measurement view

The stylus machine is used to measure the contour profile on the surface of the block (Hobson, 2011), figure 6-14 and 6-15 below show the contour profile after grinding at the location at where the weld is created. It can be seen that the residual is approximate 30 microns below the surface level, this could be due to large forces generated in the wheel caused from the stiffness of the robot. Also, there is a lip created due to the tool being lift of the surface of the block which is due to an error related to the dynamic behaviour of the robot which mainly occur from structural deformations, stiffness and robot compliance. The effect of these conditions is difficult to control. The control restrictions in the robot were the maximum of depth of cut is limited to 0.1mm along with the angle between the grinding spindle axis and surface tangent (usually 45°) overt the entire grinding process. This eventually causes errors between the tool and geometry resulting to unexpected material on the surface of the block.

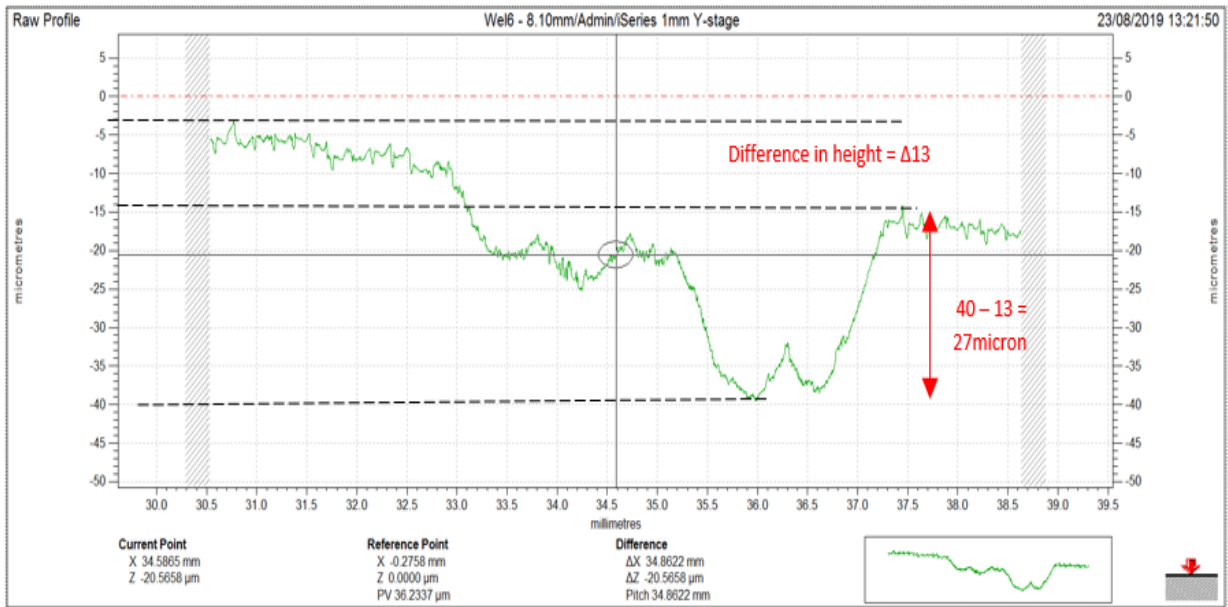


Figure 6-14: Surface profile of grinding area

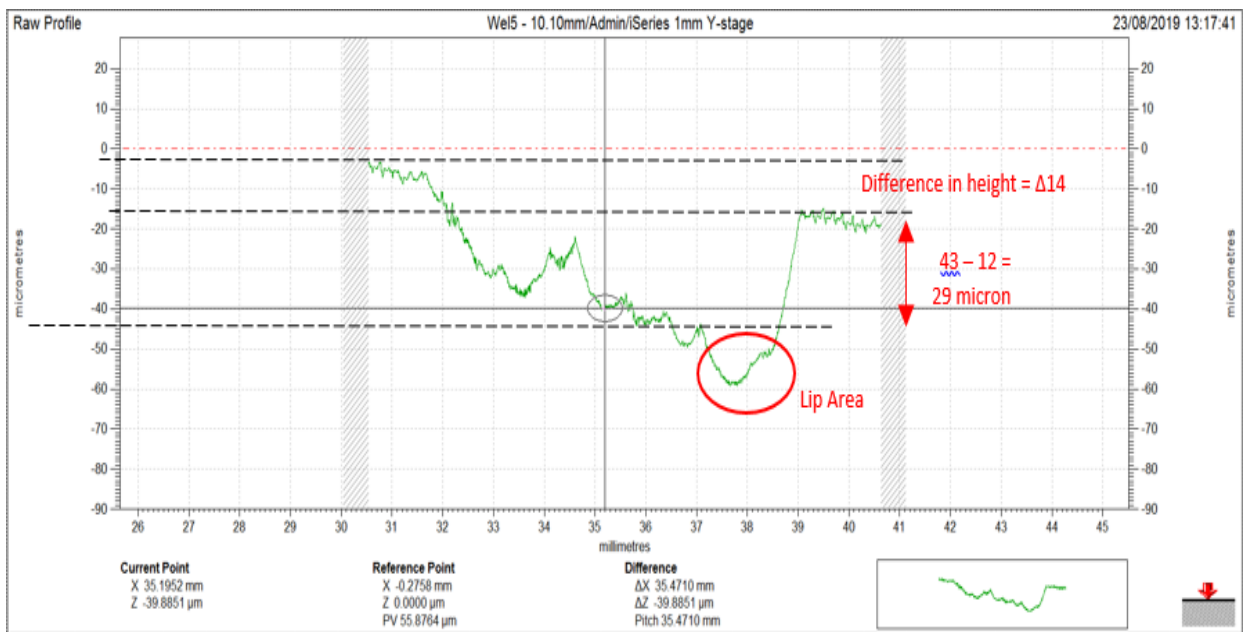


Figure 6-15: Surface profile of grinding area

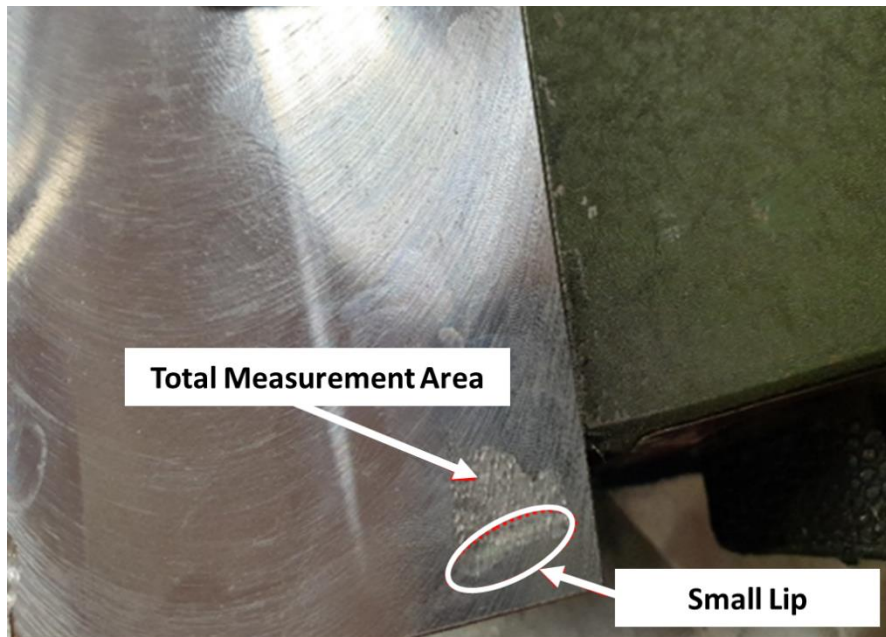


Figure 6-16: Detection of total measurement area

It can also be seen from figure 6-16 that chatter is generated on the workpiece. The generation of chatter is based on the fact that the tool cuts a surface during the previous revolution causing the arm joint to vibrate simultaneously in the directions of the cut affecting the cutting forces as well as the depth of cut. The conventional wisdom is that this is due to the obvious fact that the robot is much less stiff than CNC machine. The reason for this chatter generation is due to the lack of sensor information for force information, which produces chatter marks on the surface of the workpiece and may cause less dimensional accuracy, tool life and damage to the machine. Also, the robot joints normally categorized generally as either prismatic (linear) or revolute (rotation) joints. Preventing unwanted motions possess more challenging design problem, which can significantly affect the performance. Finally, the total repair accuracy achieved is 30micron using the robot. This proves that the strategy is efficient and could be used for repair engineering.

Remarks

Machining parameters of the robot such as the spindle speed, depth of cut, load and lubrication caused process dependent error. The robot structure transmits forces to the workpiece that eventually affects the depth of cut. Lubrication is one important factor affecting the quality of the final product as it contributes to avoiding chatter. Forces increase and produce vibrations on the robot TCP (Top Center Point) which interacts with the workpiece making the surface of the work piece becoming not as smooth as expected. The combination of process parameters, thermal effect on chip formation and waviness on the surface of workpiece are caused by the vibration of the cutting tool.

6.2. Summary

This chapter discusses the developed grinding cycle to improve the machining repair accuracy. Based on the tool-workpiece contact measurement and using acoustic emission sensing technique, the workpiece datum is estimated and aligned to the robot system to allow the generation of the tool path. The strategy applied to effectively to perform grinding for component repair using the robot. The mathematical model is used to define the number of passes required to perform the repair grinding, the repair accuracy level achieved is **30 μ m** which is controlled by considering the process influential variables, such as depth of cut, wheel speed, feed speed, dressing condition and system time constant. The proposed method provides a good level accuracy for using robot in grinding where it is believed it could help designers and manufacturers to control the final accuracy for repair work.

Chapter Seven. Conclusion

Robotic machining is an effective technique that aims to revolutionize the manufacturing industry. This thesis aims to establish a geometrical relationship between workpiece reference datum and tool probe using acoustic emission sensing technique. The error level is assessed based on the repeatability and defined measuring points on the surfaces of the workpiece. A compliance model is then designed to build an optimum grinding cycle by defining the best dressing condition, infeed speed and number of passes (spark-outs) required to verify the final grinding and repair machining. The goal of this thesis has been achieved where the developed method has improved the machining accuracy using the robot. The following points conclude the findings of this thesis work;

- The geometrical datum error has been developed based on the relationship between the workpiece and the cutting tool using three methods, Mechanical, Electrical and Acoustic Emission sensing technique. According to results, acoustic emission under the minimum speed demonstrated the best error accuracy. Based on repeatability measurements of the relative positions between workpiece and robot datum, a mathematical model is developed to predict the estimated datum. It was observed that the geometrical datum error achieved is less than **30 μ m**, which corresponds to the accuracy error found from repeatability. This supports the process monitoring and control strategy to provide a reliable and accurate grinding movement using the robot.
- A compliance model was built to help design an optimum grinding cycle by reconstructing the surface of the workpiece. The model defines the best dressing condition and infeed speed based on time constant at a discrete level to give a good indication of the compliance performance system to form a solid base for the grinding cycle. It was observed that the best speed to use to perform grinding is 20mm/s due to the condition of the wheel and time taken to achieve the required depth of cut. After that, a mathematical model is designed to determine the number of passes required to carry out grinding procedure for repairing the workpiece.

- The grinding cycle is implemented experimentally for verification. The developed grinding cycle has improved the machining repair accuracy to a level of **30 μm** . The error has been controlled by considering the process variables such as depth of cut, wheel speed, feed speed, dressing condition and system time constant which is the key for controlling the robot to conduct grinding process. It is believed it could help designers and manufacturers to control the final accuracy for machining a product

The novelty in this research have been fulfilled by developing a method to define the geometrical error accuracy by using the cutting tool as a probe whilst using acoustic emission monitoring technology that modifies robot commands accordingly. Also, a novel mathematical model is developed for compensating machining errors in relation to its geometrical position by utilising system relaxing technique. Finally, a novel improvement of repair accuracy by taking advantages of abrasive machining that has minimum depth of cut which provides a suitable solution for precision measurement for to repair components in manufacturing and maintenance operation using a robot in many industrial sectors.

Chapter Eight. Recommendations & Future Work

Robotic grinding has made significant improvements in the machining efficiency by the efforts of both academic and industrial sectors. Despite to the advantages the robot has, there still gap for improvements and future work. This chapter suggests some future work and recommendations in order to gain better accuracy when performing robotic grinding. From the author point of view, the following recommendations and future work could be put in place;

Rigidity Map

Developing a rigidity map for a given point within the robot working envelope to ease many possible joint configurations of the robot for a given machining path, If the rigidity map is known easily this may give better machining quality. We all know that robots have accuracy problems due to low arm stiffness, one way to scale down this issue is by reducing the arm reach design to decrease the effect of error and increase robot stiffness.

Chatter Control

Vibration of robot tool structure is a major limitation of the robotic machining applications. The frequency of arm causes the generation of chatter that may damage the surface being machined. Given the fact that the stiffness of a robot arm may cause machining errors and chatter, more research and experimental work is required to avoid any sort of error affecting the chatter.

Compliance Control

Robot machining efficiency such as machining large components has barely been investigated due to the limited robot rigidity, payload, feed rate, depth of cut and cutter diameter. All variables must be kept small as this limit the material removal rate and machining efficiency. One way to do that is by considering the dynamics structures of the robot and theoretically implementing into a software that takes into consideration the all sorts of error as this may improve the robot machining accuracy as well as efficiency. Good force and position control in robotic grinding aims to reduce the surface roughness of parts and pays less attention to the accuracy of form and position.

References

- Allanson, D., Rowe, W. B. & Boyle, A., (1997). Automatic Dwell Control in Computer Numerical Control Plunge Grinding. Issue 1.
- Bagci, E., (2009). Reverse Engineering Applications For Recovery of Broken or Worn Parts and Re-manufacturing: Three Case Studies. *Advances in Engineering Software*, 40(6), pp. 407-418.
- Baptista, R. & Simoes, J. A., (2010). Three and five axes milling of sculptured surfaces. *Journal of Materials Processing Technology*, 103(1), pp. 398-403.
- Batako, A. & Goh, S., (2014). Workpiece roundness profile in the frequency domain: an application in cylindrical plunge grinding. *The International journal of Advanced Manufacturing Technology*, 72(1), pp. 277-288.
- Berth, J., Vasselín, E., Lefebvre, D. & Dakyo, B., (2005). Determination of the Repeatability of the Kuka Robot Using the Stochastic Ellipsoid Approach. *IEEE International Conference on Robotics and Automation*, pp. 4336-4344.
- Bisu, C., Cherif, M., Gerard, A. & Nevez, J., (2011). *Dynamic behavior analysis for a six axis industrial machining robot*. Bucharest, Proc ICASAAM.
- Boothroyd, G. & Knight, W. A., (2006). *Fundamentals of Machining and Machine Tools*. Florida: Taylor and Francis.
- Borisenko, A. I. & E., T. I., (2012). *Vector and Tensor Analysis with Applications*. New York: Dover Publications.
- Brink, J., Hinds, B. & Haney, A., (2004). Robotics Repeatability and Accuracy: Another Approach. *Texas Journal of Science, Robotica*, 27(3), pp. 149-156.
- Caggiano, A. & Teti, R., (2013). CBN Grinding Performance Improvement in Aircraft Engine Components Manufacture. 9(1).
- Chaiyaprat, S. & Rujikietgumjorn, S., (2008). Modelling of Positional Variability of Fixture Workpiece due to locatinf Error. *Journal of Manufacturing Science and Technology*, 2(121), pp. 273-281.
- Chang, C., Chen, S. & Chang, C., (2000). Application of neural network for improving the quality of five axis machining. *Journal of Engineering Manufacture*, 214(1), pp. 47-59.

Chen, F., Zhao, H., Li, D. & Chen, L., (2019). Robotic grinding of a blisk with two degrees of freedom contact force control. Volume 101.

Cheng, K., (2008). *Fundamentals Applications and Practices*. s.l.:pringer Science & Business Media.

Chen, J. S., Huang, Y. K. & Chen, M. S., (2005). A study of the surface scallop generating mechanism in the ball-end milling process. *International Journal of Machine Tools & Manufacture*, Volume 45, pp. 1077-1084.

Chen, L., (2014). A workcell calibration method for enhancing accuracy in robot machining of aerospace part. 85(1-4).

Chen, T. & Ye, P., (2012). A tool path generation strategy for sculptured surfaces machining. *Journal of Materials Processing Technology*, 127(1), pp. 396-373.

Chen, Y. & Dong, F., (2013). Robot Machining: Recent Devalopment and Future Issue.. 9(66), pp. 1489-1497.

Chen, Y. & Fenghua, D., (2013). Robot Machining: Recent Development and future research issues. Volume 66.

Chiles, V., Black, S., A.J, L. & Martin, S., (2002). *Principles of Engineering Manufacture*. Massachusetts: Butterworth-Heinemann.

Choudhuri, S. & DeMeter, E., (1999). Tolerance Analysis of Machining Fixture Locations. *Journal of Manufacturing Science and Engineering*, 121(2), pp. 273-281.

Cui, H. & and Zhu, Z., (2006). Error Modelling and Accuracy of Parallel Industrial Robots. 1(5).

D.J, S., Jin, T. & Corbett, J., (2002). High efficiency deep grinding of a low alloy steel with plated CBN wheels. 51(1).

Damle, G. & Gadit, J., (2015). Task Programming of Robotic welding using touch sensing principle. 2(5).

David, C., (2012). *Robotic Industries Association*. [Online] Available at: www.robotics.org [Accessed 17 10 2017].

Dix, B., (2004). Aerofoild machining and polishing combined into a single automated process. *Aircraft Engineering and Aerospace Technology*, 76(5).

Draper, N. R. & Harry, S., (1998). *Applied Regression Analysis*. New York: Wiley-Interscience.

Dumas, C., CAro, S., Garnier, S. & Furet, B., (2011). Joint stiffness identification of six-revolute industrial serial robots. 27(4).

Durgumahanti , U., Singh, V. & Rao, P., (2010). A new model for grinding for prediction and analysis. 48(12).

El Mansori, M., Sura, E., Ghidossi, P. & Deblaise, S., (2007). Toward physical description of form and finish performance in dry belt finishing process by a tribo-energetic approach. 182(1-3).

Epson, (2015). <https://epson.com/For-Work/Robots/6-Axis/Epson-C8-Compact-6-Axis-Robots/p/RC8-A701ST75SS>. [Online] Available at: <https://epson.com/For-Work/Robots/6-Axis/Epson-C8-Compact-6-Axis-Robots/p/RC8-A701ST75SS>. [Accessed 12 January 2019].

Feng, H. Y. & Li, H., (2002). Constant scallop height tool path generation for three axis sculptured surface machining. *Computer Aided Design* , 34(9), pp. 647-654.

Gadit, J. & Damle, G., (2015). Task Programming of Robotic welding using touch sensing principle. 2(5).

Gao, Z., Lan, X. & Bian, Y., (2011). Structural Dimension Optimization of Robotic Belt Grinding System for Grinding Workpieces with Complex Shaped Surfaces Based on Dexterity Grinding Space. 24(3).

Gupta, A., Robinson-Westcott, J. & Arora, S. K., (2013). *Industrial Automation and Robotics*. Washington D.C: Mercury Learning & Information.

Hartenberg, R. & Danavit, J., (1955). 'a kinematics notation for lower pair mechanisms based n matirces. *journal of applied mathamatics*, 23(1), pp. 215-221.

Ha, T.-H.et al., (2004). Role of Sensors in Corrosion Monitoring and Durability Assessment in Concrete Structures: the State of the Art. *Sensors and Materials*, 16(3), pp. 133-158.

Hobson, T., (2011). *Exploring Surface Texture*. [Online] Available at: <https://www.taylor-hobson.com//media/ametektaylorhobson/files/learning%20zone/exploring%20surface%20texture%202014.pdf?la=en>. [Accessed 28 09 2019].

Hobson, T., (2016). *Form Talysurf*. [Online] Available at: https://www.taylor-hobson.com/-/media/ametektaylorhobson/files/product%20downloads/i-series%20range/fts-i-series_product%20brochure.pdf. [Accessed 22 06 2019].

Huang, H., Gong, Z., Chen, X. & Zhou, L., (2002). Robotic grinding and polishing for turbine-vane overhaul. 127(2).

Huffman, (2013). *Huffman Machine*. [Online] Available at: <http://huffman-llc.com/Laser-Grinding-Waterjet-Technology.aspx?sid=15&pid=14&red=yes>. [Accessed 07 04 2016].

Hurco, (2017). <http://www.hurco.com/pages/default.aspx>. [Online] Available at: <http://www.hurco.com/pages/default.aspx>. [Accessed 23 January 2019].

Inasaki, I., Tonshoff, H. & Howes, T., (1993). Abrasive Machining in the Future. *Annals of the CIRP*, 42(2).

International Organization for Standardisation, (1998). *Manipulating industrial robots - Performance criteria and related test methods*. Geneva: International Organization for Standardization.

Jiang, P. & Liue, D., (2009). Modelling of Machining Error Flow Based on Form Feature for Multistage Processes. *International Journal of computer integrated manufacturing*, 22(9), p. 587-876.

Jin, T. & Jiyong, K., (2007). A 3-D point sets registration method in reverse engineering. *Computers & Industrial Engineering*, 53(2), pp. 270-276.

Ji, W. & Wang, L., (2019). Industrial robotic machining: a review. 103(1-4).

J, N., (2007). Automated robotic grinding by low-powered manipulator. 23(5).

Karpuschewski, Y., Wehmeier, M. & Inasak, I., (2000). Grinding Monitoring System Based on Power and Acoustic Emission Sensors. *CIRP Annals*, 49(1), pp. 235-240.

Khodaygan, S., (2014). Manufacturing error compensation based on cutting tool location correction in machining processes. 27(11).

Kim, H. Y., Kim, S., Ahn, J. H. & Kim, S., (2001). Process monitoring of centerless grinding using acoustic emission. *Journal of Materials Processing Technology*, April, 111(1-3), pp. 273-276.

Klimchik, A., Ambiehl, A., Garnier, S. & Furet, B., (2017). Efficiency evaluation of robots in machining applications using industrial performance measure. Volume 48.

Kubla, T. & Singule, V., (2015). *Investigation of Position Accuracy of Industrial robots and online methods for accuracy improvement in machining processes*. Brno, International Conference on Electrical Drives and Power Electronics.

Kuka, (2010). *Kuka System Software 5.5*, s.l.: Kuka.

- KUKA, (2011). *KUKA System Software 8.2*. Augsburg: KUKA Roboter GmbH.
- Lartigue, C., Duc, E. & Tournier, C., (1999). Machining of free-form surfaces and geometrical specifications. *Proceedings of the Institution of Mechanical Engineers, Part B: Journal of Engineering Manufacture*, 213(1), pp. 21-27.
- Latifinavid, M. & Konukseven, E., (2017). Hybrid model based on energy and experimental methods for parallel hexapod-robotic light abrasive grinding. 1(1).
- Li, I., Fu, J. & Peklenik, J., (1980). A study of grinding force mathematical model. 29(1).
- Li, J., (2008). Calibration of a portable laser 3-D scanner used by a robot and its use in measurement.. 47(1).
- Li, J., huang, Y. & Kong, G., (2018). Loose gangues backfill body's acoustic emissions rules during compaction test: Based on solid backfill mining. 115(1).
- Liu, H., Lai, X. & Wu, W., (2013). Time-optimal and jerk-continuous trajectory planning for robot manipulators with kinematic constraints. 29(2).
- Lizarralde, R., Barrenetxea, D., Gallego, I. & Marquinez, J., (2005). Practical application of new simulation method for the elimination of geometric instabilities in centerless grinding. *CIRP Annals - Manufacturing Technology*, 54(1), pp. 273-276.
- Lo, C. C. & Lin, R. S., (2001). An improved method for scheduling the tool paths for three axis surface machining. *International Journal of Machine Tools & Manufacture*, 41(1), pp. 133-147.
- mach, (2011). *machsuporport*. [Online] Available at: <https://www.cnccookbook.com/cnc-stepover/> [Accessed 23 03 2019].
- Maksoud, T. M. A. & Atia, M. R., (2007). Review of Intelligent Grinding and Dressing Operations. 8(2).
- Marin, R. & Ferreria, P., (2003). Analysis of the influence of fixture locator errors on the compliance of work part features to Geometric Tolerance Specifications. *Journal of Manufacturing*, 3(125), pp. 609-616.
- Metrology, E., (2012). *CMM Contact Measurement (Probing)*. [Online] Available at: <http://www.exactmetrology.com/3d-scanning-technology/contact-measurement> [Accessed 05 04 2016].

- Mohammed, A., Hong, J. & Wang, D., (2018). Design of a force-controlled end-effector with low-inertia effect for robotic polishing using macro-mini robot approach. Volume 49.
- Morgan , M., Cai, R. & guidotti, A., (2007). Design and Implementation of an intelligent grinding assistant system. 1(1).
- Nageswara, P. R., (2006). *CAD/CAM Principles and Applications*. Second ed. Iowa, USA: Tata McGraw-Hill .
- Neto, P. & Moreira, A., (2013). *Robotics in Smart Manufacturing*. 1st ed. Porto: Springer Heidelberg .
- Niku, S. B., 2001. *Introduction to Robotics*. New Jersey: Prentice Hall.
- Noda, K., Yamamoto, T. & Tatsunori, K., (2003). *Robot and control method for controlling robot expressions*. United States of America, Patent No. 73631082.
- Nof, S. Y., (1999). *Handbook of Industrial Robotics, Volume 1*. New York: John Wiley & Sons.
- Overby, A., (2010). *CNC Machining Handbook: Building, Programming, and Implementation*. New York: McGraw-Hill Education .
- Owen , W. & Benhabib, B., (2006). Real-time trajectory resolution for a two-manipulator machining system. 1(22), pp. 51-63.
- Pan, Z., Zhang, H., Zhu, Z. & Wang, J., (2006). Chatter Analysis of Robic Machining Process. 173(3).
- Pires, J. N., Loureiro, A. & Bölmsjö, G., (2006). *Welding Robots: Technology, System Issues and Application*. Coimbra: Springer.
- Qi, J., Zhang, D., Li, S. & and Chen, B., (2017). Modeling of the Working Accuracy for Robotic Belt Grinding system for Turbine Blades. 9(6).
- Quin, G., Zhang, W. & Wan , M., (2006). A mathamtical approach to analysis and optimal design of a fixture locating scheme. *International Journal of Advanced Manufacturing Technology*, 1(29), pp. 349-359.
- Quintana, G. & Ciuranab, J., (2011). Chatter in machining processes: A review. *International Journal of Machine Tools and Manufacture*, 51(5), pp. 363-376.
- Rech, J; Kermouche, G; Grzesik, W; Gracia-Rosales, C; Khellouki, A, (2008). Charaterization and modelling of the residual stresses induced by belt finishing on a AISI52100 hardened stell. 208(1-3).

- Reddy, B., Padmanabhan, G. & Reddy, K., (2008). Surface roughness prediction techniques for CNC turning. *Asian journal of Scientific Research* , 1(3), pp. 256-264.
- Ren, X., Kuhlenkotter, B. & Muller, H., (2006). Simulation and verification of belt grinding with industrial robots. Volume 46.
- Ren, X., Muller, H. & Kuhlenkoetter, B., (2006). Surfel-based surface modeling for robotic belt grinding simulation. 7(7).
- Riemer, R. & Edan, Y., (2000). Evaluation of Influence of Target Location on RObot Repeatability. *Robotica* , 18(4), pp. 443-449.
- Rowe, B., (2009). *Principles of Modern Grinding Technology*. USA: Elsevier Publication.
- Rowe, W., (2009). *Principles of Modern Grinding Technology*. Oxford: Elsevier Science and Technology.
- Rubio, E. & Correa, J., (2012). A Wavelet Approach to Estimate The Quality of Ground Parts. *Journal of Applied Research and Technology*, 20(10).
- Salje, E., (1953). Grundlagen des Schleifvorganges. 86(4).
- Sariola, V., (2012). *Droplet self-alignment: High-precision robotic microassembly and self-assembly*, Helsinki: Aalto University.
- Schneider, U; Drust, M; Ansaloni, M; Lehmann, C; Pellicciari, M, (2014). Improving robotic machining accuracy through experimental error investigation and modular compensation. 1(1).
- Shiakolas, P., Conrad, K. & Yih, T., (2002). On The Accuracy, Repeatability, And Degree of Influence of Kinematics Parameters For Industrial Robots. *International Journal of Modelling and Simulation*, 22(3).
- Song, Y., Liang, W. & Yang, Y., (2011). A method for grinding removal control of a robot belt grinding system. 23(5).
- Sufian, M., Chen, X. & Yu, D., (2017). *Investigating the Capability of Precision in Robotic Grinding*. Huddersfield, Institute of Electrical & Electronic Engineers (IEEE).
- Sun, Y., Giblin, D. J. & and Kazerounian, K., (2009). Accurate robotic belt grinding of workpieces with complex geometries using relative calibration techniques. 25(1).

- Sun, Y., Giblin, D. J. & Kazerounian, K., (2013). Accurate robotic belt grinding of workpieces with complex geometries using relative calibration techniques. 25(1).
- Tahvilian, A; Liu, Z; Champliand, H; Hazel, B; Lagace, M, (2015). Characterization of grinding wheel grain topography under different robotic grinding conditions using confocal microscope. 80(5-8).
- Tang, J., Du, J. & Chen, P., (2009). Modelling and experimental study of grinding forces in surface grinding. 209(6).
- Tao, B., Zhao, X. & Ding, H., (2019). Mobile-robotic machining for large complex components: A review study. 62(8).
- Verl, A., (2019). Robots in machining.
- Wang, C., Lin, P. & Qin, H., (2018). Review on intelligent path planning algorithm of mobile robots. 37(8).
- Webb, P; Geldart, M; Larsson, H; Backstrom, M; Gindy, N; Rask, K, (2013). A direct comparison of the machining performance of a variax 5 axis parallel kinetic machining centre with conventional 3 and 5 axis machine tools. *International Journal of Machine Tools & Manufacture*, 43(1), pp. 1107-1116.
- Werner, G., (1978). Influence of work material on grinding forces. 1(27).
- Wu, H; Gao, J; Li, S; Zhang, Y; Zheng, D, (2013). A review of geometric reconstruction algorithm and repairing methodologies for gas turbine components. *International Journal of Telecommunication, Computing, Electronics and Control*, 11(3), pp. 1609-1618.
- Wu, Shuihua; Kazerounian, Kazem; Gan, Zhongxue; Sun, Yunquan, (2013). A Simulation Platform for Optimal Selection of Robotic Belt Grinding System Parameters. 64(3).
- Xiao, G. & Huang, Y., (2015). Equivalent self-adaptive belt grinding for the real-R edge of an aero-engine precision-forged blade.. Volume 83.
- Xiao, W., Traub, H. & Hoffmeister H, (2011). Closed Form inverse kinematic of 6R milling robot with singularity avoidance. 5(1).
- Xie, H., Li, W.-l., Yin, Z. & Ding, H., (2019). Variance-Minimization Iterative Matching Method for Free-Form Surfaces-Part I: Theory and Method. 16(3).
- Xiong, Y., Ding, H. & Wang, M., (2002). Quantitative Analysis of Inner Force Distribution and Load Capacity of Grasps and Fixtures. *Journal of Manufacturing*, 2(124), pp. 444-455.

Yamada, T., Lee, H. & Miura, K., (2013). Effect of Contact Stiffness of Grinding Wheel on Ground Surface Roughness and Residual Stock Removal of Workpiece. Volume 797.

Yoon, J.-H., Pottmann, H. & Lee, Y.-S., (2013). Locally optimal cutting position for 5-axis sculptured surface machining. *Computer Aided Design* , 35(1), pp. 69-81.

Young, M. L., Dae, W. B. & Hyun, G. L., (2006). Effect of maximum undeformed chip thickness on roughness and specific energy of grinding",. 20(25).

Yuan, L. e., (2018). A Review on Chatter in Robotic Machining Process Regarding Both Regenerative and Mode Coupling Mechanism. Volume 23.

Yun, C. & Wang, W., (2011). A Path Planning Method for Robotic Belt Surface Grinding. 24(4).

Zaghbani, Z., Lamraoui, M. & Songmene, V., (2011). Robotic high speed machining of aluminium alloy. Volume 188.

Zhang, Xiang; Kuhlenkotter, Bernd; Kneupner, Klaus, (2005). An efficient method for solving the Signorini problem in the simulation. *International Journal of Machine Tools & Manufacture*, Volume 45, pp. 641-648.

Zhang, Y., (2003). Research Into Engineering Application of Reverse Engineering Technology. *Materials Processing Technology*, Issue 139, pp. 472-475.

Zhao, T., Shi, Y., Lin, X. & Duan, J., (2014). Surface roughness prediction and parameters optimization in grinding and polishing process for IBR of aero-engine. 2014(74).

Zhifeng, L., Jingjing, X. & Qiang, X., (2018). Rotation-joint stiffness modeling for industrial robots considering contacts. 10(8).

Zhu, D., Xu, X., Yang, Z. & Zhuang, K., (2018). Analysis and assessment of robotic belt grinding mechanisms by force modeling and force control experimetns. Volume 120.

Appendices

Appendix 1

Position 1			Position 2		
Date	16/06/2016	1.00 pm	Date	16/06/2016	1.00 pm
Position	1	X	Position	2	X
Speed	2 m/s		Speed	2 m/s	
Operational Speed %	30%	Gauge Reading (mm)	Operational Speed %	30%	Gauge Reading (mm)
Measurement of Gauge			Measurement of Gauge		
Speed	30% of 2m/s	10% of 2m/s	Speed	30% of 2m/s	10% of 2m/s
No. of Times	Distance 100mm	Distance 100mm	No. of Times	100mm	100mm
1	1.1	0.8	1	-0.5	0.1
2	0.5	0.6	2	-1.2	0.1
3	1	1	3	-1.5	0.2
4	0.3	0.7	4	-1.3	0
5	0.5	1.5	5	-1.4	0.1
6	0.6	0.9	6	-1.5	0
7	1	1.3	7	1	0.4
8	0.8	1.5	8	-1.3	-0.4
9	0.6	1	9	-1.5	0.1
10	0.5	0.7	10	-2.1	0.3
11	1	1	11	-1.8	0.2
12	1.1	0.8	12	-1.7	0.4
13	0.8	0.5	13	-1.6	-0.2
14	0.6	0.4	14	-1.4	-0.1
15	1.1	0.1	15	-1.5	0
Date	16/06/2016	1.00 pm	Date	17/16/2016	10:30 AM
Position	1	Y	Position	2	Y
Measurement of Gauge			Measurement of Gauge		
Speed	30% of 2m/s	10% of 2m/s	Speed	30% of 2m/s	10% of 2m/s
No. of Times	100mm	100mm	No. of Times	100mm	100mm
1	-2.5	-0.5	1	0.2	0
2	-1	-0.8	2	0	0.3
3	-1.5	-0.8	3	0.1	-0.2
4	-1.7	-0.5	4	-0.5	0.3
5	-1.4	-0.6	5	0.3	-0.1
6	-2	-0.5	6	0.1	-0.2
7	-1.6	-0.3	7	-0.2	0.3
8	-1.8	-0.7	8	-0.3	0.2
9	-2	-0.6	9	-0.4	0
10	-2.1	-0.4			
11	-1.6	-0.1			
12	-0.5	-0.4			

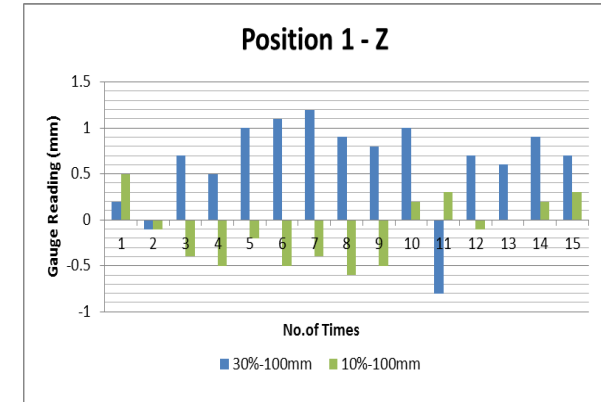
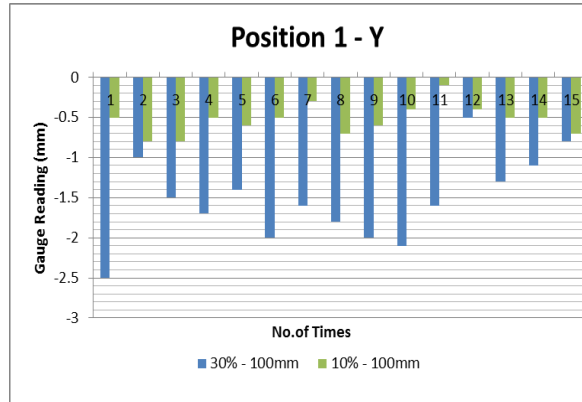
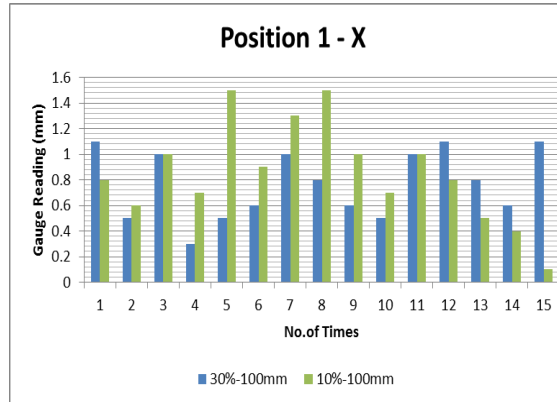
Geometrical Error Analysis and Correction in Robotic Grinding

13	-1.3	-0.5	10	-0.2	0.1
14	-1.1	-0.5	11	-0.2	0.2
15	-0.8	-0.7	12	-0.3	0.3
			13	0.2	0.2
			14	0.1	0.1
			15	0.4	-0.2
Date	16/06/2016	1.00 pm	Date	17/16/2016	1:00 PM
Position	1	Z	Position	2	Z
Measurement of Gauge			Measurement of Gauge		
Speed	30% of 1m/s	10% of 1m/s	Speed	30% of 1m/s	10% of 1m/s
No. of Times	100mm	100mm	No. of Times	100mm	100mm
1	0.2	0.5	1	0.3	0.2
2	-0.1	-0.1	2	0	0.3
3	0.7	-0.4	3	0.3	-0.2
4	0.5	-0.5	4	0.5	-0.2
5	1	-0.2	5	0.7	-0.4
6	1.1	-0.5	6	0.4	-0.2
7	1.2	-0.4	7	0.5	0.3
8	0.9	-0.6	8	0.7	-0.3
9	0.8	-0.5	9	0.5	0
10	1	0.2	10	0.9	0.1
11	-0.8	0.3	11	0.8	-0.2
12	0.7	-0.1	12	1	0.4
13	0.6	0	13	0.7	0.2
14	0.9	0.2	14	1.2	-0.3
15	0.7	0.3	15	0.5	-0.3

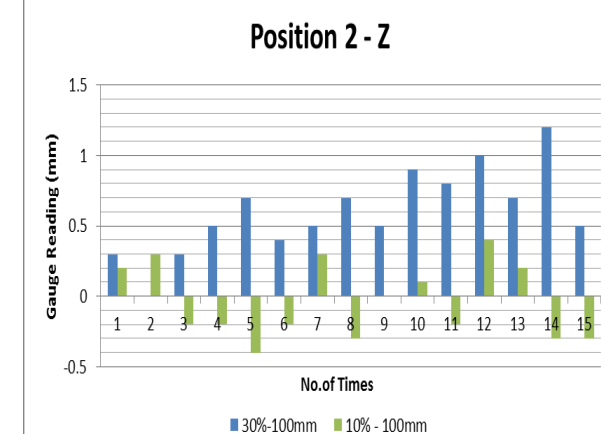
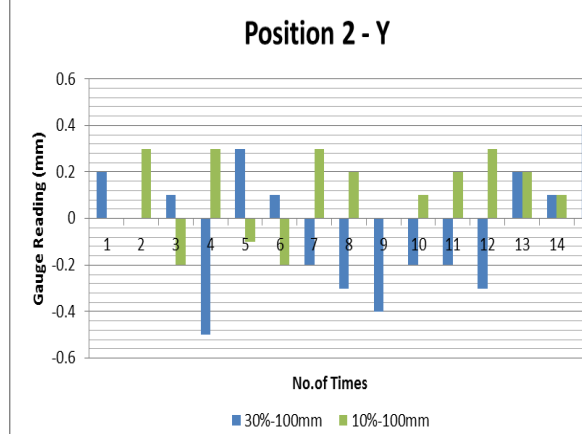
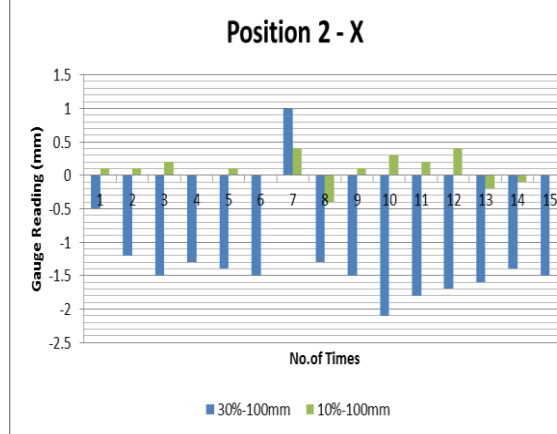
Position 3			Position 4		
Date	17/06/2016	12:00 PM	Date	20/06/2016	11:00 PM
Position	3	X	Position	4	X
Speed	2 m/s		Speed	2 m/s	
Operational Speed %	30%	Gauge Reading (mm)	Operational Speed %	30%	Gauge Reading (mm)
Measurement of Gauge			Measurement of Gauge		
Speed	30% of 1m/s	10% of 1m/s	Speed	30% of 1m/s	10% of 1m/s
No. of Times	100mm	100mm	No. of Times	100mm	100mm
1	-0.4	0.5	1	-0.1	0.1
2	-0.5	0.3	2	-0.2	-0.6
3	0.1	0.8	3	-0.4	-0.5
4	0.2	0.6	4	0.1	-0.6
5	0	0.9	5	-0.2	-0.5
6	0.2	1.2	6	0.5	-0.8
7	0.1	0.6	7	0.4	-0.2
8	0.5	1	8	-0.2	-0.6
9	0.6	0.7	9	-0.1	-0.4
10	0.2	0.4	10	0.2	-0.3
11	0.5	0.3	11	0.3	-0.9
12	0.4	0.5	12	-0.1	-0.4
13	0.5	0.3	13	0.2	-0.5
14	0.3	0.2	14	-0.3	0.2
15	0.2	0.4	15	0.2	0.3
Date	20/06/2016	12:00 PM	Date	20/06/2016	13:00 PM
Position	3	Axis	Position	4	Y
Measurement of Gauge			Measurement of Gauge		
Speed	30% of 1m/s	10% of 1m/s	Speed	30% of 1m/s	10% of 1m/s
No. of Times	100mm	100mm	No. of Times	100mm	100mm
1	0.9	-0.2	1	-0.1	0.8
2	0.5	-0.1	2	-0.1	0.3
3	0.3	-0.4	3	-0.2	0.1
4	-0.5	-0.5	4	-0.1	0.7
5	-0.3	-0.1	5	-0.5	0.8
6	0.4	0	6	-0.2	0.2
7	-0.3	0.2	7	-0.1	0.4
8	-0.4	0.1	8	-0.4	0.6
9	-0.8	0.3	9	-0.5	-0.2
10	0.4	0	10	-0.7	0.3
11	0.5	-0.1	11	-0.3	0.2
12	0.6	0.6			
13	-0.4	0.3			
14	-0.3	-0.1			

15	0.2	0.2	12	-0.5	0.5
			13	-0.2	0.3
Date	17/16/2016	2:20 PM	14	-0.3	0.6
Position	3	Axis	15	-0.5	0.5
Measurement of Gauge					
Speed	30% of 1m/s	10% of 1m/s	Date	20/06/2016	2:30 PM
No. of Times	100mm	100mm	Position	4	Z
			Measurement of Gauge		
			Speed	30% of 1m/s	10% of 1m/s
1	0	0.2	No. of Times	100mm	100mm
2	0.7	0.1	1	0.5	0
3	0.9	0	2	0.2	0.1
4	1	0.5	3	0.3	-0.2
5	0.8	0.6	4	-0.3	0.1
6	0.6	-0.2	5	-0.2	0
7	1.1	-0.3	6	0.3	0.3
8	0.8	-0.1	7	0.5	0.2
9	1	0.2	8	0.4	0.4
10	0.9	0.1	9	0.6	0.1
11	0.8	0.1	10	0.3	-0.3
12	0.7	0	11	-0.3	-0.2
13	1	-0.3	12	-0.2	0.2
14	0.6	-0.2	13	0.5	0.1
15	0.6	0.3	14	0.4	-0.3
			15	0.6	0.4

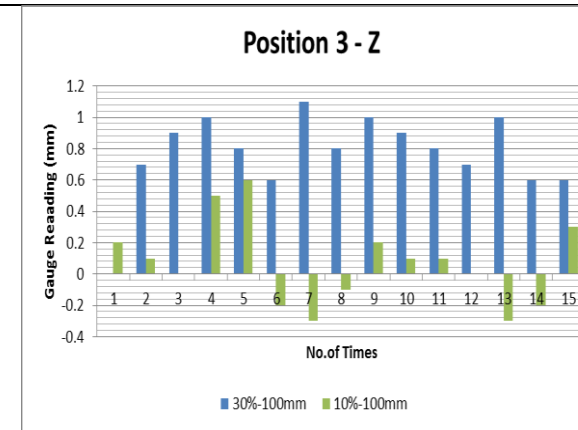
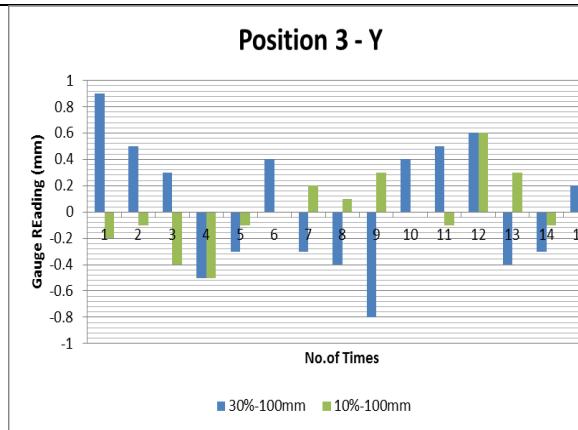
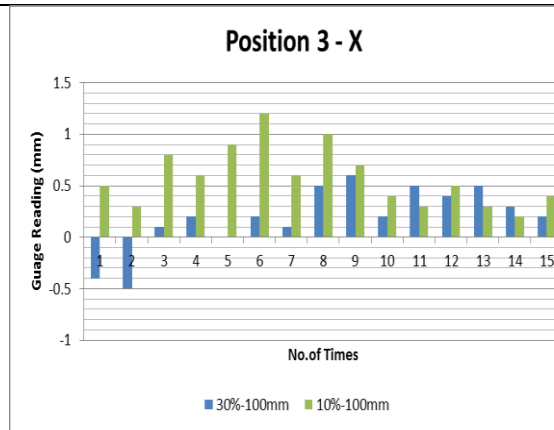
Position 1



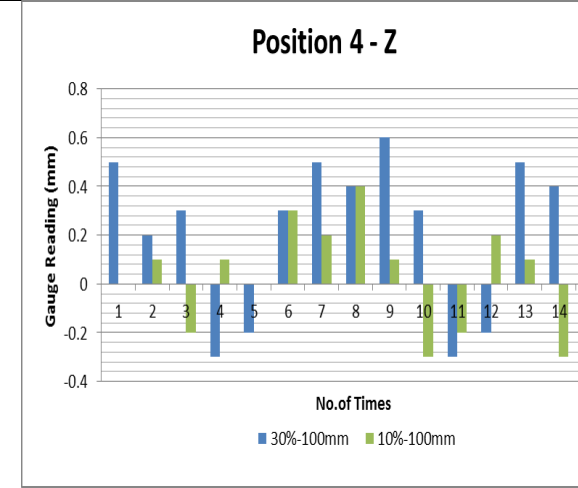
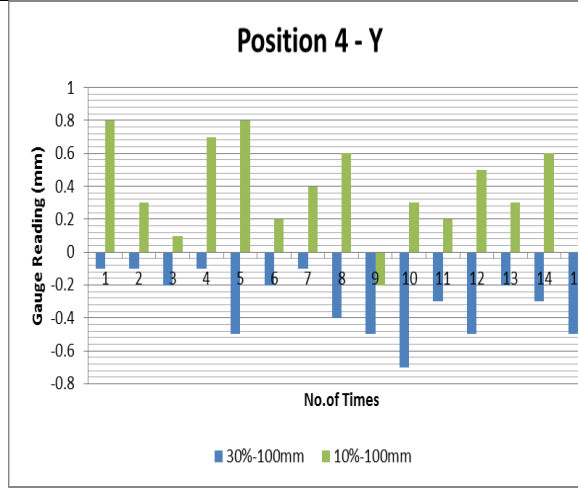
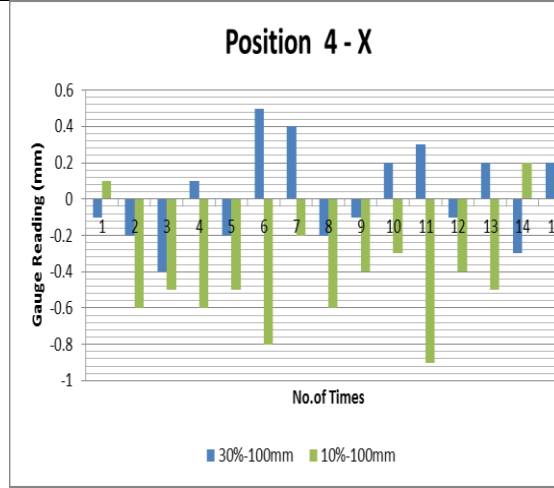
Position 2



Position 3



Position 4



Appendix 2

Datum interrupt file

ROBOT PROGRAMME COMMAND FILE - SRC

```

&ACCESS RVP
&REL 21
&PARAM TEMPLATE = C:\KRC\Roboter\Template\vorgabe
&PARAM EDITMASK = *
DEF andyz ( )
INT I
;FOLD INI
    ;FOLD BASISTECH INI
        GLOBAL INTERRUPT DECL 3 WHEN $STOPMESS==TRUE DO IR_STOPM ( )
        INTERRUPT ON 3
        BAS (#INITMOV,0 )
    ;ENDFOLD (BASISTECH INI)
;FOLD SPOTTECH INI
USERSPOT(#INIT)
;ENDFOLD (SPOTTECH INI)
;FOLD GRIPPERTECH INI
USER_GRP(0,DUMMY,DUMMY,GDEFAULT)
;ENDFOLD (GRIPPERTECH INI)
    ;FOLD USER INI
        ;Make your modifications here

    ;ENDFOLD (USER INI)
;ENDFOLD (INI)

FOR I=1 TO 16
$OUT[I]=TRUE ; activate all Outputs
ENDFOR

GLOBAL INTERRUPT DECL 1 WHEN $IN[1]==TRUE DO RECORD ( )

;FOLD PTP HOME Vel= 100 % DEFAULT;{%PE}%MKUKATPBASIS,%CMOVE,%VPTP,%P
1:PTP, 2:HOME, 3:, 5:100, 7:DEFAULT
$BWDSTART = FALSE
PDAT_ACT=PDEFAULT
FDAT_ACT=FHOME
BAS (#PTP_PARAMS,100 )
$H_POS=XHOME
PTP XHOME
;ENDFOLD
;FOLD PTP P1 Vel= 50 % PDAT1 Tool[5]:25mm ball Base[7]:Grinding
Block;{%PE}%R 5.2.25,%MKUKATPBASIS,%CMOVE,%VPTP,%P 1:PTP, 2:P1, 3:,
5:50, 7:PDAT1
$BWDSTART = FALSE
PDAT_ACT=PPDAT1
FDAT_ACT=FP1
BAS (#PTP_PARAMS,50)
PTP XP1
;ENDFOLD

```

```
;FOLD LIN P2 Vel= 1 m/s CPDAT5 Tool[5]:25mm ball Base[7]:Grinding
Block;{%PE}%R 5.2.25,%MKUKATPBASIS,%CMOVE,%VLIN,%P 1:LIN, 2:P2, 3:, 5:1,
7:CPDAT5
$BWDSTART = FALSE
LDAT_ACT=LCPDAT5
FDAT_ACT=FP2
BAS(#CP_PARAMS,1)
LIN XP2
;ENDFOLD
;FOLD LIN P3 Vel= 1 m/s CPDAT6 Tool[5]:25mm ball Base[7]:Grinding
Block;{%PE}%R 5.2.25,%MKUKATPBASIS,%CMOVE,%VLIN,%P 1:LIN, 2:P3, 3:, 5:1,
7:CPDAT6
$BWDSTART = FALSE
LDAT_ACT=LCPDAT6
FDAT_ACT=FP3
BAS(#CP_PARAMS,1)
LIN XP3
;ENDFOLD
;FOLD LIN P4 Vel= 1 m/s CPDAT7 Tool[5]:25mm ball Base[7]:Grinding
Block;{%PE}%R 5.2.25,%MKUKATPBASIS,%CMOVE,%VLIN,%P 1:LIN, 2:P4, 3:, 5:1,
7:CPDAT7
$BWDSTART = FALSE
LDAT_ACT=LCPDAT7
FDAT_ACT=FP4
BAS(#CP_PARAMS,1)
LIN XP4
;ENDFOLD

MOVEP ( )

MOVEP1 ( )

MOVEP2 ( )

MOVEP3 ( )

MOVEP4 ( )

MOVEP5 ( )

MOVEP6 ( )

MOVEP7 ( )

MOVEP8 ( )

MOVEP9 ( )

MOVEP10 ( )

MOVEP11 ( )

MOVEP12 ( )

;FOLD PTP HOME Vel= 100 % DEFAULT;{%PE}%MKUKATPBASIS,%CMOVE,%VPTP,%P
1:PTP, 2:HOME, 3:, 5:100, 7:DEFAULT
```

```
$BWDSTART = FALSE
PDAT_ACT=PDEFAULT
FDAT_ACT=FHOME
BAS (#PTP_PARAMS,100 )
$H_POS=XHOME
PTP XHOME
;ENDFOLD
```

```
END
```

```
;MOVEP ( ) PROGRAMME
```

```
DEF MOVEP ( )
$ADVANCE=0
INTERRUPT ON 1
LIN_REL {Z+20}
END
```

```
;MOVEP1 ( ) PROGRAMME
```

```
DEF MOVEP1 ( )
$ADVANCE=0
INTERRUPT ON 1
LIN_REL {Y+7}
LIN_REL {Z+20}
END
```

```
;MOVEP2 ( ) PROGRAMME
```

```
DEF MOVEP2 ( )
$ADVANCE=0
INTERRUPT ON 1
LIN_REL {Y+7}
LIN_REL {Z+20}
END
```

```
;MOVEP3 ( ) PROGRAMME
```

```
DEF MOVEP3 ( )
$ADVANCE=0
INTERRUPT ON 1
LIN_REL {Y+22}
LIN_REL {Z+20}
END
```

```
;MOVEP4 ( ) PROGRAMME
```

```
DEF MOVEP4 ( )
$ADVANCE=0
INTERRUPT ON 1
LIN_REL {Y+7}
LIN_REL {Z+20}
END
```

```
;MOVEP5 ( ) PROGRAMME
```

```
DEF MOVEP5 ( )
```

```
$ADVANCE=0
INTERRUPT ON 1
LIN_REL {Y+7}
LIN_REL {Z+20}
END

;MOVEP6 ( ) PROGRAMME

DEF MOVEP6 ( )
$ADVANCE=0
INTERRUPT ON 1
LIN_REL {X-40}
LIN_REL {Z+20}
END

;MOVEP7 ( ) PROGRAMME

DEF MOVEP7 ( )
$ADVANCE=0
INTERRUPT ON 1
LIN_REL {Y-7}
LIN_REL {Z+20}
END

;MOVEP8 ( ) PROGRAMME

DEF MOVEP8 ( )
$ADVANCE=0
INTERRUPT ON 1
LIN_REL {Y-7}
LIN_REL {Z+20}
END

;MOVEP9 ( ) PROGRAMME

DEF MOVEP9 ( )
$ADVANCE=0
INTERRUPT ON 1
LIN_REL {Y-22}
LIN_REL {Z+20}
END

;MOVEP10 ( ) PROGRAMME

DEF MOVEP10 ( )
$ADVANCE=0
INTERRUPT ON 1
LIN_REL {Y-7}
LIN_REL {Z+20}
END

;MOVEP11 ( ) PROGRAMME

DEF MOVEP11 ( )
$ADVANCE=0
INTERRUPT ON 1
LIN_REL {Y-7}
```

```
LIN_REL {Z+20}
END

;MOVEP12 ( ) PROGRAMME

DEF MOVEP12 ( )
LIN_REL {Z-100}
END

;SUB PROGRAMME
DEF RECORD ( )
INTERRUPT OFF 1
BRAKE F
$OUT[1]=TRUE
LIN_REL {Z-10} ;point at which interrupt is read
WAIT SEC 1
RESUME
END
```

Appendix 3

Z – Plane Calculations

$$Z_{\text{Theoretical}} = D + (aX) + (bY)$$

Known:	Value:	Found by:
a	0.000765	Matlab
c	0.001865	Matlab
d	-12.4445	Matlab
X	60.29546 mm	Practical Experimentation
Z	13.23640 mm	Practical Experimentation

Hence, by running the programme and inspection of the results within the Matlab workbook, the regression coefficients d, a, and c, can be found. This is implemented for all Planes

Y Plane - Y Point 2 (Sample)

$$Y_{\text{Theoretical}} = d + (aX) + (cZ)$$

Known:	Value:	Found by:
a	0.016491121	Matlab
c	-0.00315637	Matlab
d	-13.9813368	Matlab
X	59.73188 mm	Practical Experimentation
Z	9.280461 mm	Practical Experimentation

Inserting the known values:

$$Y_{\text{Estimated}} = -13.9813368 + (0.016491121 \times 59.73188) + (-0.00315637 \times 9.280461) \text{ mm}$$

∴

$$Y_{\text{Theoretical}} = -13.02558 \text{ mm}$$

From the point detection exercise, the actual value of Y is:

$$Y_{\text{Experimental}} = -13.03617 \text{ mm}$$

By inserting the values in to **Equation 11**:

$$Y_{\text{Theoretical}} - Y_{\text{Experimental}} = \Delta_Y$$

∴

$$-13.02558 + 13.03617 = \Delta_Y$$

$$\Delta_Y = 10.59 \mu\text{m}$$

X Plane - X Point 9 (Sample)

$$X_{\text{Estimated}} = d + (bY) + (cZ)$$

Known:	Value:	Found by:
b	-0.013743064	Matlab
c	-0.003697439	Matlab
d	-10.45683307	Matlab
Y	47.12934 mm	Practical Experimentation
Z	22.6794 mm	Practical Experimentation

Inserting the known values:

$$X_{\text{Estimated}} = -10.45683307 + (-0.013743064 \times 47.12934) + (-0.003697439 \times 22.6794) \text{ mm}$$

∴

$$X_{\text{Theoretical}} = -11.1907235 \text{ mm}$$

From the point detection exercise, the actual value of Y is:

$$X_{\text{Experimental}} = -11.18107 \text{ mm}$$

By inserting the values in to **Equation 11**:

$$X_{\text{Theoretical}} - X_{\text{Experimental}} = \Delta_X$$

∴

$$-11.1907235 + 11.18107 = \Delta_X$$

$$\Delta_X = 9.65 \mu\text{m}$$

Appendix 4

Measurement Data

ZX-Plane	Point1	Point2	point 3	point 4
x	18.96116	53.95994	53.95922	18.9595
y	9.65432	9.65386	59.65188	59.6485
z	-13.53528	-13.43599	-13.49653	-13.67748

YZ-Plane	Point1	Point2	point 3	point 4
x	68.96665	68.96383	23.96347	23.96554
y	-12.01869	-12.00135	-12.63366	-12.67575
z	9.61960	34.61897	34.61565	9.61183

XY-Plane	Point1	Point2	point 3	point 4
x	-13.06790	-13.18500	-13.80750	-13.68550
y	6.63600	6.63639	56.63482	56.63440
z	5.23590	30.23607	30.23911	5.23752

Regression

ZX-Plane	Regression Values		
	$0.0040x - 0.00203y - Z + 13.612 = 0$		
	Z (mm) Measurements	Z (mm) Estimated	Error (mm)
Point 1	-13.53528	-13.55569705	0.02042
Point 2	-13.43599	-13.4155745	0.020415505
Point 3	-13.49653	-13.51694498	-0.02041498
Point 4	-13.67748	-13.65706348	0.020416522

YZ-Plane	Regression Values		
	$0.01432x + 0.00119z - Y + 13.0243 = 0$		
	Y (mm) Measurements	Y (mm) Estimated	Error (mm)
Point 1	-12.01869	-12.05062289	-0.03193
Point 2	-12.00135	-12.05064265	-0.04929
Point 3	-12.63366	-12.69606821	-0.06241
Point 4	-12.67575	-12.69608865	-0.02034

XY-Plane	Regression Values $-0.0124y - 0.00478z - X + 12.9593 = 0$		
	X (mm) Measurements	X (mm) Estimated	Error (mm)
Point 1	5.23590	-13.06667676	0.00122
Point 2	30.23607	-13.18622324	-0.00122
Point 3	30.23911	-13.80627683	0.00122
Point 4	5.23752	-13.68672318	-0.00122

Appendix 5

Define Roughing process

- defining coefficient of deformation (α)

$$\delta_1 = \frac{1}{1 + \alpha} \delta'$$

δ = Real depth cut of first cut

δ' = Nominal depth of cut (0.3mm)

$$0.20 = \frac{1}{1 + \alpha} \times 0.3$$

$$1 + \alpha = \frac{0.3}{0.20}$$

$$\alpha = 1 - \frac{0.3}{0.20} = 0.500$$

- Calculating the number of rough infeeds $\delta_1, \delta_2, \dots$

$$\delta_{r1} = \left[1 - \left(\frac{\alpha}{1 + \alpha} \right)^1 \right] \delta'$$

$$\delta_{r1} = \left[1 - \left(\frac{0.500}{1 + 0.500} \right)^1 \right] \times 0.3$$

$$\delta_{r1} = 0.200$$

Calculating roughing 2

$$\delta_{r2} = \left[1 - \left(\frac{0.500}{1 + 0.500} \right)^2 \right] \times 0.3$$

$$\delta_{r2} = 0.266$$

.

.

$$\delta_{r_1} = 0.200, \delta_{r_2} = 0.2666, \delta_{r_3} = 0.2888, \delta_{r_4} = 0.2963, \delta_{r_5} = 0.2987, \delta_{r_6} = 0.2995, \delta_{r_7} = 0.2998$$

According to rough stage, a 7 number of roughing is required. Therefore, Position at which roughing ends is as follows:

$$2.27 - 0.200 - 0.2666 - 0.2888 - 0.2963 - 0.2987 - 0.2995 - 0.2998 = \mathbf{0.3199}$$

Where **2.27mm** is the height of the weld form the surface of the block.

Step 2 – Define Finishing process

Calculate the number of finishing δ_{f1}, δ_{f2}

Where:

$$\delta' = 0.1 \text{ mm}$$

$$\alpha = 0.5 \text{ (assumed to be constant)}$$

$$\delta_{f1} = \left[1 - \left(\frac{\alpha}{1 + \alpha} \right)^1 \right] \delta'$$

$$\delta_{f1} = \left[1 - \left(\frac{0.5}{1 + 0.5} \right)^1 \right] \times 0.1$$

$$\delta_{f1} = 0.066$$

Calculating Finishing 2

$$\delta_{f2} = \left[1 - \left(\frac{\alpha}{1 + \alpha} \right)^1 \right] \delta'$$

$$\delta_{f2} = \left[1 - \left(\frac{0.5}{1 + 0.5} \right)^2 \right] \times 0.1$$

$$\delta_{f2} = 0.1111$$

$$\delta_{f1} = 0.066, \delta_{f2} = 0.111$$

According to finishing stage, a two number of finishing is required. Therefore, Position at which finishing ends is as follows:

$$0.3199 - 0.066 - 0.111 = \mathbf{0.1421}$$

Where **0.1421mm** is the amount of residual left on the surface. This needs a couple of spark outs to achieve the final finish

Finally, the spark out stage is used to approach the final dimension after the infeed stages. On the last finishing stage a few additional passes is made until no sparks is visual and minimum residual is achieved.

Where:

$$\delta' = 0.1421$$

$$\delta_i = \left(\frac{\alpha}{1+\alpha} \right)^n \delta'$$

First Spark Out

$$\delta_{i1} = \frac{0.5}{(1 + 0.5)} \times 0.1421 = 0.0473$$

Second Spark Out

$$\delta_{i2} = \left(\frac{0.5}{1 + 0.5} \right)^2 \times 0.1421 = 0.0157$$